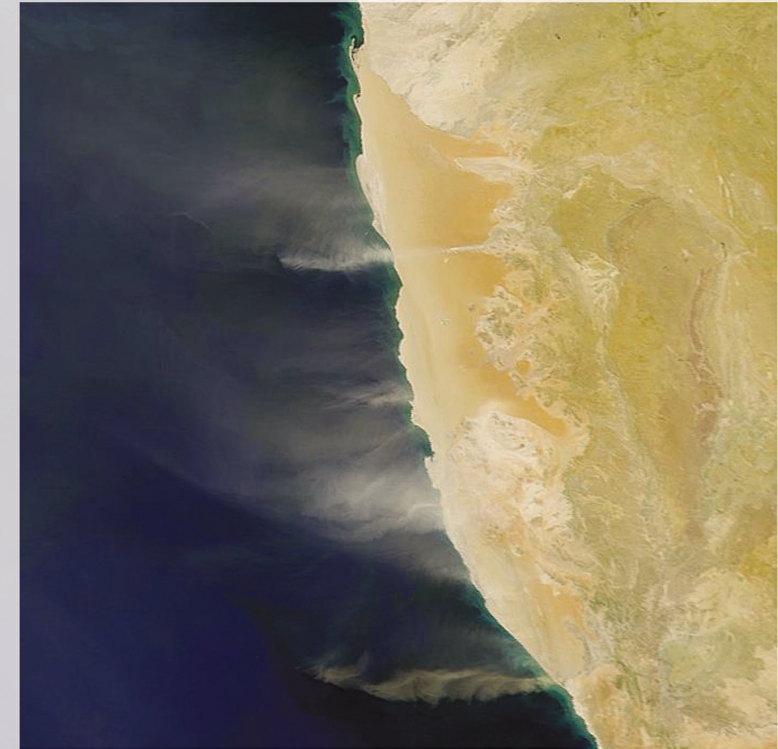


GEOLOGICA ULTRAIECTINA

Mededelingen van de
Faculteit Aardwetenschappen
Universiteit Utrecht

No. 212



Late Quaternary Southwestern African
terrestrial-climate signals
in the marine record of Walvis Ridge,
SE Atlantic Ocean

Jan-Berend W. Stuut

GEOLOGICA ULTRAIECTINA

Mededelingen van de Fakulteit Aardwetenschappen
Universiteit Utrecht

No. 212

**Late Quaternary southwestern African terrestrial-climate signals
in the marine record of Walvis Ridge, SE Atlantic Ocean**

Jan-Berend Willem Stuut

Front cover: Satellite image of southwestern Africa

From SeaWiFS - <http://seawifs.gsfc.nasa.gov/>

© Orbital Imaging Corporation and processing by NASA Goddard Space Flight Center

This research was carried out as part of the NSG-NIOZ-Bremen co-operation,
supported by NWO

ISBN 90-5744-069-5

**Late Quaternary southwestern African terrestrial-climate signals
in the marine record of Walvis Ridge, SE Atlantic Ocean**

**Laat Kwartaire zuidwestelijk Afrikaanse terrestrische
klimaatsignalen in mariene tijdseries van Walvis Rug,
zuidoostelijke Atlantische Oceaan**

(met een samenvatting in het Nederlands)

PROEFSCHRIFT

ter verkrijging van de graad van doctor
aan de Universiteit Utrecht
op gezag van de Rector Magnificus, Prof. Dr. W.H. Gispen,
ingevolge het besluit van het College voor Promoties
in het openbaar te verdedigen op
maandag 3 december 2001 des middags om kwart over vier

door

Jan-Berend Willem Stuut

Geboren op 26 augustus 1971 te Weener, Duitsland

PROMOTOR:

Prof. Dr. Poppe L. de Boer

Faculty of Earth Sciences, Utrecht University
Utrecht, The Netherlands

CO-PROMOTORES:

Dr. J.H. Fred Jansen

Netherlands Institute for Sea Research
Den Burg, The Netherlands

Dr. George Postma

Faculty of Earth Sciences, Utrecht University
Utrecht, The Netherlands

*Aan mijn ouders
Voor Meta en Mathilde*

MEMBERS OF THE DISSERTATION COMMITTEE:

Prof Dr Jan W. de Leeuw

Nederlands Instituut voor Onderzoek der Zee (NIOZ)
Den Burg, The Netherlands

Prof Dr Dick Kroon

Faculteit Aardwetenschappen, Vrije Universiteit Amsterdam
Amsterdam, The Netherlands

Prof Dr Jef Vandenberghe

Faculteit Aardwetenschappen, Vrije Universiteit Amsterdam
Amsterdam, The Netherlands

Dr Gert J. de Lange

Faculteit Aardwetenschappen, Universiteit Utrecht
Utrecht, The Netherlands

Dr Ralph R. Schneider

Fachbereich Geowissenschaften, Universität Bremen
Bremen, Germany

This study was carried out at the Institute for Palaeoenvironments and Palaeoclimate of Utrecht University (IPPU) of the Netherlands Research School of Sedimentary Geology (NSG) and the Netherlands Institute for Sea Research (NIOZ).

Contents

Bibliography	11
Chapter 1. Introduction and summary.	13
Chapter 2. Southeastern Atlantic deep-sea sediments characterised by CORTEX (Core scanner Texel, XRF).	21
Chapter 3. Precision, accuracy and resolution of the laser particle sizer Malvern Mastersizer S and unmixing of artificial sediment mixtures.	35
Chapter 4. Fast reconnaissance of carbonate dissolution based on the size distribution of calcareous ooze on Walvis Ridge, SE Atlantic Ocean.	53
Chapter 5. A 300 kyr record of aridity and wind strength in Southwestern Africa: inferences from grain-size distributions of sediments on Walvis Ridge, SE Atlantic Ocean.	65
Chapter 6. Palaeo- wind strength and continental aridity based on the terrigenous fraction of sediments from the continental slope offshore Walvis Bay, SE Atlantic Ocean.	77
Chapter 7. Southern Hemisphere aridity signals in the grain-size distributions of terrigenous sediments.	87
Chapter 8. Concluding remarks	101
Appendix A: Analytical methods	105
References	109
Samenvatting (summary in Dutch)	117
Acknowledgments	125
Curriculum Vitae	128

Bibliography

Chapter 3:

Jan-Berend W. Stuut^{1,2} & Maarten A. Prins³

Precision, accuracy and resolution of the laser particle sizer Malvern Mastersizer S and unmixing of artificial sediment mixtures.
submitted to Sedimentology (October 2001)

Chapter 4:

Jan-Berend W. Stuut^{1,2}, Maarten A. Prins³ & J.H. Fred Jansen¹

Fast reconnaissance of carbonate dissolution based on the size distribution of calcareous ooze on Walvis Ridge, SE Atlantic Ocean.
submitted to Marine Geology (April 2001)

Chapter 5:

Jan-Berend W. Stuut^{1,2}, Maarten A. Prins³, Ralph R. Schneider⁴, Gert Jan Weltje⁵, J.H. Fred Jansen¹ & George Postma²

A 300 kyr record of aridity and wind strength in Southwestern Africa: inferences from grain-size distributions of sediments on Walvis Ridge, SE Atlantic Ocean.
Marine Geology 180 (1-2) (reprinted with permission from Elsevier Science)

The following chapters were co-authored by:

CHAPTER 2 Southeastern Atlantic deep-sea sediments characterised by CORTEX (Core scanner Texel, XRF)
Mattias Zabel[†] & J.H. Fred Jansen¹

Chapter 6 Palaeo- wind strength and continental aridity based on the terrigenous fraction of sediments from the continental slope offshore Walvis Bay, SE Atlantic Ocean.
Rik H. Tjallingii² & George Postma²

Chapter 7 Southern Hemisphere aridity signals in the grain-size distributions of terrigenous sediments.
Frank Lamy⁴, Maarten A. Prins³, Luc J. Lourens², Klaas van der Borg⁶, Poppe L. de Boer² & J.H. Fred Jansen¹

¹Netherlands Institute for Sea Research (NIOZ), Den Burg, The Netherlands

²Faculty of Earth Sciences, Utrecht University, Utrecht, The Netherlands

³Faculty of Earth Sciences, Vrije Universiteit Amsterdam, Amsterdam, The Netherlands

⁴Fachbereich Geowissenschaften, Universität Bremen, Bremen, Germany

⁵Faculty of Civil Engineering and Applied Geosciences, Delft University of Technology, Delft, The Netherlands

⁶R.J. Van de Graaff laboratory, Utrecht University, Utrecht, The Netherlands

1. Introduction

The first written observations of aeolian dust over the open ocean probably stem from the second half of the 12th century, when the famous explorer Edrisi (1100–1166) found dust on his ship during his expeditions. More than 7 centuries later, Charles Darwin, after one of his famous expeditions with the “Beagle”, published one of the first papers on Saharan dust off the coast of West Africa entitled: “An account of the fine dust which often falls on vessels in the Atlantic Ocean”. Nowadays aeolian dust has become a ‘hot topic’ and is covered in numerous publications, since it is thought that iron-rich dust, from areas like the Sahara and the Namib Desert, could have contributed to the evolution of glacials through fertilisation of the oceans. Algae living in the surface ocean utilise iron and they lower the atmospheric CO₂ content when their remains are buried in the sediments.

The major part of this thesis deals with aeolian dust. Aeolian dust was recovered from deep-sea sediments offshore Southwestern Africa. It originates from the large deserts on the southern part of the African continent. Aim of the study is to reconstruct the climate history of this part of Africa using the physical properties of terrigenous part of the sediments that were deposited in the Southeastern Atlantic Ocean. Aeolian dust is only one of the terrigenous components that are carried to the sea. Terrigenous sediments are also transported to the ocean by rivers and glaciers. In the studied area, however, no large rivers or glaciers are active at present nor in the studied time interval.

Deposition of sediments in the deep oceans is continuous and has been continuous throughout most of the geologic past. This allows reconstruction of the climate and oceanographic history from the deep-sea sedimentary record. Large-scale changes in the composition and flux of the terrigenous fraction, for example, are recorded in the sedimentary record. In general, the supply of terrigenous sediments to the open ocean is affected by tectonics (exposure of rock to erosion), climate and climate change (weathering and transport of erosion products) and sea level and sea-level change (erosion and transport capacity of rivers). Especially climate change and sea-level change determined the high-frequency changes in marine sedimentary sequences throughout the Late Quaternary.

Owing to continuous changes in the position and orientation of the Earth relative to the Sun, the temporal and spatial distribution of energy received from the Sun varied through time. The resulting large-scale temperature variations caused variation in the amount of ice in glaciers around the planet and in the North and South-Polar regions. The waxing and waning of these ice sheets can be recognised in the ratio of oxygen isotopes in the oceans because this ratio varies with the amount of water that is stored in the ice sheets. Calcium-carbonate producing organisms that live in the oceans register the prevailing oxygen-isotope ratio in their calcium-carbonate tests. When the organisms perish, they rain down to the sea floor and the few that get preserved there, hold a record of palaeo-ice-volume. By measuring the ratio of oxygen isotopes from these fossil remains in the sedimentary record, we can reconstruct the global ice volume through time, and have a measure for palaeotemperature as well.

Chapter 1

The large temperature differences on Earth are redistributed through large-scale circulation patterns in both the atmosphere and the oceans. These circulation patterns and the accompanying precipitation patterns caused large climate differences on the continents. Large differences between dry and wet conditions on Earth are reflected in the transport mechanisms of terrigenous sediments to the oceans. A relatively wet climate, for example, will result in increased fluvial runoff of sediments, whereas a relatively dry climate will cause desertification and promote aeolian transport of sediments. The occurrence of these two climate-driven end members of transport of terrigenous sediments (fluvial transport and aeolian transport) can potentially be recognised in the terrigenous fraction of deep-sea sediments, and be translated into relative climate conditions in the source area of the sediments. This hypothesis is the major rationale for this thesis.

The purpose of long-term climate reconstructions is clear: if we don't have a profound knowledge of climate change in the past, we cannot put for example the dramatic rise in atmospheric CO₂ since the industrial revolution into perspective. For that reason it is very important to continue looking for new tools that can help to reconstruct and to understand palaeoclimate from before the recent instrumental records. In this thesis one such tool will be discussed: the spatial and temporal variations in grain size of deep-sea sediments.

Grain size

Leading thread in this thesis is the grain size of sediments. Both the size of shells of plankton that lives in the water column and the grain size of the terrigenous fraction of deep-sea sediments contain a wealth of information. On the basis of the size of plankton shells and shell fragments, a 300-kyr record of Southwestern African wind strength was reconstructed. The prevailing wind system in this part of the South Atlantic influences the oceanic circulation patterns and the dissolution of the carbonate shells produced by planktonic organisms. The dissolution of the calcium carbonate causes the shells to fall apart, which is reflected in the size of the carbonate shell fragments (Chapter 4). The wind that drives the ocean currents also carries large amounts of aeolian dust to the ocean. From the grain size of the terrigenous part of the sediments deposited on Walvis Ridge (Figure 1.1), a 300-kyr Southwestern African climate reconstruction was established in terms of continental aridity and trade wind strength (Chapters 5 and 6).

Southeastern Atlantic Ocean

The study area comprises parts of the Angola and Cape Basins in the Southeastern Atlantic Ocean (Figure 1.1). These two basins are separated by the northeast-southwest trending Walvis Ridge, a submarine volcanic mountain ridge that was formed during the opening of the southern part of the Atlantic Ocean in Late Cretaceous times. Walvis Ridge is covered predominantly with calcareous marine sediments. The oceanography of the area is determined by two large current systems: the southward flowing Angola Current and the northward flowing Benguela Current. These currents meet at the Angola-Benguela Front, which is presently located at a few hundreds of kilometres North of Walvis Ridge. The continental expression of the Angola-Benguela Front is the boundary between the arid climate of Namibia and the (sub)tropical rainforest of Angola. The latitudinal position of the Angola-Benguela Front has varied through geologic time and so has the continental expression of it. A characteristic feature of the Cape Basin is the occurrence of coastal upwelling: surface waters are pushed oceanward by the southeastern trade winds and replaced by cold and nutrient-rich deep waters. Upwelling cells are topographically controlled and cause high biogenic production in the surface waters of Namibia and South Africa. Because of the upwelling-induced high productivity, the sediments that are preserved on the sea bottom consist primarily of tests of foraminifers (unicellular organisms that thrive in the upper 200 m of the water column and produce calcium carbonate shells of $\sim 2\text{ }\mu\text{m}$ to 1 mm) and tests of diatoms (unicellular plants that thrive in the water column and produce silica shells of $\sim 2\text{--}200\text{ }\mu\text{m}$). The main sources of terrigenous sediments are the Namib Desert ($\sim 140,000\text{ km}^2$) and the Kalahari Desert ($\sim 360,000\text{ km}^2$). In combination with the southeastern trades, these deserts deliver large amounts of aeolian dust. Moreover, there are two large perennial rivers; the Cunene River in the North and the Orange River in the South. The Orange River drains almost entire South Africa West of the Drakensbergen and a large part of Namibia, and is therefore the largest contributor of fluvial sediments. Beside these two large rivers there is a number of ephemeral rivers that reach the ocean only once every 10 – 15 years. In the course of the Late Quaternary, the amounts of fluvial and aeolian sediments transported to the Southeastern Atlantic Ocean have varied dramatically. To study these variations, a number of sediment cores was retrieved from Walvis Ridge (Figure 1.1).

Walvis Ridge rises on average about 2000 m above the surrounding sea floor. Therefore, its sediments offer the opportunity to construct a continuous Late Quaternary record. Walvis Ridge is situated next to the Namib Desert, which must be, in combination with the southeastern trades, largely the source area for aeolian dust. Special attention was given to sediment core MD962094 (Figure 1.1) that was studied in detail. This 30.68 m long core was retrieved from 2281 m water depth. The sediments from this core were dated using stable-oxygen isotopes and AMS ^{14}C -dates. This study focuses on the last 300,000 years, which makes up the top 15 m of the core.

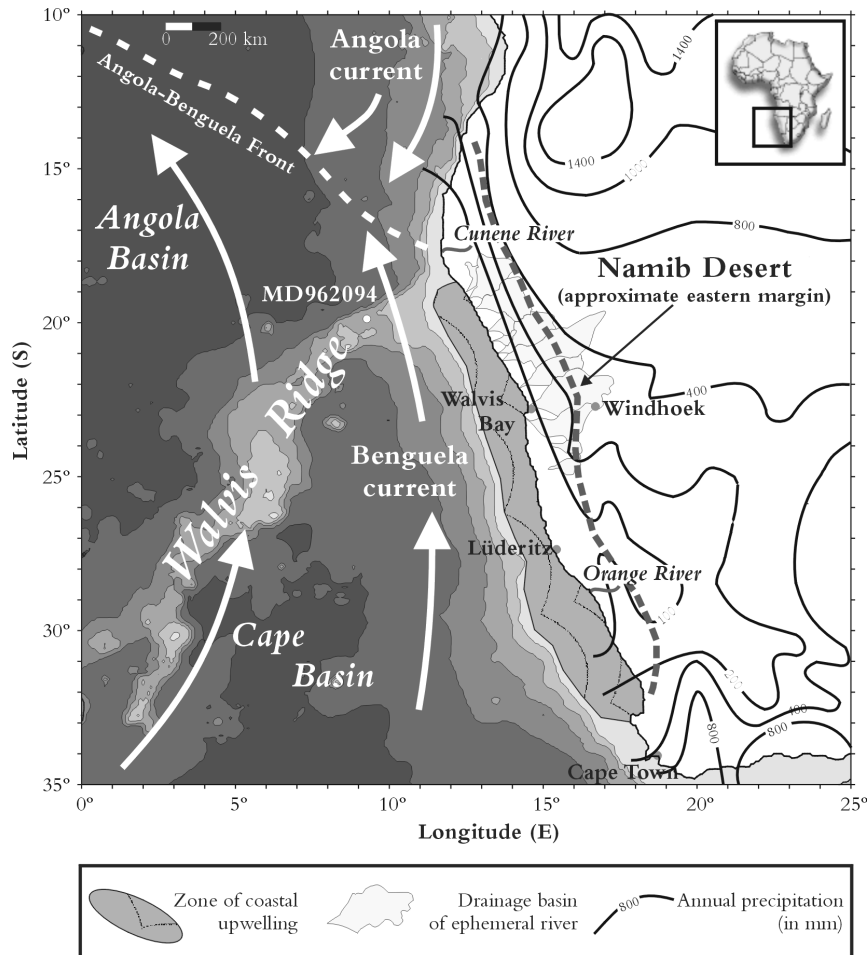


Figure 1.1. Bathymetric map of the Southeastern Atlantic Ocean and Southwestern Africa, showing the most characteristic features in the sea as well as on the land. Bathymetry is given in 1000-m contours.

Abstract and organisation of this thesis

Bulk-chemical (CORTEX) analyses of a transect of seven cores through the Southeastern Atlantic Ocean show that the variations observed in core MD962094 are characteristic for this part of the Atlantic Ocean (Chapter 2). Therefore, the physical properties of the terrigenous fraction of the sediments from this core will be studied. First, the quality of the laser particle sizer *Malvern Mastersizer S* will be examined. The combination of grain-size analyses and an end-member algorithm appears to be ideal for the analysis of mixtures consisting of several subpopulations (Chapter 3). The grain size of bulk sediments (predominantly composed of calcium carbonates) appears to be a good tool to reconstruct the carbonate dissolution on Walvis Ridge (Chapter 4). The interpretation of the downcore bulk size record as an upwelling-induced carbonate-

dissolution record correlates well with the wind-strength record obtained from the grain size of terrigenous sediments on Walvis Ridge (Chapter 5). The interpretation of the end members from Walvis Ridge is supported by the end members that result from three time slices of sediments from the continental slope offshore Walvis Bay (Chapter 6). The continental-aridity record that can be derived from the terrigenous fraction of sediments from the SE Atlantic Ocean, correlates well with other palaeoclimate records from the Southern Hemisphere (Chapter 7). The chemical and physical properties of the sediments from the Southeastern Atlantic Ocean are closely linked to each other (Chapter 8). The bulk chemistry results from CORTEX, which seem to show a palaeoclimate record, are in fact predominantly caused by dissolution of calcium carbonate.

Chapter 2

CORTEX

The chemical composition of seven cores along a transect from the continental slope offshore Walvis Bay to the distal parts of Walvis Ridge was studied. The CORTEX (CoreScanner Texel, XRF) was used to analyse the downcore distributions of seven chemical elements in the seven cores. The CORTEX results are quantitative as appears from the comparison with results from other bulk-chemical analyses. The CORTEX results are a good tool for the correlation of the various cores from the Southeastern Atlantic Ocean, and the good correlation of the seven cores indicates that the sediments from core MD962094 are representative for the sediments from this part of the Atlantic Ocean.

Chapter 3

‘Malvern Mastersizer S’

Nearly all sediments are mixtures of different components. These components differ from each other, amongst others in size, for instance because they have been produced differently (e.g. foraminifers versus diatoms) or have been carried to the site of deposition by different transport mechanisms. In this chapter the quality of the new laser particle sizer *Malvern Mastersizer S* is evaluated by studying the precision (which is the reproducibility of the measurements?), the accuracy (how well is the true grain size reproduced?), and the resolution (how well can the machine discern the mixing ratios of different components in the mixtures?). An end-member algorithm is applied to the data set of mixtures, to check if they can be unmixed into their original subpopulations. In contrast to natural sediments, here the components of the matrix of grain-size distributions are known beforehand, and hence their reconstruction can be checked. The results show that the combination of grain-size analyses and an end-member modelling algorithm are a good tool to distinguish between subpopulations in glass-bead mixtures.

Chapter 4

Grain size of bulk sediments

The size distributions of Walvis Ridge sediments consist of three dominant modes, which can be ascribed to calcium-carbonate tests of different organisms living in the water column. Since these sediments consist of 70-95% calcium carbonate, the bulk size distributions are considered representative for the composition of the calcium carbonate. The fine mode in the size distributions consists of coccospheres (unicellular algae producing calcium-carbonate parts) and fragments of those. The two coarsest modes in the size distributions are predominantly caused by foraminifers (unicellular organisms producing a calcium-carbonate shell) and fragments of those. From microscope analyses of the sediments it appears that there have been periods in which the foraminifers' shells have been preserved well and periods in which most shells have been damaged. Since the shells have been broken along the edges of their chambers, they have most probably been caused by carbonate dissolution. Most dissolution appears to have taken place in the samples of which the coarsest mode in the size distribution is low. The ratio of the two coarse modes thus reflects the fragmentation of the calcium carbonate, caused by carbonate dissolution. In the case of the Southeastern Atlantic Ocean, carbonate dissolution can be related to wind-driven upwelling, which will be discussed further in the next chapter.

Chapter 5

Grain size of terrigenous sediments

Variations in the grain-size distributions of the terrigenous fraction of the Walvis Ridge sediments reflect the transport mechanisms that carried the terrigenous material there. These variations are closely linked to climate conditions on land. The grain-size distributions of the terrigenous (CaCO_3 , C_{org} and biogenic-opal free) fraction of the sediments from core MD962094 (Figure 1.1) were analysed and unmixed with an end-member modelling algorithm into three end members. These were interpreted as coarse-silt aeolian dust, fine-silt aeolian dust, and fine-silt to clayey hemipelagic mud. Assuming that the hemipelagic component eventually originates from fluvially transported material, the proportions of the end members can be interpreted in terms of changes in climate. The ratio of the two aeolian end members is a measure of the (Southeastern trade) wind strength. The ratio of the two aeolian and the hemipelagic end members is interpreted as a measure of continental aridity. The wind-strength record is compared to a published wind-induced upwelling record. These records strongly resemble each other. The observed variations in the continental-aridity and wind-strength records are ascribed to meridional changes in the position of oceanic- and atmospheric frontal zones, possibly related to changes in the volume of the Antarctic ice sheet.

Spatial distribution of terrigenous sediments

Chapter 7

Aeolian dust partly regulates the heat-transporting capacity of the atmosphere. In this chapter, Southern Hemisphere aeolian-dust records are compared to study the response of this hemisphere to changes in atmospheric circulation patterns. The Southern Hemisphere shows a continental aridity record that seems the opposite of published aridity records from the Northern Hemisphere; wet glacials versus dry interglacials. Comparison of two marine continental-aridity records from the Southern Hemisphere (Northern Chile and Southwestern Africa) with $\delta^{18}\text{O}$ -records and temperature records from Antarctica (Vostok ice core), results in a correlation that points to the Antarctic ice volume as the driving mechanism of the southern-hemisphere climate. The waxing and waning of the Antarctic ice sheet causes the various oceanic and atmospheric frontal zones to move equatorward and poleward, respectively. One of these frontal zones is the front of moisture bearing Southern Westerlies that causes increased precipitation in South America and Southwestern Africa North of 35°S during glacials.

Comparison of the bulk chemical and grain-size data from core MD962094 shows that although changes in these data are probably closely related to changes in climate, they may not always directly be interpreted as such. Variations in the Ca and Fe records from Walvis Ridge seem to correlate well to the flux of (iron-rich?) aeolian dust by the trade winds. However, this relationship is not causal, as it is the direct product of dissolution of calcium carbonate. The dissolution is caused by the trade-wind driven upwelling and is thus indirectly related to trade-wind intensity. Hence, the correlation of the Fe record and the wind-strength record is real but not as 'cause and effect'. The complex combination of supply of iron-coated aeolian dust on the one hand, and Fe enrichment of the sediments through carbonate dissolution on the other, excludes the possibility to relate bulk chemistry to continental climate in the Southeastern Atlantic Ocean. The combination of grain-size analyses of bulk and terrigenous sediments, unmixed into the various subpopulations, provides the necessary information about continental aridity and trade-wind strength in Southwestern Africa during the last 300 kyr BP.

2. Southeastern Atlantic deep-sea sediments

characterised by CORTEX

(Core scanner Texel, XRF)

Abstract

Seven cores along a transect from the continental slope offshore Walvis Bay to the distal part of Walvis Ridge (SE Atlantic Ocean) have been scanned with CORTEX (XRF) to study the major-element content and their potential use for palaeoclimate studies. CORTEX results of the carbonate-rich sediments ($\text{CaCO}_3 = 70\text{--}90\%$) are quantitative; calibration with chemical data measured with Inductively Coupled Plasma results in a correlation coefficient of $r^2 = 0.85$. On the basis of the calcium and iron records, the cores can be correlated very well. The bulk chemical data show that sedimentation on Walvis Ridge is uniform over a large area and therefore, sediments from core MD962094 can be used to study late Quaternary sedimentation changes in the southeastern Atlantic Ocean.

Introduction

The physical properties of (deep-) marine sediments in sediment cores can be studied in two ways: either by scanning the unopened or split core, or by analysing samples retrieved from the sediment core. The advantages of core scanners are numerous; they are relatively quick, are able to scan at high resolutions and leave the sediment intact. The most widely used core-scanner techniques are Colour Reflectance Spectroscopy (Mix et al., 1992; Balsam et al., 1995), Magnetic Susceptibility (An et al., 1991; Frederichs et al., 1999), Gamma Ray Transmissivity (Weber et al., 1997) and P-wave velocity (Vidal et al., 1998; Best & Gunn, 1999; Weber & Pisias, 1999). Since the scans can be carried out onboard the ship that collects the cores, they can be used as a first correlation tool for sediments from the same region (Mix et al., 1992; Frederichs et al., 1999). A new core-scanning device was built at the Netherlands Institute for Sea Research with which quantitative XRF measurements can be carried out on split core sections (Jansen et al., 1998). With this core scanner (CORTEX) a suite of major elements can be measured at any resolution down to 1 mm. The CORTEX makes use of the process of X-Ray emission. Incident X-rays eject an electron from an inner shell of an atom. The energy that is emitted when the resulting vacancy is filled by an electron from an outer shell is characteristic for that particular atom and can be recorded (for a detailed description of the machine see Jansen et al., 1998). Since specific amounts of energy have to be applied for each suite of major elements, only limited numbers of elements can be measured at a time (Jenkins, 1976). CORTEX data have been widely used for the study of deep-marine sediments and have often been interpreted in terms of palaeoclimate (Arz et al., 1998; Arz et al., 1999; Lamy et al., 2001; Richter et al., 2001). Since bulk chemistry data alone are very difficult to interpret in terms of palaeoclimate change, we use the CORTEX data for correlation of the seven cores from the SE Atlantic only.

Our objectives are: (1) to characterise the sediments from the SE Atlantic Ocean through quantification of their bulk chemistry and by comparing XRF (CORTEX) data with ICP analyses of discrete samples. (2) to examine if sedimentation is sufficiently uniform throughout the Cape Basin and Walvis Ridge to use data of one core for inferences on regional change in palaeoclimate.

Material and methods

Seven cores from a NE-SW transect on Walvis Ridge (see Figure 2.1 and Table 2.1) were scanned with CORTEX at intervals of 0.5 – 5 cm, a time resolution of ~300 – 500 years. In the set-up used, 6 major elements were measured; K, Ca, Ti, Mn, Fe and Sr. Major elements of core GeoB 1028-5 were also analysed using an Inductively Coupled Plasma emission spectrometer.

To study the condition of the iron more specifically, microscope studies were carried out on selected samples from cores MD962094 (Walvis Ridge) and MD962097 (continental slope offshore Walvis Bay, Figure 2.1). The calcium carbonate, C_{org} and biogenic-opal free fractions of three samples from core MD962094 were studied using a light microscope (for a detailed description of the applied chemical treatments, see Stuut et al., 2001, Chapter 5). Four selected intervals from core MD962097 were

studied using a scanning electron microscope (SEM) and an energy-dispersive X-ray analysis (EDAX) system. Samples of 6*2*1 cm taken from this core were sealed in epoxy glue and ground to 2 mm thickness. The hardened samples were polished and prepared for SEM analysis using a carbon coating. SEM images were made by Saskia Kars at the Faculty of Earth Sciences, Vrije Universiteit Amsterdam on a JEOL JSM 6400 Scanning Electron Microscope using a 500* magnification.

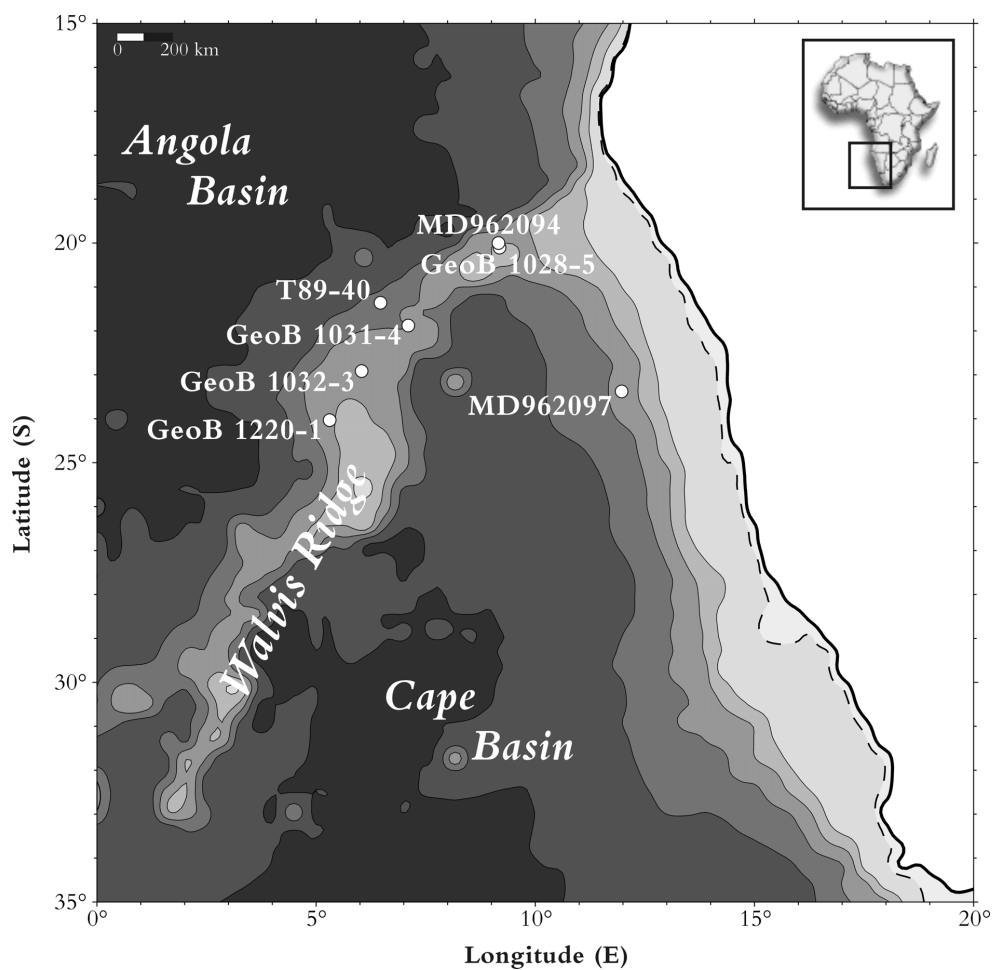


Figure 2.1. Study Area. Position of the studied cores in the SE Atlantic Ocean. Bathymetry is shown in contour intervals of 1000 m, the 125-m isobath is presented as a dotted line.

Table 2.1: Position, water depth, core length and resolution of scanned cores

Core	Longitude	Latitude	Water depth	Core Length	Sampled interval
MD962097	11.97 E	23.38 S	2,662 m	31.68 m	5 cm
MD962094	9.16 E	20.00 S	2,281 m	30.68 m	2 cm
GeoB 1028-5	9.11 E	20.06 S	2,209 m	10.79 m	1 cm
T 89-40	6.47 E	21.36 S	3,073 m	16.24 m	1 cm
GeoB 1031-4	7.06 E	21.53 S	3,105 m	10.78 m	1 cm
GeoB 1032-3	6.02 E	22.55 S	2,505 m	5.24 m	0.5 cm
GeoB 1220-1	5.18 E	24.02 S	2,266 m	4.65 m	0.5 cm

Age models

Core MD962094 was sampled at 5-cm intervals with 10 ml syringes. These samples were used for stable oxygen-isotope analysis. Eight to ten well-preserved and clean specimens of the planktonic foraminifer *Globorotalia inflata* d'Orbigny were hand-picked under a binocular microscope from the 250–500 μm fraction to achieve an analytical weight of 0.05 to 0.10 mg. The stable oxygen-isotope composition of *G. inflata* were measured with a Finnigan MAT 252 mass spectrometer at the Fachbereich Geowissenschaften in Bremen. The oxygen-isotope record of *G. inflata* was correlated with the stacked record of Martinson et al. (1987) to obtain an age model for core MD962094 (Figures 2.2B and C). Correlation of the oxygen-isotope records was established using the software package Analyseries version 1.1 (Paillard et al., 1996). Twenty-two marine isotope events (MIE) were taken as calibration points for the age model. For further chronostratigraphic control, radiocarbon ages were measured on planktonic foraminifera from five selected samples (Table 2.2 and Figure 2.2). At least 400 well-preserved and clean specimens of the planktonic foraminifer *Globogerinoides ruber* were hand-picked under a binocular microscope from the 250–500 μm fraction to achieve an analytical weight of at least 800 μg per sample. AMS- ^{14}C dates were determined at the R.J. van de Graaff laboratory (Utrecht University, The Netherlands). The ages were corrected for a reservoir age of 400 yr as the mean value for the South Atlantic Ocean at 20°S latitude (Bard, 1988). The ^{14}C ages were converted to calendar years with the Calib 4 software (Stuiver & Reimer, 1993). The final age model resulted from linear interpolation between the age-calibration points. The upper 14.7 m of the sediment record in core MD962094 appear to span the last ~300 kyr, i.e. marine isotope stages (MIS) 1 to 8. MIE 7.5 does not appear as a full interglacial substage with associated low $\delta^{18}\text{O}$ values relative to the SPECMAP (Martinson et al., 1987) curve. This phenomenon is typical for the area (Schneider et al., 1996).

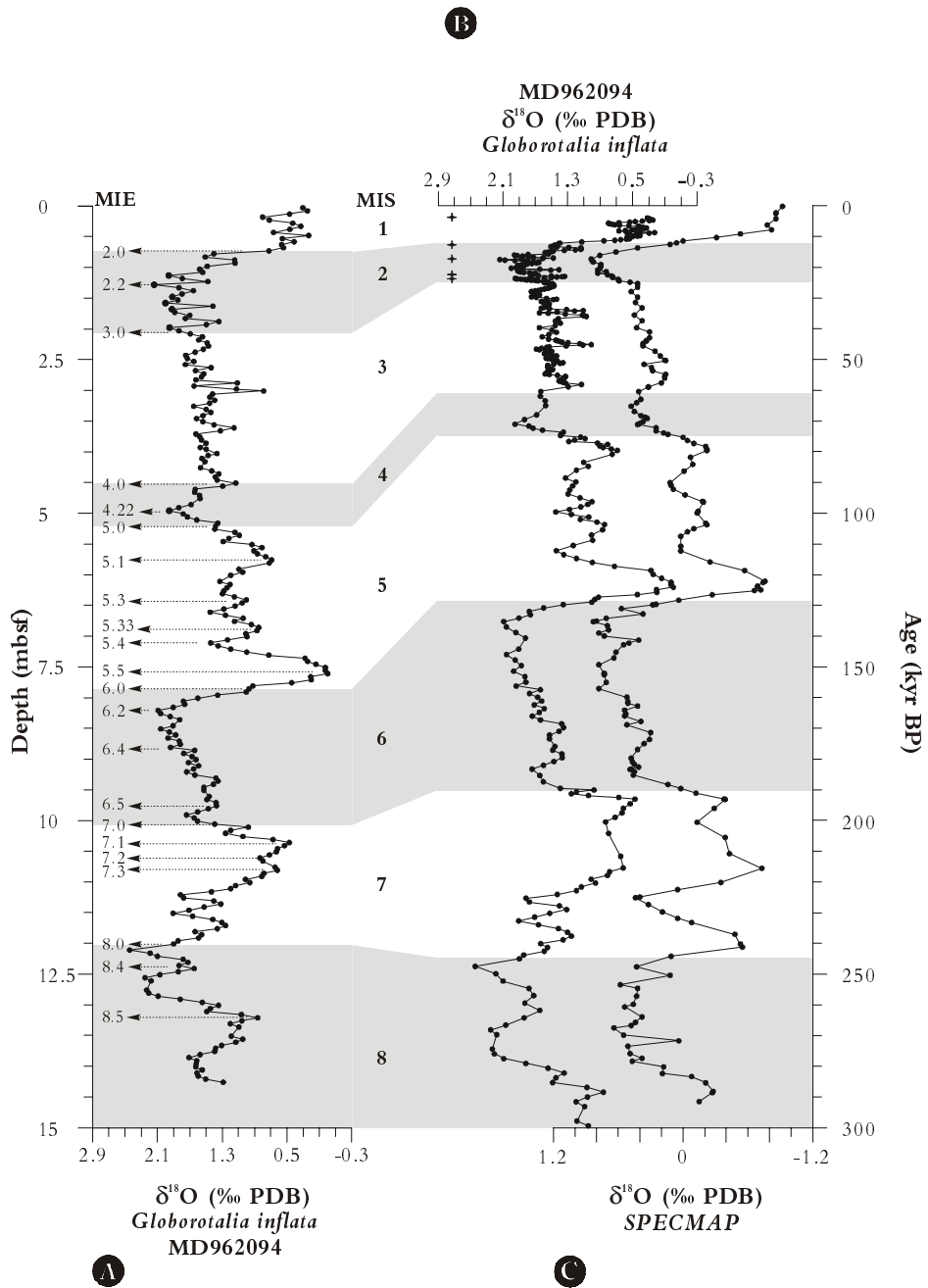


Figure 2.2. Age model of core MD962094. **A**) *Globorotalia inflata* $\delta^{18}\text{O}$ -record versus depth. Marine Isotopic Events (MIE) and Marine Isotopic Stages (MIS) after Martinson et al. (1987) are indicated.. **B**) *Globorotalia inflata* $\delta^{18}\text{O}$ -record versus age. AMS- ^{14}C dates are indicated (+) **C**) SPECMAP $\delta^{18}\text{O}$ -record after Martinson et al. (1987). Glacial stages are shaded.

Table 2.2: ^{14}C AMS Results from core MD962094

Depth (cmbsf)	Age (^{14}C yr)	Error	Age (cal. yr)	Error
3	4130	50	4175 ^a	75
83	11940	80	13310 ^a	130
128	15150	90	17540 ^a	270
188	19870	120	22990 ^a	400
198	21690	150	25000 ^c	400

^aAges converted to calendar years using Calib 4.1 (Stuiver & Reimer, 1993).

^bAge extrapolated from conversion in Stuiver & Reimer (1993)

The Fe record of core MD962097 was correlated to the one of core MD962094 using the software package Analyseries (Paillard et al., 1996). In this way an age model for the last 300 kyr (the upper 17.9 m) of core MD962097 was established (Figure 2.3).

Stable-oxygen isotope based age models of the other five cores were taken from Schmidt, (1992, four GeoB cores), and Ufkes et al., (2000, core T89-40). The downcore $\delta^{18}\text{O}$ records of the six cores plotted versus age for the last 300 kyrs are shown in Figure 2.4.

Results

CORTEX data of the element iron (Fe) from the transect of seven cores are plotted for the last 300 kyr (Figure 2.5). The sedimentation rates gradually decrease from East to West along the ridge. Along with the decreasing sedimentation rates, the Fe contents decrease from core MD962097 (~1925 c/s) to core GeoB 1220-1 (~195 c/s). All cores show the same pattern: low Fe contents during interglacial stages compared to high contents in glacial stages. From microscope analyses it appears that the terrigenous fraction of the samples from core MD962094 consists primarily of quartz and feldspar grains with an orange coating, which could be iron oxy-hydroxides. The selected samples from core MD962097 however, clearly show that all the mineral iron is concentrated in pyrite crystals (Figure 2.6).

The CORTEX data were compared for the element Ca, with CaCO_3 measurements on discrete samples (Schmidt, 1992, Figures 2.7A & B). A high correlation coefficient is observed ($r^2=0.76$, Figure 2.7G). The CORTEX data from core GeoB 1028-5 were also compared with ICP data (Fe and Ti) measured on discrete samples from the same core. Despite some differences in downcore resolution, the similarity of the records is clear. The Fe-data measured with the two different methods show a high correlation coefficient ($r^2=0.85$, Figure 2.7H). The correlation coefficient for the Ti-data is considerably lower ($r^2=0.38$, Figure 2.7I) owing to the low radiation yield of this element.

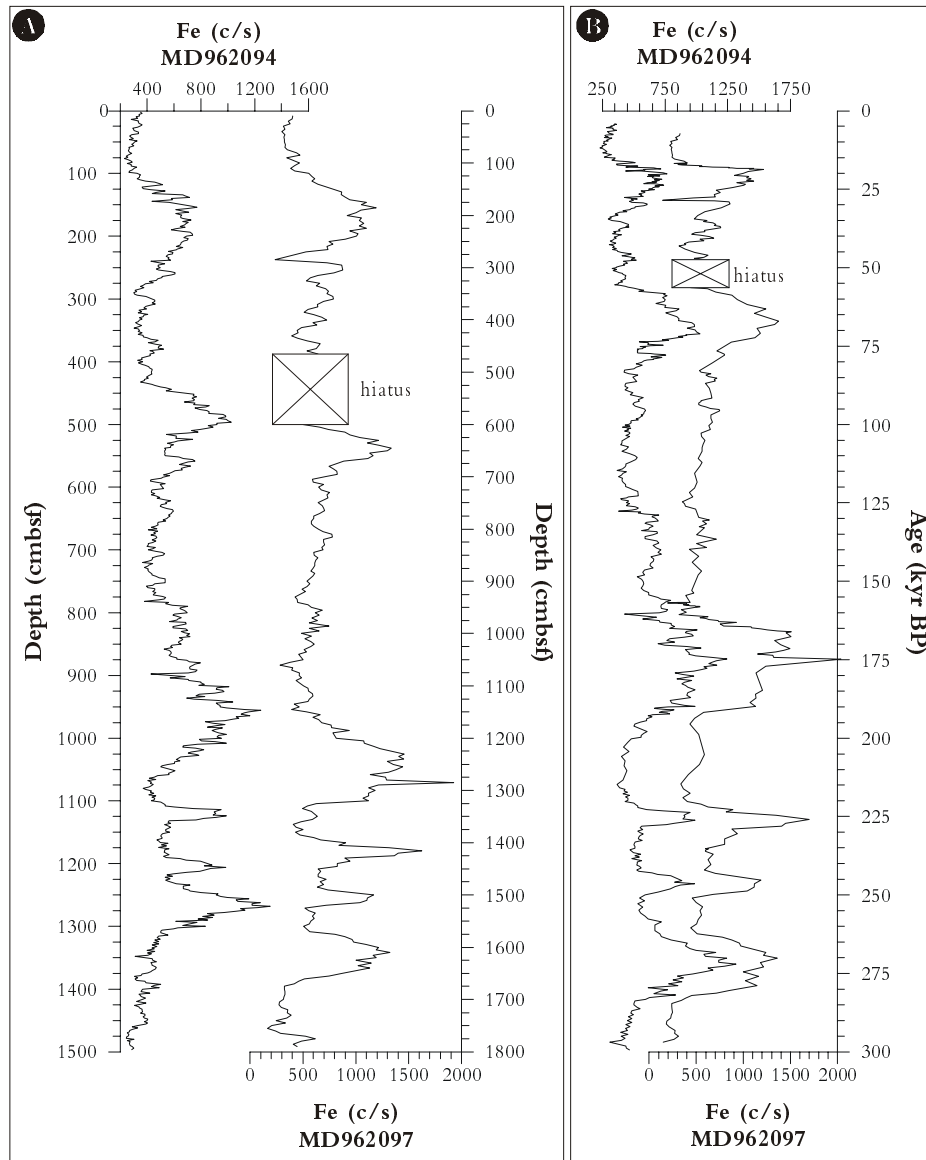
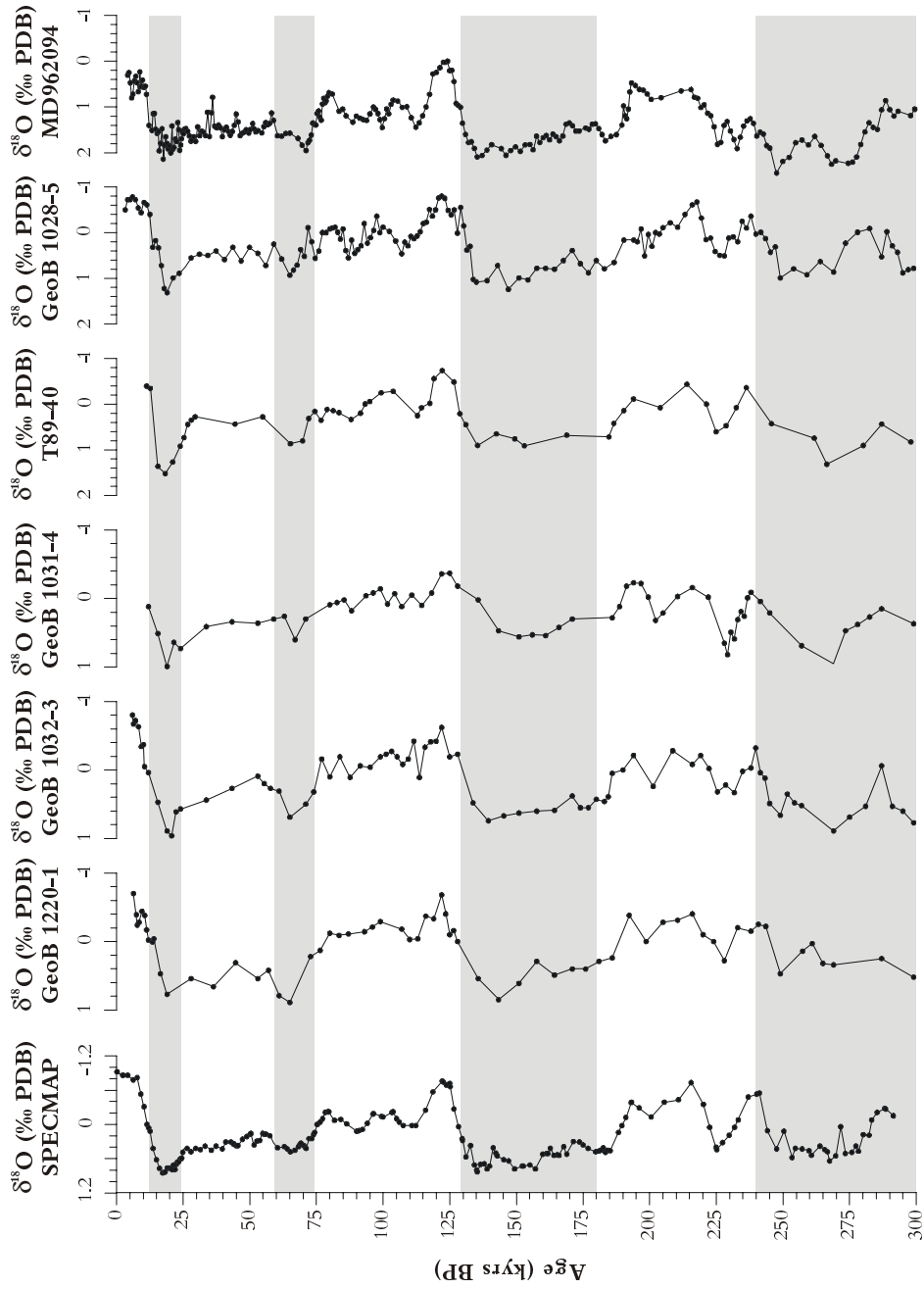


Figure 2.3. Correlation of core MD962097 with MD962094 for the last 300 kyr.
A) Fe records versus depth. **B)** Fe records versus age.



Discussion

The seven sediment cores from the continental slope offshore Walvis Bay and along Walvis Ridge can be correlated very well using their CORTEX Ca and Fe records. This indicates that sedimentation in the area is persistent and sediments from core MD962094 are representative for those in the southeastern Atlantic Ocean. Detailed study of the mineral iron in the sediments from core MD962094 (Walvis Ridge) and MD962097 (continental slope offshore Walvis Bay) shows that the iron in the distal core is present as a coating of iron-oxyhydroxides around single particles, whereas closer to the coast, the iron is present in pyrite crystals (Figure 2.6). We ascribe this to the location of the Benguela upwelling below which core MD962097 is located. Due to the presence of the upwelling cells, the sediments in this core contain relatively large amounts of organic carbon, promoting the formation of FeS_2 through reducing conditions in and near the sea bottom. In contrast, the sediments of the cores on Walvis Ridge, just outside the reach of the upwelling cells, consist predominantly of calcium carbonate and contain $< 1\%$ organic carbon. The iron that is present in the sediments from the southeastern Atlantic most probably originates from the Namib Desert. It is transported to the ocean by fluvial transport and by the southeastern Trades. The decrease in the amount of iron down the Walvis Ridge is explained by the increasing distance to the source of the iron, which most probably is the Southwestern African continent. However, the high amounts of calcium carbonate in the sediments obscures interpretation of the Fe and Ti records in terms of palaeoclimate. The fact that the records of the three elements show the same downcore pattern (Figure 2.7) is probably related to variations in the Ca-curve. The good correlation of the cores show that the reduction of the iron oxyhydroxides to pyrite occurs relatively quick and does not lead to migration of the iron through the sediments.

(Previous page) Figure 2.4. Oxygen-isotope based age models. Martinson (Martinson et al., 1987) $\delta^{18}\text{O}$ record compared with $\delta^{18}\text{O}$ record of *Globorotalia inflata* (MD962094) and of *Globigerinoides ruber* (w) (GeoB-cores and T89-40) records versus age (kyr BP). Glacial stages are shaded. Age models of the four GeoB cores from Schmidt (1992), age model of core T89-40 from Ufkes et al. (2000).

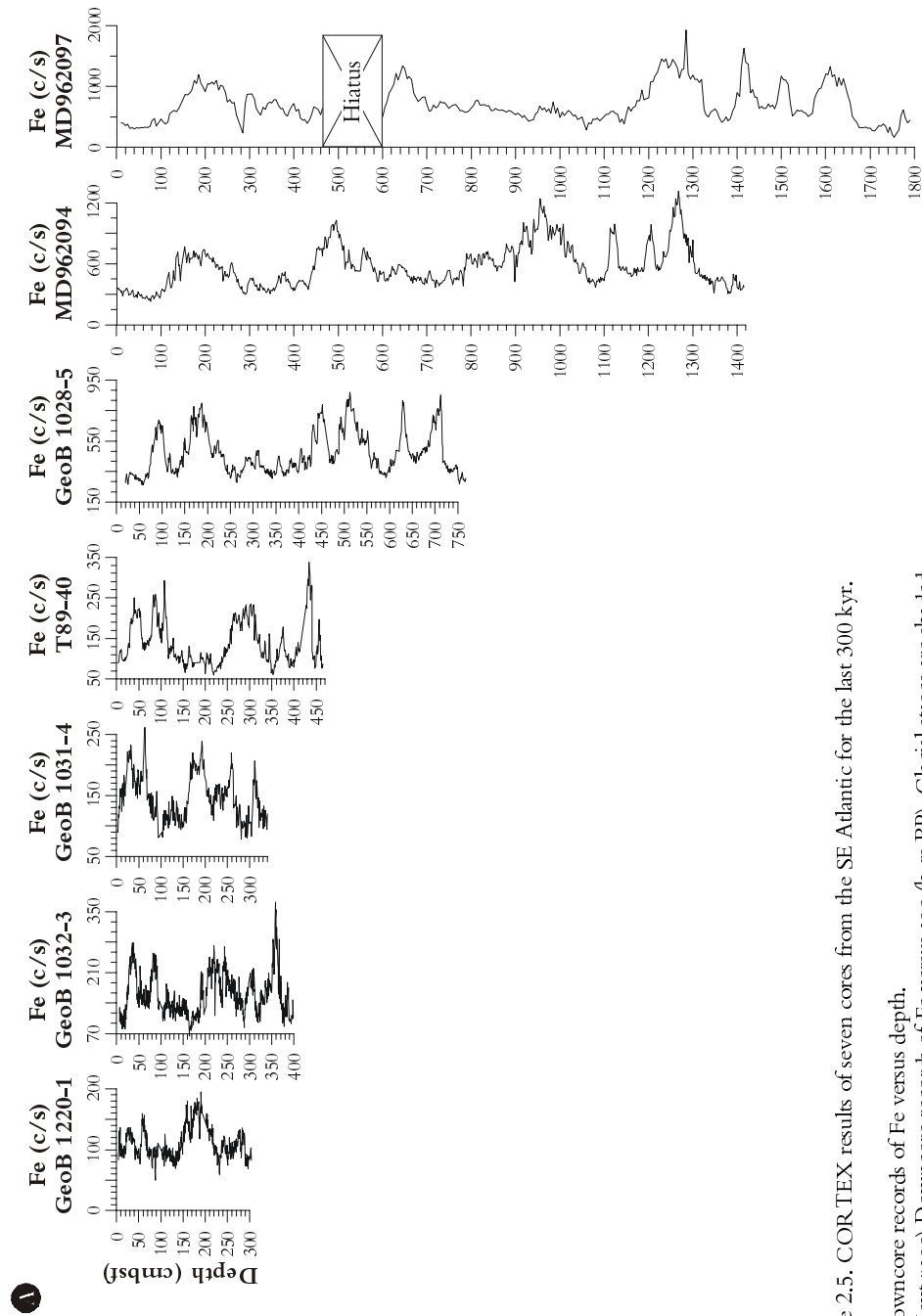
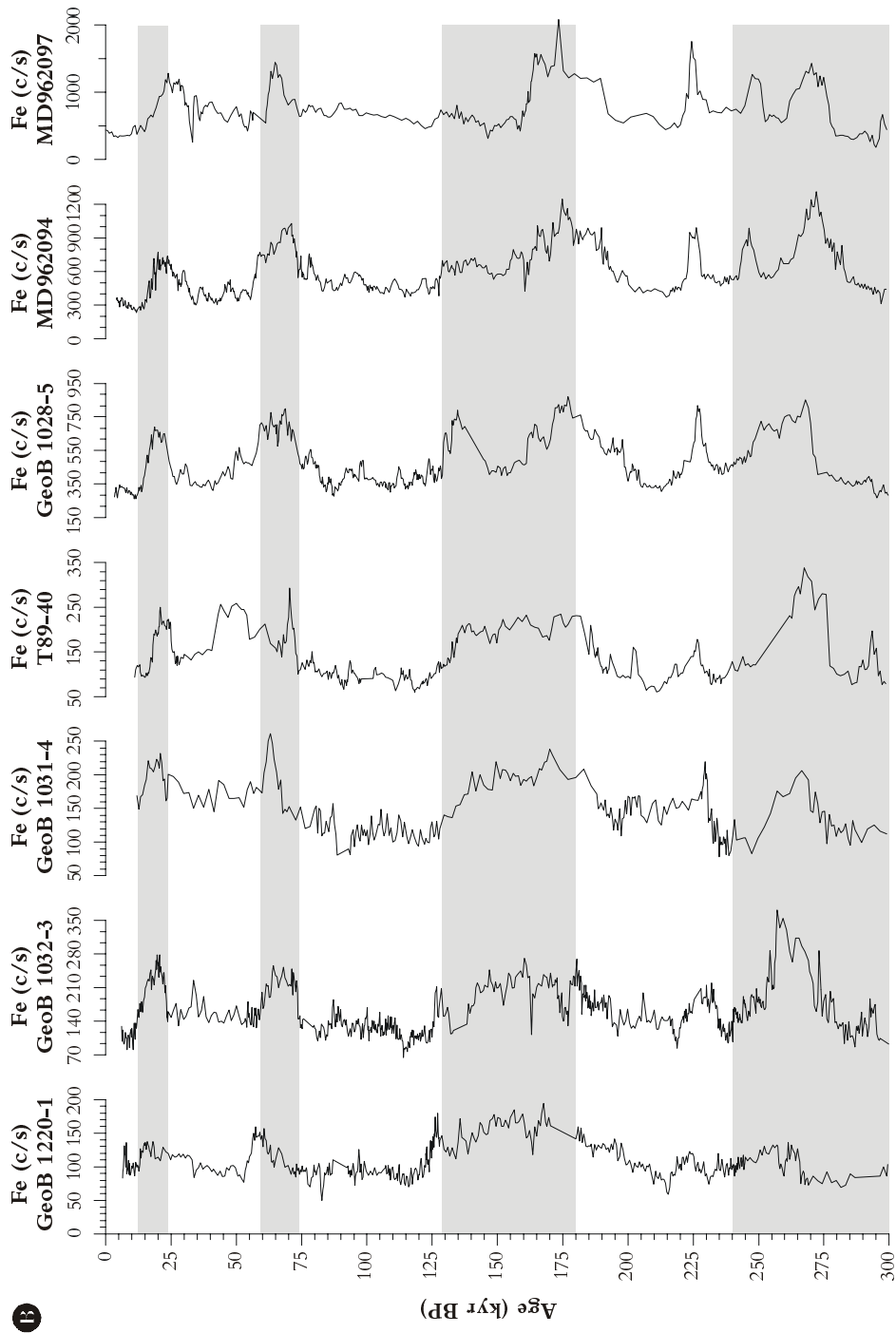


Figure 2.5. CORTEX results of seven cores from the SE Atlantic for the last 300 kyr.

A) Downcore records of Fe versus depth.

B) (Next page) Downcore records of Fe versus age (kyrs BP). Glacial stages are shaded.



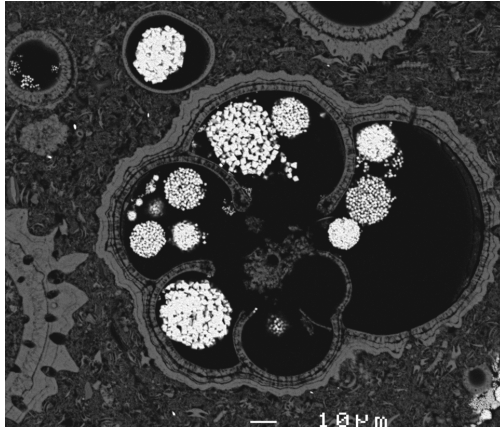


Figure 2.6. Scanning Electron Microscope image of a sample from core MD962097, 1362-1368 cm core depth. Scale bar indicates 10 μm (500 \times magnification). Image created by S. Kars.

The good correlation between the CORTEX and ICP results for the element iron (Figure 2.7) demonstrates that CORTEX produces quantitative data for iron. The low correlation coefficient ($r^2=0.38$) for the element titanium is caused by the low radiation yield of this element; count rates do not exceed 44 counts per second (Figures 2.7 F and I). The yields of the elements Ca and K are somewhat less reliable owing to the similarity of their energy levels (Jenkins, 1976) and also because of the so-called sand-paper effect: the presence of so many calcareous shells results in a relatively rough surface, which decreases the accuracy of the measurements (Jansen et al., 1998). This problem occurs when sediments contain over 70% of calcium carbonate. It can be resolved by expressing the signal of the elements as a ratio of the total suite of elements measured (Jansen et al., 1998). After this conversion, the calcium record is reliable, as shown by the high correlation coefficient with measurements of calcium carbonates (Figure 2.7). From the correlation of the Ca (c/s) with the CaCO_3 data, the Ca-data can be translated into CaCO_3 data. Thus, the calcium carbonate content of the sediments from core MD962094 vary from 70 to 90%.

In the case of the Walvis Ridge sediments, the CORTEX data provide a good tool for the correlation of the different cores, owing to the fact that sedimentation is continuous throughout the area.

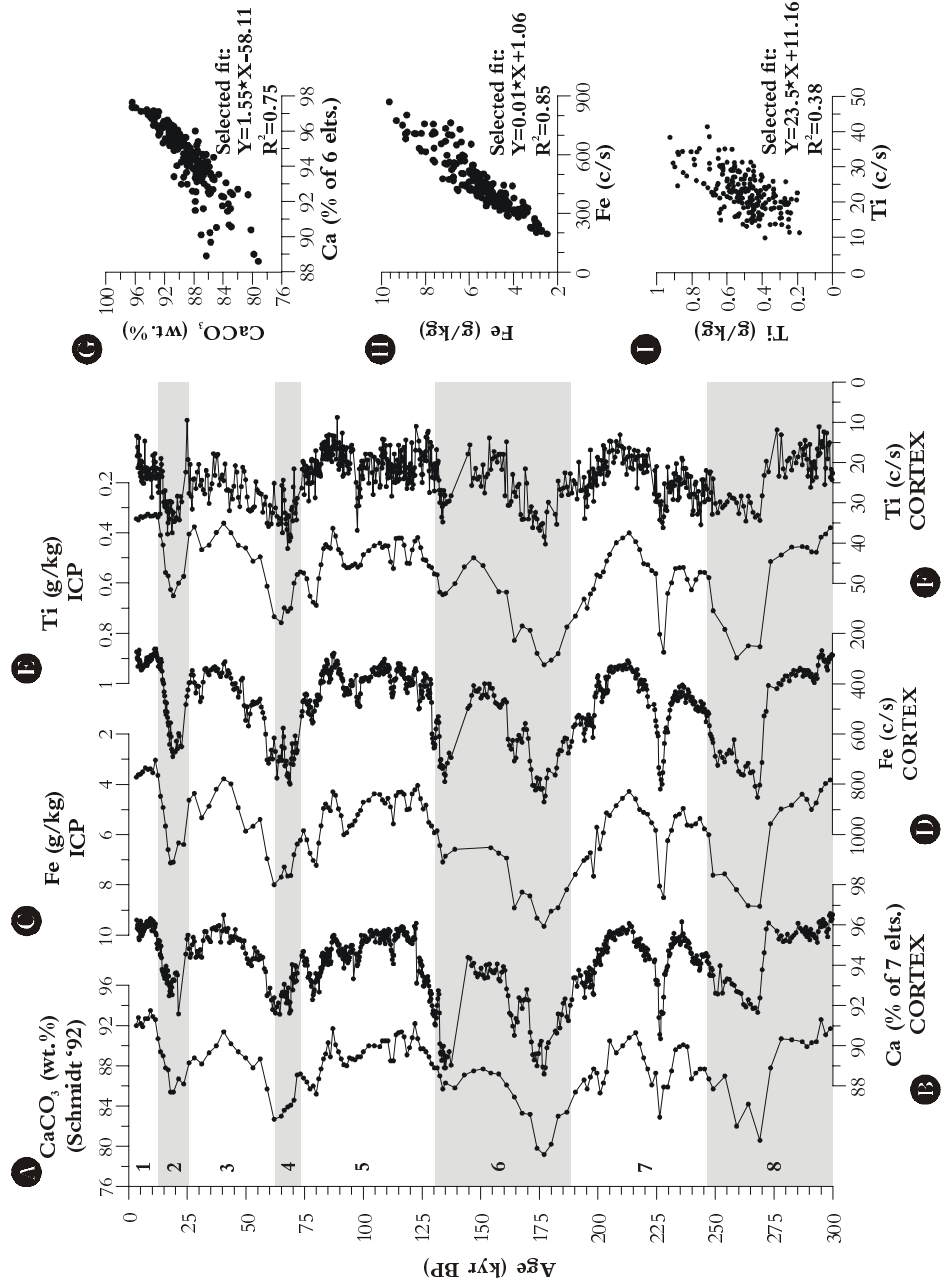


Figure 2.7. Fe and Ca records in core GeoB 1028-5. Glacial stages are shaded. **A)** CaCO_3 (wt.%) (Schmidt '92) **B)** Ca normalised against 6 elements (Ca, K, Sr, Mn, Fe, Ti) **C)** Fe (g/kg) from ICP **D)** Fe (c/s) from CORTEX. **E)** Ti (g/kg) from ICP. **F)** Ti (c/s) from CORTEX. **G)** Linear regression plots of the Ca and CaCO_3 data. **H)** Linear regression plots of the Fe data. **I)** Linear regression plots of the Ti data.

Conclusions

- CORTEX provides quantitative chemical data that provide a good tool for correlating sediment cores from the same area on the basis of the elements calcium, iron and titanium.
- From the good correlation between the iron records of the transect of cores from the continental slope offshore Walvis Bay to the distal part of Walvis Ridge we conclude that sedimentation is consistent over this part of the SE Atlantic.
- Sediments from core MD962094 are representative for sediments in the SE Atlantic Ocean and hence, are suitable for inferences on regional palaeoclimate.
- The downcore bulk chemical variations observed in the CORTEX data are probably caused by variations in the downcore record of Ca owing to the high amounts (70-90%) of calcium carbonate. Therefore, care has to be taken in interpreting the downcore Fe and Ti records.

Acknowledgements

The Images II and N.O. Marion Dufresne staff are acknowledged for retrieving core MD962094 and MD962097, Ralph Schneider is thanked for providing the $\delta^{18}\text{O}$ data of the four GeoB-cores, and Els Ufkes for providing $\delta^{18}\text{O}$ data of core T89-40. Furthermore we are indebted to Monica Segl and Birgit Meyer-Schack (Universität Bremen) for carrying out the oxygen-isotope measurements of core MD962094. Saskia Kars (VU Amsterdam) is thanked for assistance with the SEM photographs. Kaj Beets (VU Amsterdam) is thanked for valuable discussion and help with the Fe analyses. Susanne Lassen (NIOZ) and Klaas van de Borg (Utrecht University) are acknowledged for support with the picking of the foraminifera and for carrying out the AMS- ^{14}C datings, respectively.

3. Precision, accuracy and resolution of the laser particle sizer *Malvern Mastersizer S*, and unmixing of artificial sediment mixtures.

Abstract

The qualities of a laser-diffraction particle sizer, the Malvern Instruments Mastersizer S, are evaluated using glass-bead standards. Precision (reproducibility), accuracy (approximation of the 'real' size) and resolution (recognition of subpopulations) of measurements of discrete glass-bead standards and of mixtures of glass beads are tested. Optical imagery of the glass beads is used to test the accuracy of the Malvern Mastersizer-S. Binary mixtures were prepared by mixing series of glass beads of known optical and physical characteristics. Measurements of these mixtures allow evaluation of the ability of the laser particle sizer to 'discern' subpopulations within sediment mixtures. Precision of the measurements is very high for both the single glass bead standards and the mixtures.

The mixing experiments show that the Malvern Mastersizer-S is able to distinguish sediment subpopulations from the grain-size distributions. Approximation of the measured grain-size distributions by the 'best-fit' grain-size distribution of the mixed standards provides the apparent mixing proportions of the sediment standards as seen by the Malvern Mastersizer-S. Owing to the relatively poor resolution of the Malvern Mastersizer-S for mixtures where the proportions of the standards are <5 wt.%, variations in the relative proportions of the subpopulations < 5% appear not to be significant. To unravel the composite mixtures of standards into their original subpopulations, an end-member algorithm was applied to the data set of the binary mixtures. A three-end member model appears to provide the best balance between the smallest number of end members and best possible fit of the data set. The three end members that result from the model resemble the grain-size distributions of the initial glass-bead standards almost perfectly. The combination of the grain-size analyses and the application of the end-member algorithm proves to be a powerful tool for the unmixing of grain-size populations from large data sets of grain-size distributions.

Introduction

The grain-size distribution of natural sediments is a property often used to characterise natural sediments in terms of sedimentary environment and/or transport mechanism of sediments (Koopmann, 1981; Lamy et al., 1998; Prins and Weltje, 1999; Stuut et al., 2001). However, there is still a lot of debate on how to determine the grain size of natural sediments. Different techniques have been developed, applied and compared (see for an overview Syvitski, 1991). Next to sieve analysis there are in general four automated techniques: Image analysis, SediGraph, Electroresistance particle sizers, and Laser particle sizers. The different techniques all have their advantages and pitfalls. Image analysis clearly analyses particles in the most objective way, although it always considers the two longest axes of the particles. It is specifically suitable for small samples and for selected analysis of specific components within a sample (Kennedy and Mazzullo, 1991). Image analysis is very accurate and precise but also very time consuming and therefore not specifically useful for the analysis of large sets of samples. The SediGraph considers the hydrodynamic properties of the particles. With this technique, the settling velocity of the particles determines the grain-size distribution. This is probably the most 'natural' way to study the size of sediments since it resembles the 'real-life' depositional environment closest. However, settling velocities are not only influenced by the size of the particles, both the shape and the density of the particles play a major role as well (Coakley and Syvitski, 1991; Syvitski et al., 1991; Beuselinck et al., 1998). Therefore, it is difficult to compare SediGraph results to other size-analysis techniques that do not take into account the density of the particles. Besides, with the SediGraph only a small fraction of the size distribution of sediments ($< 63 \mu\text{m}$) can be considered, which strongly limits its applicability to natural sediments. Electroresistance particle sizers measure the actual volume of each individual particle. All particles are suspended in an electrolytic suspension and drawn through a small aperture of known diameter (Milligan and Kranck, 1991). The great advantage of this technique is that the volume of each individual particle is analysed independent of shape or density. The great disadvantage however, is that the size interval of particles that can be measured at a time is dependent on the aperture width. Therefore, the sample has to be fractionated in a number of size fractions that increases with decreasing sorting of the sample. This takes a lot of time and introduces errors. Besides, the electric properties of the sediments, especially of clay particles, may influence the outcome of the measurements strongly. Laser particle sizers are applied more and more for the analysis of large sample sets since they are precise and accurate (Prins, 1999) and measurements can be carried out in relatively short time (< 5 minutes). The new generation of laser particle sizers is able to measure large size intervals in one analysis and hence, the problems arising with the use of different lenses (McCave et al., 1986; Agrawal et al., 1991) do not exist anymore. The lasers' underestimation of the clay fraction in natural sediments appeared to be caused by the fact that the shape of the particles plays a major role in the hydrodynamic properties of the particles. The definition of clay particles is still based on measurements obtained with settling tubes, which assumes spherical particles. However, Konert and Vandenberghe (1997) showed that platy particles of $8 \mu\text{m}$ (v.f. silt) have the same hydrodynamic properties as spherical particles of $2 \mu\text{m}$ (clay), and therefore, the grain-size distribution produced by the laser particle sizer is correct.

To interpret the grain-size data most users express the distribution into a statistical value like the median grain size (Koopmann, 1981; Rea, 1994; Zinck and Sayago, 2001). Prins and Weltje (1999) showed that a large data set of grain-size data measured on deep-sea sediments from a number of core sites in the Indian Ocean can be expressed as the product of a small number of end members. The end-member modelling approach is a new way to look at the data. It assumes that all sediments are the result of linear mixing of a number of subpopulations in various proportions. It tries to explain the variance in the total data set without any 'a priori' knowledge of the number of subpopulations or their composition. The number of end members is chosen by looking at the goodness of fit, a measure of how well the variance in the data set can be explained. This approach has been successfully applied to grain-size distributions of deep-sea sediments (Prins and Weltje, 1999; Prins et al., 2000a; Prins et al., 2000b; Stuut et al., 2001) and to biological data (Van Dam and Weltje, 1999).

Prins and Stuut (Prins, 1999, chapter 2) evaluated the quality of the laser particle sizer Malvern Instruments M 2600 by mixing certified polystyrene standards and natural sediments in known weight proportions. The results were then unmixed using the end-member modelling approach by Prins and Weltje (Prins, 1999, chapter 3). The results appeared to be strongly influenced by variations in the shape and density and probably also the optical characteristics of the natural sediments. In this chapter therefore, we use glass beads sieved into narrow size fractions to evaluate the quality of the laser particle sizer Malvern Instruments Mastersizer S. The glass-bead standards are used to test the precision (reproducibility), accuracy (approximation of the 'real' size), and resolution (recognition of subpopulations) of the Mastersizer S. Glass beads are ideal for mixing experiments since 1) the optical properties (absorption coefficient, refraction index) are known, 2) the density is constant so that weight percentages can be translated to volume percentages, 3) the particles are almost perfect spheres (see Fig 1) so variations related to differences in particle shape can be excluded. Finally, an end-member algorithm (Weltje, 1997) is applied to unmix the size distributions that gives the impression to consist of single modes (Figure 3.1), to see if the glass-bead standards used to create the mixtures can be reconstructed from the data set.

Material and Method

Glass beads normally used for sand blasting were fractionated into narrow size fractions using sieves with mesh sizes of 30 μm and 53 μm . Four standards were constructed that are close to the size fractions of terrigenous sediments recovered from Walvis Ridge (Chapter 5). The first two standards were made by splitting the original glass-bead sample of 20–90 μm into A1 (<53 μm) and A2 (53–90 μm). Then, A1 was split up in A1x (<30 μm) and A1y (30–53 μm). For each standard the amount (dry weight) was determined at which an obscuration of the laser of $20 \pm 1\%$ was established. Thus, variations related to changing sample density during measurement were excluded. All analyses were carried out on a Malvern Instruments Mastersizer S, available at the Sedimentology Division of the Faculty of Earth Sciences, Utrecht University. The analyses were performed with a lens with 300 mm focal length resulting in 64 size classes ranging from 0.05–878 μm (Table 3.1). For each analysis the entire dry weighed sample was introduced in the sample cell of the Mastersizer S using demineralised water. Total dispersion of the sample in the sample cell was ensured using a sonic dismembrator attached to the tank containing the suspended sample.

Table 3.1: Size range of Malvern Mastersizer S

Size class	Lower boundary (μm)	Upper boundary (μm)	Size class	Lower boundary (μm)	Upper boundary (μm)
1	0.05	0.06	33	6.63	7.72
2	0.06	0.07	34	7.72	9.00
3	0.07	0.08	35	9.00	10.48
4	0.08	0.09	36	10.48	12.21
5	0.09	0.11	37	12.21	14.22
6	0.11	0.13	38	14.22	16.57
7	0.13	0.15	39	16.57	19.31
8	0.15	0.17	40	19.31	22.49
9	0.17	0.20	41	22.49	26.20
10	0.20	0.23	42	26.20	30.53
11	0.23	0.27	43	30.53	35.56
12	0.27	0.31	44	35.56	41.43
13	0.31	0.36	45	41.43	48.27
14	0.36	0.42	46	48.27	56.23
15	0.42	0.49	47	56.23	65.51
16	0.49	0.58	48	65.51	76.32
17	0.58	0.67	49	76.32	88.91
18	0.67	0.78	50	88.91	103.58
19	0.78	0.91	51	103.58	120.67
20	0.91	1.06	52	120.67	140.58
21	1.06	1.24	53	140.58	163.77
22	1.24	1.44	54	163.77	190.80
23	1.44	1.68	55	190.80	222.28
24	1.68	1.95	56	222.28	258.95
25	1.95	2.28	57	258.95	301.68
26	2.28	2.65	58	301.68	351.46
27	2.65	3.09	59	351.46	409.45
28	3.09	3.60	60	409.45	477.01
29	3.60	4.19	61	477.01	555.71
30	4.19	4.88	62	555.71	647.41
31	4.88	5.69	63	647.41	754.23
32	5.69	6.63	64	754.23	878.67

Repeated measurements (N=10) were carried out for each of the standards (Figure 3.1 and Table 3.2).

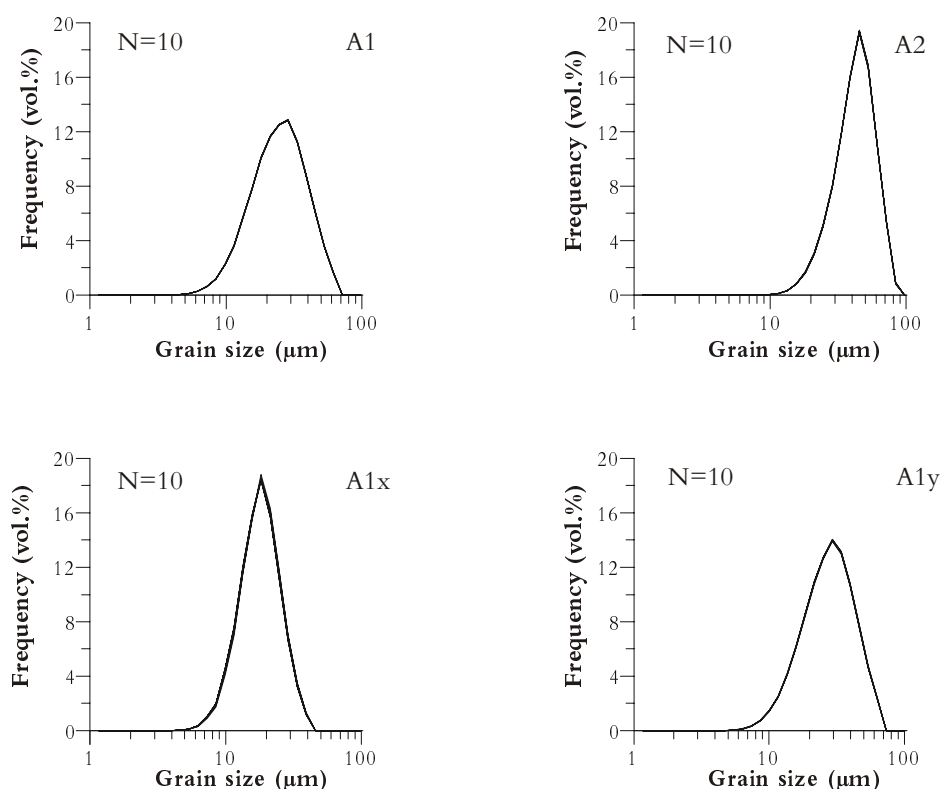


Figure 3.1. Multiple analysis: Precision of the Mastersizer. Grain-size distributions of multiple analyses (n=10) of all four standards are plotted. Data are listed in tables 3.2 and 3.3.

SEM images (n=111) were made by Saskia Kars at the Faculty of Earth Sciences, Vrije Universiteit Amsterdam on a JEOL JSM 6400 Scanning Electron Microscope using a 300[×] magnification. At least 12 photos of each standard were analysed with the software package AnalySIS v3.0 (Soft Imaging System GmbH, 1999) to ensure a minimum of 800 particles per standard. According to Kennedy and Mazzullo (1991) this should be sufficient to describe well-sorted samples.

The AnalySIS data consist of the lengths of the intermediate and longest axes measured for each particle. These data were used to calculate the mean diameter and the volume of the particles to be able to calculate the analySIS-volume distribution, distributed over the 64 size classes used in the software of the Mastersizer S (Figure 3.2, Table 3.3).

Table 3.2: Grain-size distributions of glass-bead standards

Size class	A1	A2	A1x	A1y	Size class	A1	A2	A1x	A1y
1	0.00	0.00	0.00	0.00	33	0.63	0.00	1.00	0.33
2	0.00	0.00	0.00	0.00	34	1.19	0.00	1.91	0.73
3	0.00	0.00	0.00	0.00	35	2.26	0.03	4.45	1.43
4	0.00	0.00	0.00	0.00	36	3.62	0.11	7.39	2.50
5	0.00	0.00	0.00	0.00	37	5.68	0.31	11.82	4.15
6	0.00	0.00	0.00	0.00	38	7.82	0.80	15.72	6.17
7	0.00	0.00	0.00	0.00	39	10.06	1.67	18.51	8.60
8	0.00	0.00	0.00	0.00	40	11.66	3.05	15.89	10.89
9	0.00	0.00	0.00	0.00	41	12.51	5.08	11.40	12.66
10	0.00	0.00	0.00	0.00	42	12.85	7.99	6.83	13.99
11	0.00	0.00	0.00	0.00	43	11.24	11.80	3.34	13.07
12	0.00	0.00	0.00	0.00	44	8.79	15.97	1.25	10.74
13	0.00	0.00	0.00	0.00	45	6.03	19.33	0.00	7.62
14	0.00	0.00	0.00	0.00	46	3.58	16.76	0.00	4.66
15	0.00	0.00	0.00	0.00	47	1.69	10.83	0.00	2.30
16	0.00	0.00	0.00	0.00	48	0.00	5.41	0.00	0.00
17	0.00	0.00	0.00	0.00	49	0.00	0.86	0.00	0.00
18	0.00	0.00	0.00	0.00	50	0.00	0.00	0.00	0.00
19	0.00	0.00	0.00	0.00	51	0.00	0.00	0.00	0.00
20	0.00	0.00	0.00	0.00	52	0.00	0.00	0.00	0.00
21	0.00	0.00	0.00	0.00	53	0.00	0.00	0.00	0.00
22	0.00	0.00	0.00	0.00	54	0.00	0.00	0.00	0.00
23	0.00	0.00	0.00	0.00	55	0.00	0.00	0.00	0.00
24	0.00	0.00	0.00	0.00	56	0.00	0.00	0.00	0.00
25	0.00	0.00	0.00	0.00	57	0.00	0.00	0.00	0.00
26	0.00	0.00	0.00	0.00	58	0.00	0.00	0.00	0.00
27	0.00	0.00	0.00	0.00	59	0.00	0.00	0.00	0.00
28	0.00	0.00	0.00	0.00	60	0.00	0.00	0.00	0.00
29	0.01	0.00	0.01	0.00	61	0.00	0.00	0.00	0.00
30	0.03	0.00	0.03	0.00	62	0.00	0.00	0.00	0.00
31	0.10	0.00	0.11	0.04	63	0.00	0.00	0.00	0.00
32	0.26	0.00	0.35	0.12	64	0.00	0.00	0.00	0.00

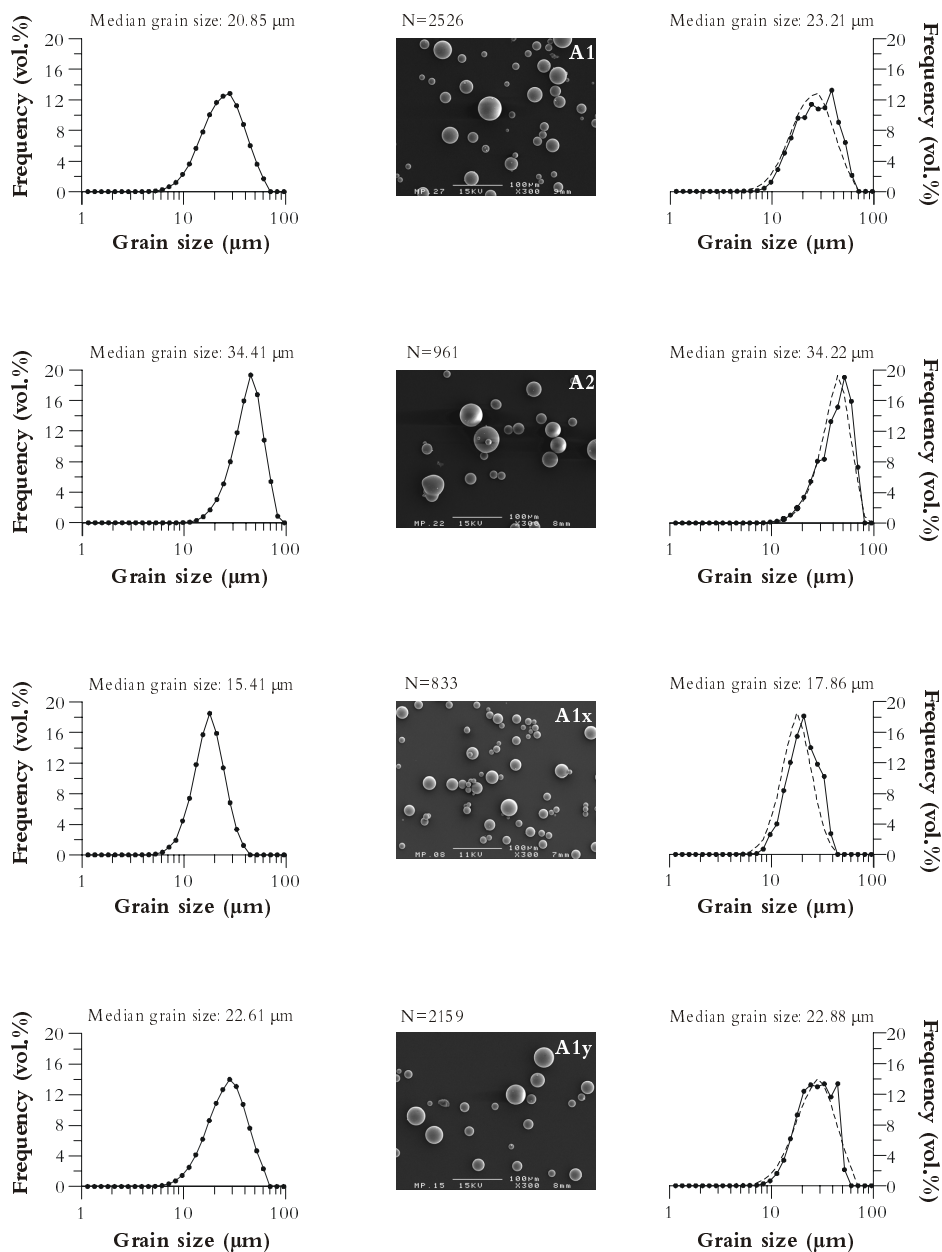


Figure 3.2. Comparison of grain-size distributions: Accuracy of the *Malvern Mastersizer S*. Grain-size distributions of all four standards are plotted. The left column shows the distributions measured with Mastersizer S. The distributions obtained from the optical analysis of SEM photographs and calculation with the software package AnalySIS are shown in the right column. For comparison, the Mastersizer distributions are dashed. Examples of SEM photographs are shown, total number of particles analysed are indicated. Median grain sizes, resulting from the two methods, are also indicated.

Table 3.3: Statistics of glass-bead standards

Glass-bead standard	A1	A2	A1x	A1y
Malvern median diameter $\pm 1\sigma$ (μm)	20.85 ± 0.051	34.41 ± 0.065	15.40 ± 0.126	22.61 ± 0.088
Sorting $\pm 1\sigma$ (μm)	11.62 ± 0.016	13.77 ± 0.037	6.27 ± 0.024	11.806 ± 0.029
Number of measurements	10	10	10	10
AnalySIS median diameter (μm)	23.21	34.22	17.86	22.88
Number of particles analysed	2526	961	833	2159
Deviation (%) between Malvern and AnalySIS median diameter	10.16	0.54	13.76	1.19

Bimodal mixtures of standards A1-A2 and A1x-A1y were constructed by weighing varying proportions of the standards in quantities where an obscuration of $20 \pm 1\%$ was ensured (Figure 3.3 and Table 3.4).

An end-member algorithm (Weltje, 1997) was applied to the whole data set of bimodal mixtures. Because the glass-bead standards are very well sorted, the data set contains 43 size classes with zero values (Table 3.2). These size classes were removed prior to modelling so that the data set consisted of data in 21 size classes in the range 4.19–103.58 μm . To estimate the minimum number of end members required for a satisfactory approximation of the data, the coefficients of determination were calculated. The coefficients of determination represent the proportion of the variance of each size class that can be reproduced by the approximated data. This proportion is equal to the squared correlation coefficient (r^2) of the input variables and their approximated values (Weltje, 1997; Prins and Weltje, 1999).

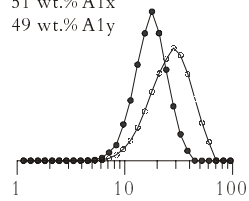
(Next page) Figure 3.3. Evaluation of mixture data.

Schematic presentation of the evaluation of the data produced by the Mastersizer S. As an example the results of mixture 65 (Table 3.4) are used. **A)** Size distributions of standards A1x and A1y measured with the Malvern Mastersizer S. **B)** Calculated size distribution of sample 65 based on the weight proportions of standards A1x and A1y. This is the *expected* size distribution. **C)** Size distribution of mixture 65 as measured with the Malvern Mastersizer S. This is the *measured* size distribution. **D)** Calculated size distribution of standards A1x and A1y that fits the *measured* size distribution of mixture 65 as close as possible according to the methods of least squares. This is the *least-squares fit* distribution. **E)** To express the fit into an independent number the absolute difference between the *measured* and the *least-squares fit* distributions (shaded area) is calculated as the ‘sum of least squares’.

Evaluation of Mastersizer data

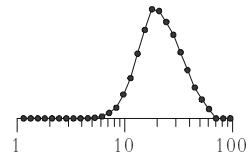
A

51 wt.% A1x
49 wt.% A1y



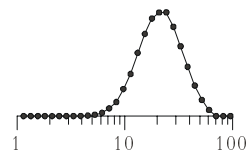
Standards are mixed
on basis of weight

B



Expected size distribution
on basis of weight proportions

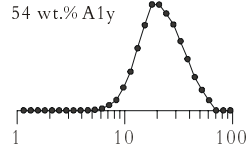
C



Measured size distribution

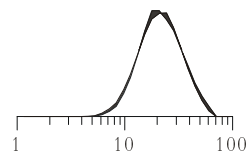
D

46 wt.% A1x
54 wt.% A1y



Best fit of standards and measured
size distribution.

E



Difference between **measured**
and **best-fit** distributions
(Sum of least squares)

Results

Precision

Precision of the Mastersizer S was tested by performing multiple analyses ($N=10$) of the four standards (Figure 3.1). The very high precision is demonstrated by small deviations in the median diameter and the sorting of the size distribution (Table 3.3). Measurements of standard A1, for example, result in a median diameter of $20.85 \pm 0.051 \mu\text{m}$ (0.25 % variation) and a standard deviation (measure of sorting) of $11.62 \pm 0.016 \mu\text{m}$ (0.14 % variation). Owing to the high precision, the grain-size distributions of the ten measurements of each sample shown in Figure 3.1 appear as a single one.

Accuracy

Accuracy of the Mastersizer S was tested by comparing the laser-sizer results with the image-analysis results (Figure 3.2). In both the Malvern and the AnalySIS results particles larger than the cut-off values of the used sieves do occur. Although the standards were created using sieves with mesh sizes of $53 \mu\text{m}$ and $30 \mu\text{m}$, the two methods still 'see' particles in at least one size class larger than the cut-off values. The median grain size obtained by the analysis of the SEM photos results in slightly greater values for standards A1 and A1x (Figure 3.2 and Table 3.3). Deviation between the median diameter obtained with the Mastersizer S and the image analysis vary between 0.54 and 13.76 %, corresponding to absolute deviations between 0.19 and $2.46 \mu\text{m}$. Thus, the Mastersizer S produces accurate measurements of the glass-bead standards. It appears that the discrepancy between the Malvern and the AnalySIS observations are larger for the fine sieve fractions (A1 and A1x, Table 3.3). This may be caused by the fact that the particles are not perfect spheres. The elongate particles do get through the sieve due to their smallest axis but their size is overestimated by the fact that on the picture they are always oriented such that their intermediate and longest axes show. Besides, the fine tail of the distribution may be underrepresented in the image analysis relative to the Malvern analysis. Another possibility of the mismatch between the size distributions of these two standards may be sorting of the samples before SEM analysis.

Resolution

Figure 3.3 shows how the comparison of the measured and the two calculated grain-size distributions leads to an evaluation of the resolution of the Mastersizer S. The 'expected' distribution is the distribution the Mastersizer S should produce if it would generate correct measurements that one expects on the basis of the linearly mixed standards. The 'expected' distribution is calculated by summing the grain-size distributions of the two standards (as listed in Table 3.2) in relative proportions according to the mixing weight proportions (as listed in Table 3.4). However, the Mastersizer S does not produce fully accurate measurements of the mixtures and therefore, the measured distribution should be 'unmixed' into the relative proportions of the mixed standards. This 'unmixing' was performed by the method of least squares (Davis, 1973): for each sample the 'best-fit' mixing ratio of the standards was calculated for which the absolute deviation between the measured and 'least-squares fit' (LSF) distribution is smallest (Figure 3.3).

Two series of samples were prepared by mixing two standards in various, accurately known, weight proportions (Table 3.4). Samples 1–38 are mixtures of standards A1 and A2 (median grain sizes 20.85 and 34.41 μm , Figure 3.4A), samples 39–85 are mixtures of standards A1x and A1y (median grain sizes 15.40 and 22.61 μm , Figure 3.4B).

Table 3.4: Mixing coefficients of glass-bead mixtures

Mixture nr.	Fraction A1 (wt. %)	Fraction A1 (LSF)	Mixture nr.	Fraction A1x (wt. %)	Fraction A1x (LSF)
1	96	96	39	99	99
2	94	94	40	97	93
3	91	91	41	96	92
4	90	91	42	95	95
5	89	89	43	94	88
6	87	88	44	93	91
7	82	83	45	92	87
8	81	82	46	91	86
9	78	79	47	90	85
10	75	76	48	89	83
11	67	69	49	88	83
12	67	69	50	87	80
13	57	60	51	86	79
14	55	58	52	86	80
15	50	53	53	85	80
16	49	53	54	85	80
17	49	52	55	84	79
18	48	51	56	79	74
19	42	46	57	73	68
20	39	43	58	72	67
21	35	40	59	71	65
22	34	38	60	69	65
23	26	32	61	65	61
24	24	30	62	59	53
25	21	29	63	57	50
26	21	29	64	56	50
27	20	28	65	51	46
28	17	25	66	48	44
29	13	22	67	45	41
30	11	20	68	42	39
31	10	19	69	39	35
32	9	18	70	37	34
33	6	15	71	35	33
34	6	15	72	32	29
35	3	4	73	27	24
36	3	12	74	22	20
37	3	10	75	20	18
38	3	2	76	18	16
			77	14	13
			78	11	10
			79	10	9
			80	9	8
			81	7	6
			82	5	4
			83	5	0
			84	4	4
			85	2	2

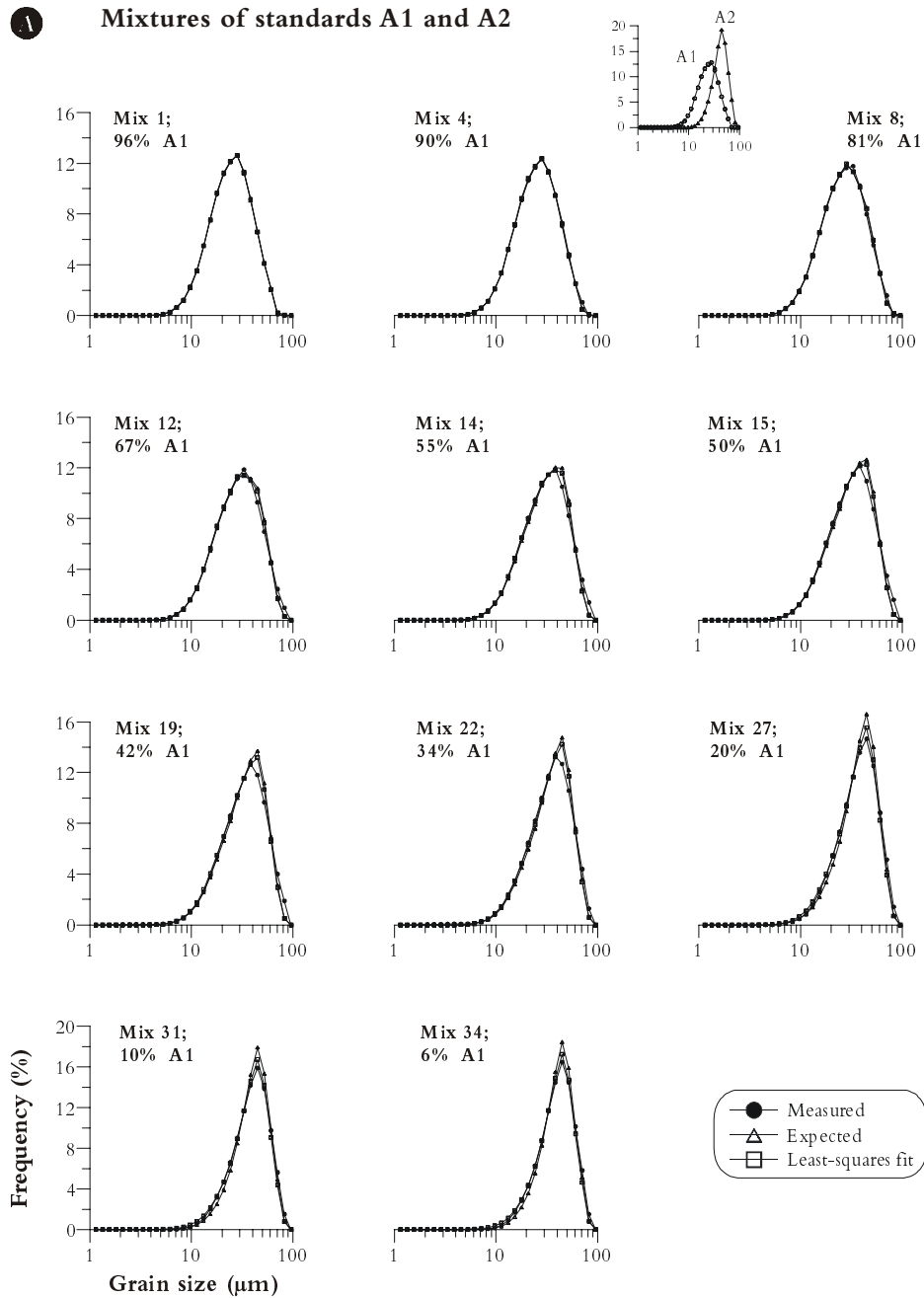


Figure 3.4A. Mixtures of standards A1 and A2. Grain-size distributions of mixtures of standards A1 and A2 are shown. For each mixture the *measured*, *expected* and *least-squares fit* grain-size distributions are shown. Sample numbers correspond to those listed in table 3.4.

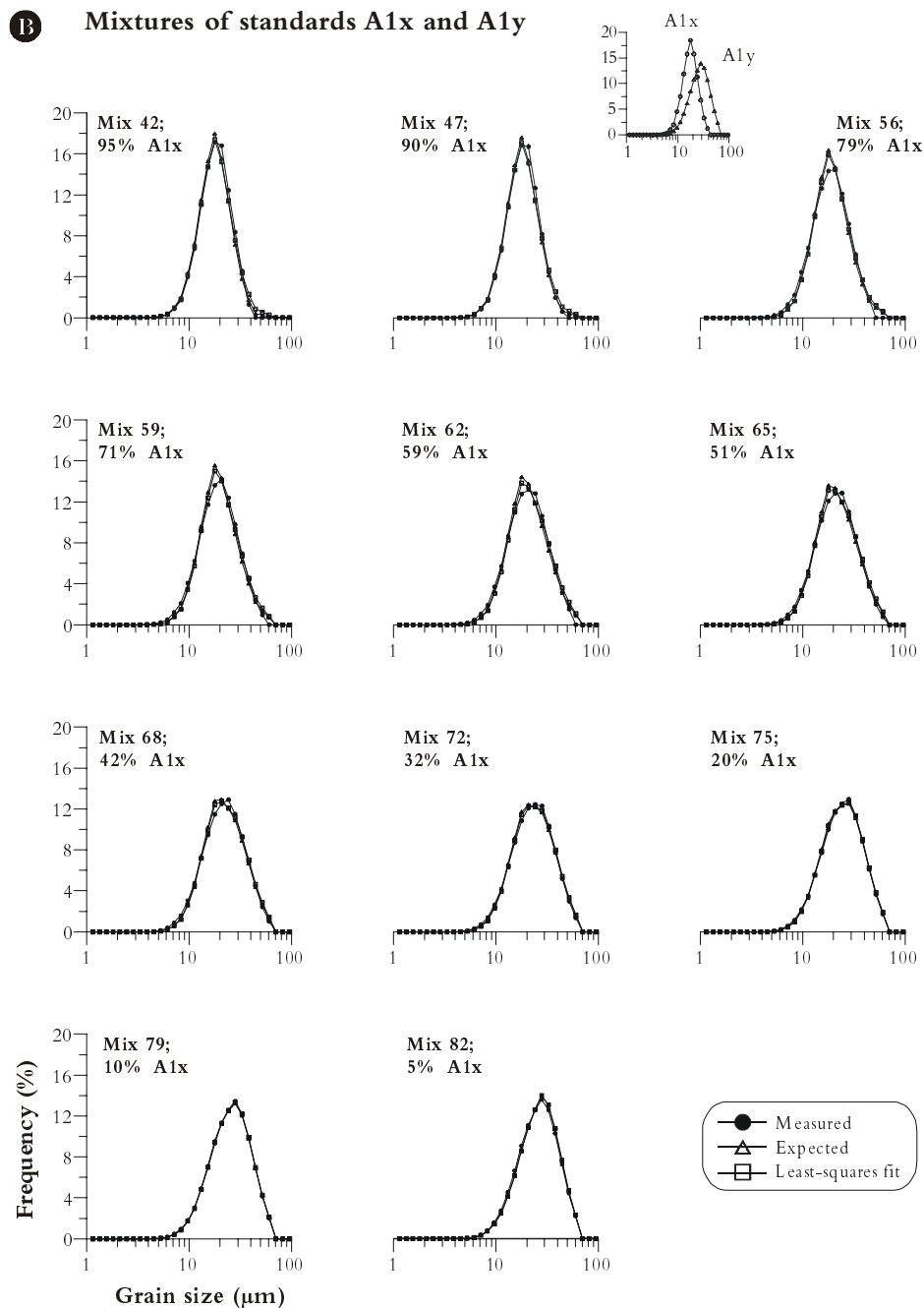


Figure 3.4B. Mixtures of standards A1x and A1y. Grain-size distributions of mixtures of standards A1x and A1y are shown. For each mixture the *measured*, *expected* and *least-squares fit (LSF)* grain-size distributions are shown. Sample numbers correspond to those listed in table 3.4.

Chapter 3

Figures 3.4A and B show grain-size distributions of a number of mixtures listed in Table 3.4. The grain-size distributions of all mixtures appear as unimodal distributions. The measured grain-size distributions are compared to two calculated distributions; the ‘expected’ and the ‘least-squares fit’ distributions. Figure 3.4A shows results for ten mixtures composed of standards A1 and A2 in steps of about 10 wt.% A1. Only very small differences are observed between the measured and calculated distributions. From 100 to about 70 wt.% A1, the measured distributions are fitted almost perfectly. The misfit then increases slightly and is largest at about 20 to 40 wt.% A1. Figure 3.4B shows results for ten mixtures composed of standards A1x and A1y in steps of about 10 wt.% A1x. Also for these mixtures only very small differences are observed between the measured and calculated distributions. From 100 to about 90 wt.% A1x, the measured distributions are fitted almost perfectly. The misfit then increases slightly and is largest at about 80 to 60 wt.% A1. From about 30 to 0 wt.% A1x, the measured distributions are fitted almost perfectly again.

The approximation of the measured grain-size distributions with the method of least squares results into the LSF distributions (Figure 3.3). The known weight proportions and the approximated (LSF) proportions of the standards correlate well with one another. This is shown in Figure 3.5 (data are listed in Table 3.4) where for both sample series the known and approximated proportional contributions of the standards are correlated. Both mixture series plot close to the line $y=x$. In case of mixtures of standards A1 and A2 (Figure 3.5A) the finer-grained standard (A1) is overestimated whereas with mixtures of standards A1x and A1y (Figure 3.5B) the finer-grained standard (A1x) is underestimated.

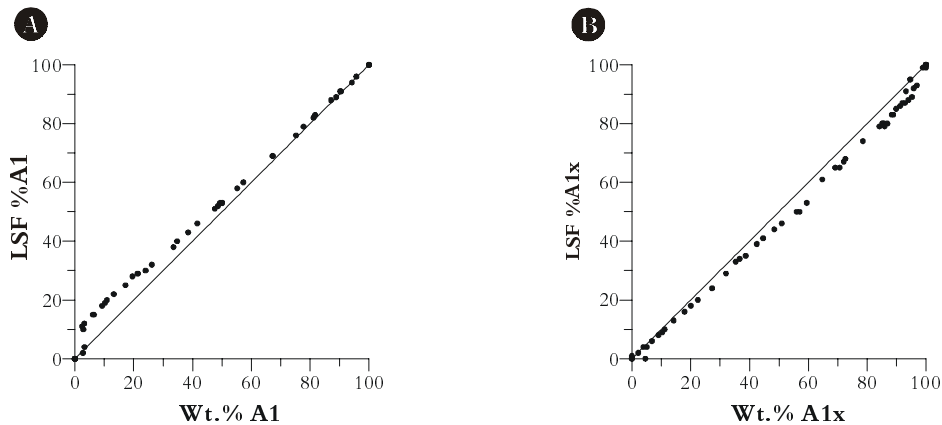


Figure 3.5. Correlation of mixture data. Correlation diagrams of known weight fractions (Wt.%) and calculated fractions (LSF %) of the fine-grained standard in the binary mixtures of **A)** standards A1-A2, and **B)** and those of A1x-A1y. The equation $y=x$ is also plotted in both graphs.

The total absolute deviation between the standards and the LSF distributions, the 'sum of least squares', is a measure of the fit of the two standards to the analysed size distribution. Figure 3.6 shows the sum of least squares versus the weighed proportion of the smallest standard for the two mixture series. The distribution of weight proportion A1 versus the sum of least squares (Figure 3.6A) indicates that the largest misfit occurs at low proportions (5–40%) of the finest standard. The distribution of weight proportion A1x versus the sum of least squares (Figure 3.6B) indicates that the largest misfit occurs at high proportions (70–95%) of the finest standard.

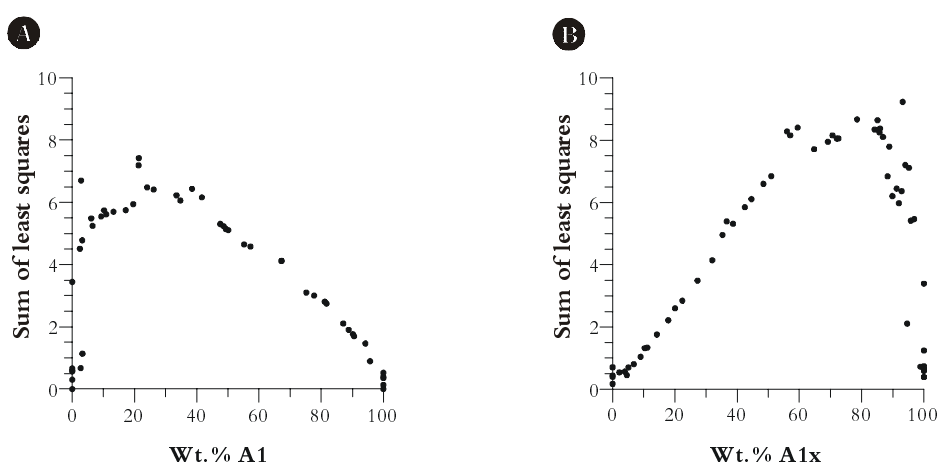


Figure 3.6. Variations in the fits of mixture data. Distribution of the known weight fractions (Wt.%) and 'goodness of fit' expressed as the 'sum of least squares' of the fine-grained standard in the binary mixtures of **A)** standards A1-A2 and **B)** those of A1x-A1y. Note that in case of mixtures A1-A2 the distribution is positively skewed, meaning an overestimation of the finer-grained standard, whereas in case of mixtures A1x-A1y the distribution is negatively skewed, meaning an underestimation of the finer-grained standard.

End-member model

An end-member algorithm (Weltje, 1997) was applied to the total data set of unimodal glass-bead mixtures (Figures 3.4A and B) to see if the four glass-bead standards can be unmixed from these data. Figure 3.7A shows the coefficients of determination (r^2) per size class for end-member models with two to ten end members. From this plot it is clear that the coefficients of determination increase with the number of end members. The two-end member model poorly reproduces the size range of about 20–40 μm . The three-end member model explains the middle part of the size range well but has trouble with the tails of the distribution. End member models of four or more end members reproduce all but the coarsest size classes very well. The mean coefficient of determination (r^2_{mean}) describes the goodness of fit over the whole size range (Figure 3.7B). The balance between the number of end members and the goodness of fit is found at the inflection point of the curve, i.e., at three end members (Figure 3.7B, $r^2_{\text{mean}}=0.91$). Below this point an additional end member will significantly increase the

goodness of fit. Beyond this point the goodness of fit will not be enhanced significantly, in other words, predominantly noise is being modelled. The end members that are described by the three end-member model are shown in Figure 3.7C. The three end members compare very well to the glass-bead standards A2, A1y and A1x. Since standards A1x and A1y result from the fractionation of standard A1, the end-member model does not 'need' this fourth standard to describe the variance in the data set. The ratio of the proportions of standards A1x and A1y in mixtures of A1 and A2 is therefore constant since $A1 = 0.2 \cdot A1x + 0.8 \cdot A1y$.

Discussion

Glass-bead standards

The Malvern Mastersizer S produces accurate and very precise measurements of the four glass-bead standards. The median particle sizes and the sorting of the size distributions are correctly measured. Differences between the Mastersizer size distributions and the distributions resulting from the optical analyses of the SEM photos can be explained by the fact that the glass beads are not perfect spheres. Therefore, the particles observed on the SEM photos will always be oriented such that the intermediate and longest axes show. The calculated mean diameter used to compute the equivalent volume of the particle will therefore be too large. The laser particle sizer analyses the average of the longest and shortest axis, which is taken as the diameter of a sphere of which the volume is calculated. Therefore, the Mastersizer S grain-size distributions will have slightly smaller median values than those obtained by analysis of the SEM photos. This effect seems to be greater in the finest sieve fractions (Standard A1 and A1x). Another possible explanation for the observed mismatch is the fact that shaking of the sample causes an inverse gradient. Despite careful sample treatment, this may have happened during transport of the samples.

Mixtures of standards

Mixtures of the glass-bead standards are analysed to a high resolution. The Mastersizer perfectly 'sees' that the applied sample is a mixture of two standards when these standards are fitted onto the measured size distribution. Although not all mixtures are measured as accurately, even very small changes in the composition of the mixtures are recognised. It appears that resolution is poorest at lowest (<5 %) proportions of the finest standard in both mixture series. Multiple analyses of the same low weight proportion of standards A1 and A1x result in LSF proportions that vary widely. In other words, if the proportion of one of the standards becomes smaller than 5 %, the Mastersizer S is still able to recognise it but has difficulty to estimate its exact proportion. In case of the mixture series of A1 and A2, the finer standard is overestimated throughout the series, whereas in the mixture series of A1x and A1y, the finer standard is underestimated. To be able to solve this problem one would have to look at the software used by the laser particle sizer, which is beyond the scope of this study.

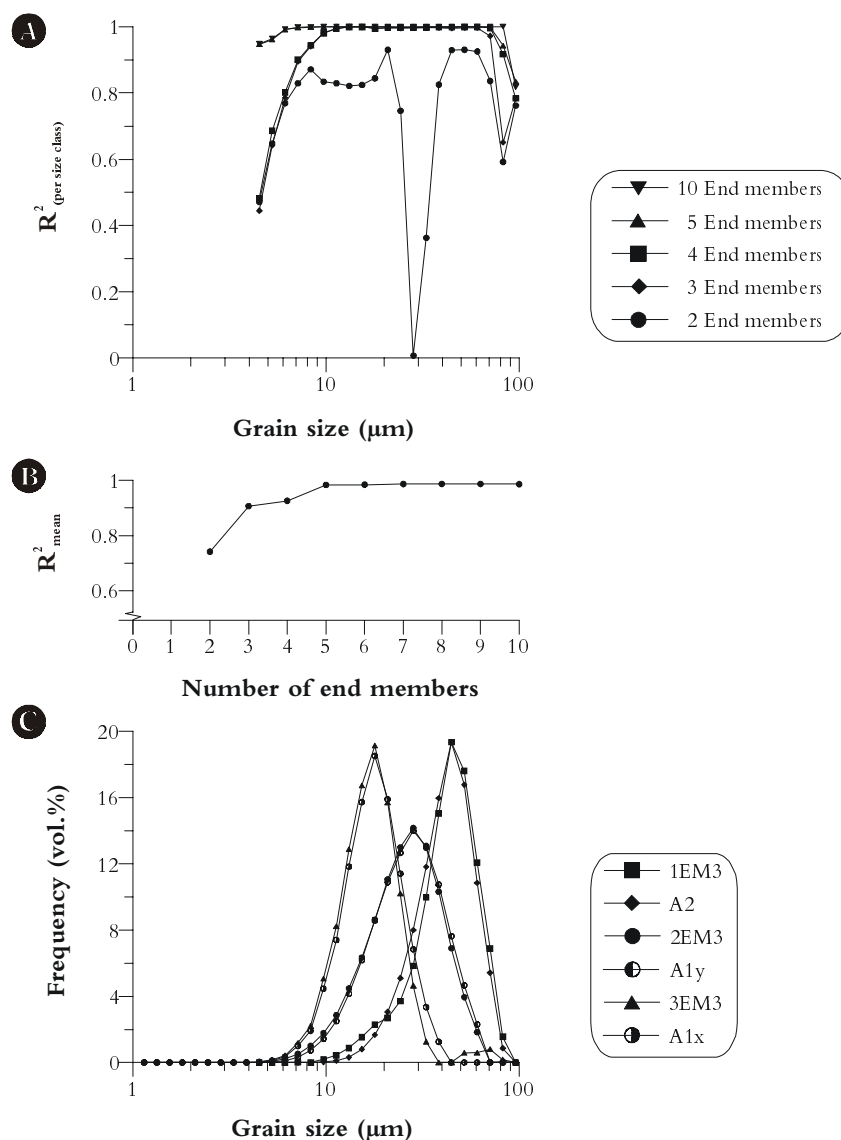


Figure 3.7. End-member results. Goodness of fit statistics of the end-member model.

A) Coefficients of determination for each size class for end-member models with two, three, four, five and ten end members. At least three end members are needed to reproduce most variables adequately; the two end-member model shows distinct lack of fit in several size ranges. Use of five or more end members hardly improves the goodness of fit relative to a four end-member model. **B)** The plot of the mean coefficient of determination per number of end members shows that three end members provide the best balance between the smallest amount of end members and the best approximation of the data. **C)** Size distributions of the end members are compared to those of the standards used in the construction of the data set. Note that except for a small mode at $\sim 70 \mu\text{m}$ in end member 3, the standards are approximated very nicely by the end members of the three end-member model.

Chapter 3

The promising outcome of the mixture-series analyses is the fact that the Mastersizer S is able to recognise bimodal mixtures down to a level of 5 % relative abundance of one of the standards. If the grain-size distribution of the standards is known beforehand, the relative contribution of each of the standards can be calculated accurately.

End-member modelling of the glass-bead mixtures

From the fact that the misfit between the measured and calculated size distributions of the glass-bead mixtures is small (largest deviation <9 %, Figure 3.6), this data set looks promising to be unmixed by the end-member model. The modelling experiment results in a three end-member model of which the end members resemble standards A1x, A1y and A2. The fact that standard A1 was not reproduced as an end member logically results from the fact that standards A1x and A1y were constructed by physically splitting (sieving) of standard A1. Therefore, A1 is considered a mixture of A1x and A1y. Except for a small mode in end member three at about 70 μm , the end members perfectly resemble the initial standards. With these three end members, 91 % of the variance in the total data set can be explained. The small mode is a small artefact of the model and may account for part of the ‘missing’ 9 %. The modelling experiment thus shows that even if the grain-size distribution of the standards is not known beforehand, as is the case in most geological studies, the end-member algorithm developed by Weltje (1997) is a powerful tool to unmix the whole data set of mixtures into its original subpopulations.

Conclusions

- The Malvern Instruments Mastersizer S produces accurate and precise measurements of both the glass-bead standards and mixtures of those.
- If the grain-size distributions of the glass-bead standards are known beforehand, the grain-size distributions of the mixtures can be unmixed accurately into their original components.
- If the grain-size distributions of the glass-bead standards are not known beforehand, the end-member algorithm developed by Weltje (1997) can be successfully applied to unmix the composite mixtures into their original subpopulations.
- The combination of the Malvern Instruments Mastersizer S and Weltje’s (1997) end-member algorithm forms a powerful tool for the analysis of the grain-size distributions of subpopulations in sediment mixtures.

Acknowledgements

Saskia Kars (Vrije Universiteit Amsterdam) is thanked for making all the SEM images of the standards. Kathrin Reimer (Netherlands Institute for Applied Geosciences) is thanked for assistance with the AnalySIS software package. Gert Jan Weltje (Technical University Delft) is thanked for providing the end-member algorithm.

4. Fast reconnaissance of carbonate dissolution based on the size distribution of calcareous ooze on Walvis Ridge, SE Atlantic Ocean.

Abstract

The size distribution of bulk sediments in core MD962094, retrieved from Walvis Ridge, is used as a proxy for carbonate dissolution. The coarsest two fractions ($>90\text{ }\mu\text{m}$ and $25\text{--}90\text{ }\mu\text{m}$) of the bulk size distribution are dominated by complete shells and fragments of adult foraminifera, and juvenile foraminifera shells and fragments, respectively. The ratio of the two fractions is a measure of fragmentation of the foraminifera shells caused by carbonate dissolution. Our carbonate-fragmentation curve compares very well with the coarse-carbonate fragmentation index defined as the ratio of whole foraminifera over foraminifera fragments as seen with a light microscope in the $>150\text{ }\mu\text{m}$ fraction in sediments from a nearby core on Walvis Ridge. Fragmentation is relatively high in glacial stages and relatively low in interglacial stages during the last 300 kyr. Correlation of the carbonate-dissolution curve and a proxy record of SE trade-wind intensity, i.e. the grain size record of aeolian dust in core MD962094, suggests a possible cause for carbonate dissolution in the Walvis Ridge area. Carbonate dissolution may be caused by the combined effect of upwelling of corrosive water and an increased production of organic matter, decreasing the preservation potential of carbonates both during and after deposition.

Introduction

The lysocline and carbonate compensation depth are boundaries in the present ocean below which carbonate dissolution starts and below which dissolution exceeds deposition of carbonate, respectively. The position of these boundaries is mainly a result of the interplay between the carbonate saturation of deep waters and organic carbon production in the surface waters (Broecker and Takahashi, 1980; Emerson and Bender, 1981; Le and Shackleton, 1992; Kucera et al., 1997). Temporal changes in carbonate dissolution therefore, can be used to reconstruct changes in the position of the lysocline and carbonate compensation depth through time (Jansen, 1985; Peterson and Prell, 1985; Farrell and Prell, 1989; Lé and Shackleton, 1992).

Carbonate dissolution has been inferred in a number of ways, e.g. from CaCO_3 -content (Farrell and Prell, 1989; 1991), fragmentation of foraminifera shells (Le and Shackleton, 1992; Schmidt, 1992; Kucera et al., 1997), nannofossils (Zachariasse et al., 1984), SEM studies of the shell thickness of single foraminiferal species from a specific size (Lohmann et al., 1999; Dittert and Henrich, 2000; Huber et al., 2000), and coarse carbonate fraction (Bassinot et al., 1994; Bickert and Wefer, 1996; Broecker and Clark, 1999). Defining the coarse carbonate fraction as $> 63 \mu\text{m}$, Broecker and Clark (1999) were able to reconstruct CO_3^{2-} ion concentrations for the late Quaternary ocean to a very high accuracy. Their study indicates that a high-precision estimate of carbonate dissolution can be obtained in a relatively simple way. However, the construction of their and most other dissolution indicators is rather labour-intensive as samples have to be washed, sieved and dried and foraminifera have to be picked and counted and studied with a (electron) microscope.

In this paper we present a fast and high-precision method that allows the establishment of a carbonate-fragmentation record on the basis of the size distribution of calcareous ooze from Walvis Ridge, SE Atlantic Ocean. Size measurements are carried out on a laser-diffraction particle sizer, allowing for a fast and high-precision analysis of the sediment's size distributions. The results from core MD962094 were compared with results from Schmidt (1992), who constructed a foraminifera-fragmentation record on sediments from core GeoB 1028-5. The two cores were retrieved from about the same location on Walvis Ridge (figure 4.1). Walvis Ridge is a northeast-southwest volcanic ridge that rises on average 2000 m above the surrounding sea floor. Sedimentation in this part of the SE Atlantic is controlled by the coastal upwelling off Namibia and South Africa. The trade-wind driven upwelling determines the amount of primary productivity in the surface waters, thereby also controlling the rain rate of both the carbonate shells and the organic carbon to the sea floor. The upwelling intensity is related to both the atmospheric and oceanic circulation in the area, and therefore has been studied extensively (Fischer and Wefer, 1999, and references therein). Bickert and Wefer (1996) have shown that changes in the proportions of northern and southern intermediate and deep waters also influence carbonate preservation in the Southeastern Atlantic Ocean. We will show that the size distribution of the bulk sediments describes changes in carbonate fragmentation and dissolution driven by changes in the atmospheric circulation patterns.

Material and Method

Core MD962094 was recovered from Walvis Ridge at 19°59,97 S / 9°15,87 E and 2280 m waterdepth, core GeoB 1028-5 (Schmidt, 1992) was retrieved at a distance less than 4.5 nautical miles from this core (Figure 4.1). The two cores can be correlated very well on the basis of the $\delta^{18}\text{O}$ curves of planktonic foraminifers (Figure 4.6). The dominant lithology of core MD962094 is foraminifer nannofossil ooze. The core is 30.75 m long and covers the last ~650 kyr (Bertrand et al., 1996). For this study we concentrate on the last 300 kyr; the upper 15 m of the core (for age model see Chapter 2). The core was sampled at 5-cm intervals with two series of 10-ml syringes for stable oxygen-isotope and grain-size analyses.

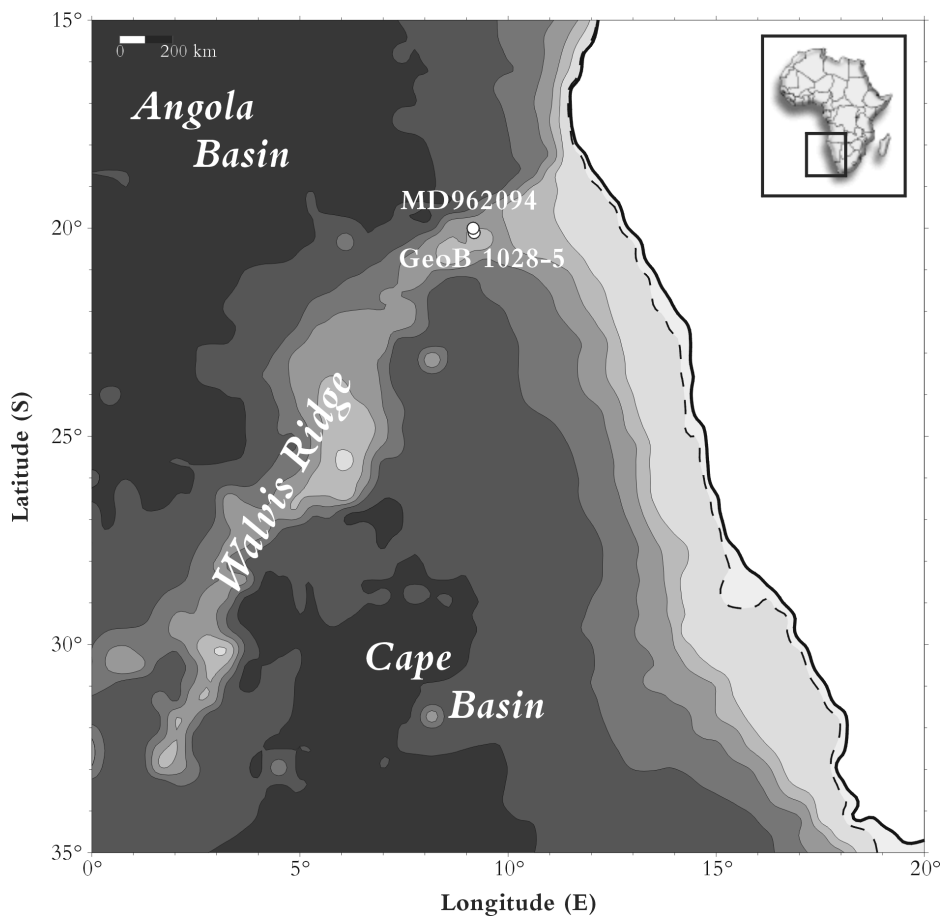


Figure 4.1. Location of cores MD962094 and GeoB1028-5 (Schmidt, 1992) in the SE Atlantic Ocean. Bathymetry is shown in contour intervals of 1000 m, the 125-m isobath is presented as a dotted line.

Size analyses of the bulk sediments were carried out with a Malvern Instruments Mastersizer S, using a lens with 300-mm focal length. The measured size distributions were analysed from 0.73–814 μm . A sample of ~500 mg was suspended in demineralised water by stirring. A subsample was taken from this suspension with a 10-ml pipette and introduced into the sample cell of the laser-particle sizer. All samples were suspended in the sample cell by stirring and ultrasonic dispersion for 15 seconds before analysis.

Reproducibility of the laser-particle size measurements was tested by multiple analyses ($n=9$) of two extreme size distributions (Figure 4.2A). Reproducibility of the two samples was good, of sample 491, $D_{50} = 10.77 \mu\text{m} \pm 0.42$, of sample 766, $D_{50} = 16.34 \mu\text{m} \pm 1.87$. The size distribution of the samples appeared to be affected by the time of exposure to ultrasonic dispersion during analysis. The carbonate-rich sediments contain large amounts of foraminifera shells that break because of the ultrasonic dispersion thereby altering the size distribution dramatically. The effect of ultrasonic dispersion on the size distribution is shown in Figure 4.2B. The initial mode at 45 μm in the size distribution at $t = 0$ shifts to 15 μm after 60 minutes. Figure 4.2C shows the rapid decrease of the proportion $>90 \mu\text{m}$ through time. It is clear from these figures that the size distribution changes most dramatically during the first few minutes of ultrasonic dispersion. However, ultrasonic dispersion is needed to ensure 100% suspension of the sample. Therefore, to minimise physical fragmentation of the foraminifera shells before analysis and yet to ensure suspension, we chose to expose the samples to 15 seconds ultrasonic dispersion prior to the measurements.

Size distributions of foraminifer ooze

The $\delta^{18}\text{O}$ -curve of *Globorotalia inflata* (Chapter 2) is plotted in Figure 4.3A for the last 300 kyr showing marine-isotope stages one to eight. The size-spectra map of the bulk sediments from core MD962094 is shown in Figure 4.3B. Here, the size distributions of the 276 samples are represented as a contour plot showing higher frequencies (volume %) in darker shades of grey. Interglacials clearly show coarser size distributions with modes at about 50–60 μm , indicating low fragmentation, compared to finer grained sediments in glacial periods with modes at about 5–15 μm , indicating high fragmentation. The position of the samples plotted in Figures 4.2, 4.4 and 4.5 are indicated in Figure 4.3B.

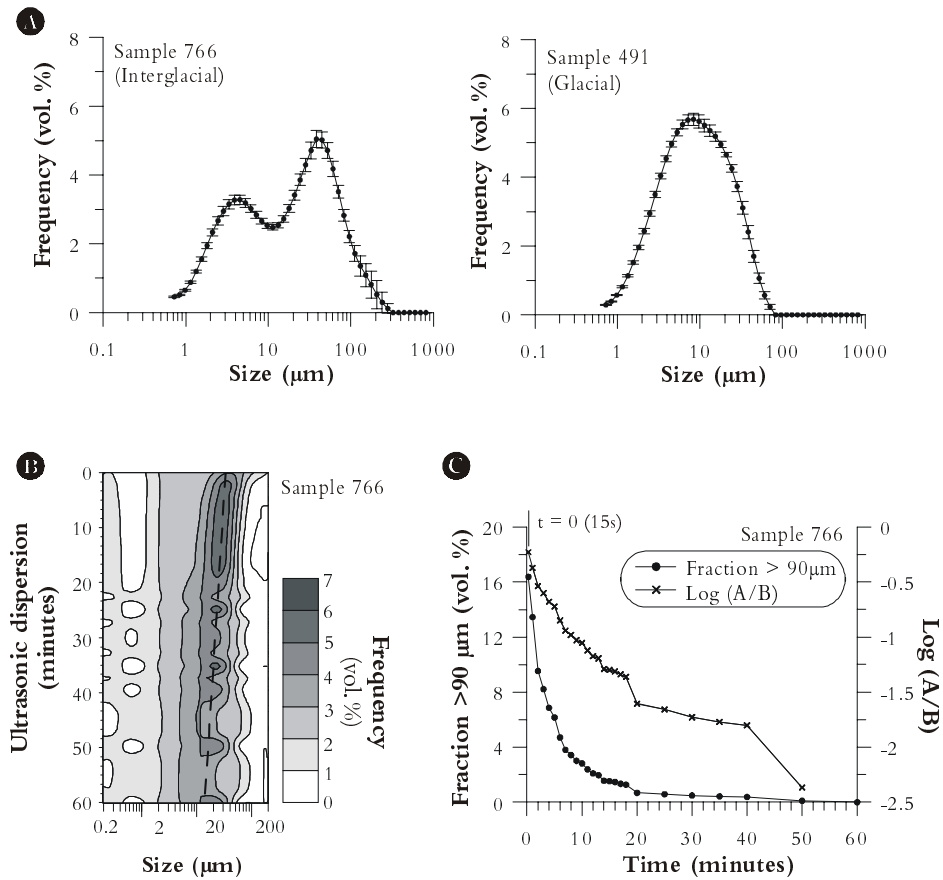


Figure 4.2. Measurements of bulk size distributions.

A Reproducibility of the size analysis described in this paper tested for sample 491 (glacial, M.I.S. 4, 491 cm core depth) and sample 766 (interglacial, M.I.S. 5E, 766 cm core depth). **B** Physical break-up of foraminifera shells in sample 766 owing to ultrasonic dispersion. Bulk size distributions of this sample measured repeatedly during 60 minutes represented as a contour plot showing higher frequencies (volume %) in darker colours. **C** Break-up of the >90 μm fraction through time and resultant effect on the log-ratio of the coarsest two fractions from the size distributions, example from sample 766.

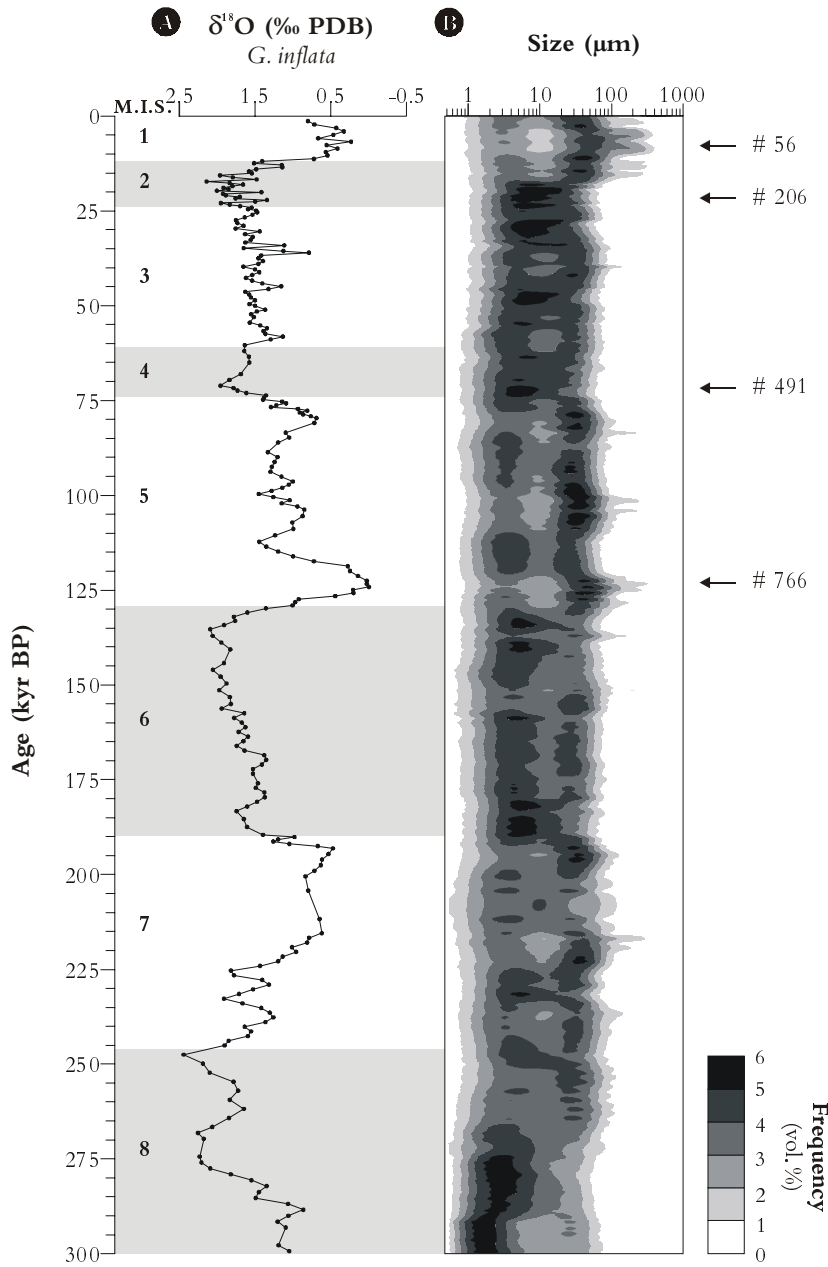


Figure 4.3. Bulk size data. **A)** $\delta^{18}\text{O}$ -curve of *G. inflata* in core MD962094 (Chapter 2), Marine Isotopic Stages (M.I.S.) after Martinson et al. (1987) are indicated. **B)** Bulk size distributions of all 276 samples plotted versus age (kyr BP) represented as a contour plot showing higher frequencies (volume %) in darker colours. Positions of the samples shown in Figures 4.2, 4.4 and 4.5 are indicated with arrows.

The average size distribution of the 276 bulk-sediment samples in core MD962094, covering the last 300 kyr, is shown in Figure 4.4A. The average distribution is polymodal with clear modes at about 5 μm , 30 μm and a small mode at $>100 \mu\text{m}$. Figure 4.4B shows two extreme size distributions of samples from the Late Holocene and the Last Glacial Maximum. It shows that the contribution of the terrigenous fraction to the size distribution of the bulk sediments is negligible. The three modes in the size distributions are mainly attributed to coccoliths, juveniles and small fragments of foraminifera shells, and adult foraminifera shells and large fragments, respectively. We defined fraction A as $> 90 \mu\text{m}$, and fraction B as 25–90 μm (Figure 4.4A).

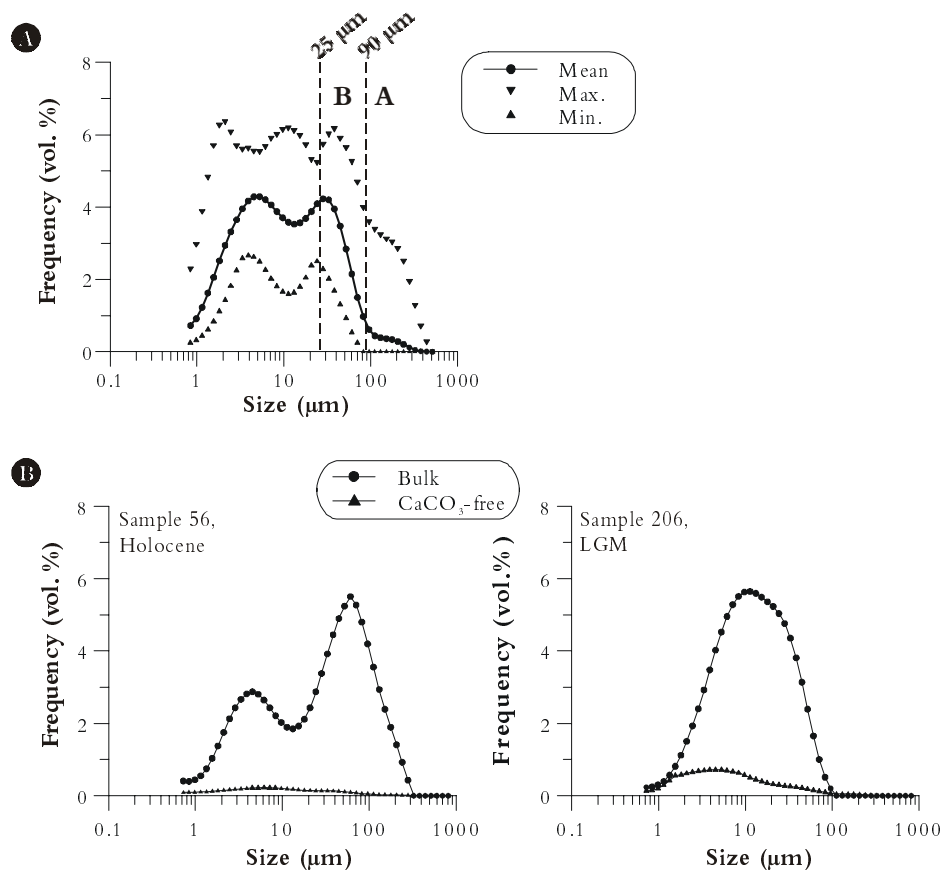


Figure 4.4. Sample statistics. **A)** Sample statistics of all 276 samples. Also indicated are the boundaries between the coarsest two fractions A and B. **B)** Typical size distribution of two extreme samples. Sample 56 (Holocene, 56 cm core depth) shows good preservation, sample 206 (LGM, 206 cm core depth) shows a large amount of dissolution. To show the negligible effect of the contribution of the carbonate-free fraction of the samples on the bulk size distribution, they are plotted in relative abundance using calcium-carbonate concentrations of 90 and 70% respectively.

It appears that the foraminifera shells in fraction A ($> 90 \mu\text{m}$) from sample #56 (Holocene) are predominantly complete although a few shells are broken (Figure 4.5A). Fraction B ($25\text{--}90 \mu\text{m}$) shows considerably more fragments, but complete foraminifera shells prevail in the sample (Figure 4.5B). Sample #206 (Last Glacial) shows significantly more broken foraminifera shells, both in fraction A as well as in B (Figures 4.5C and D).

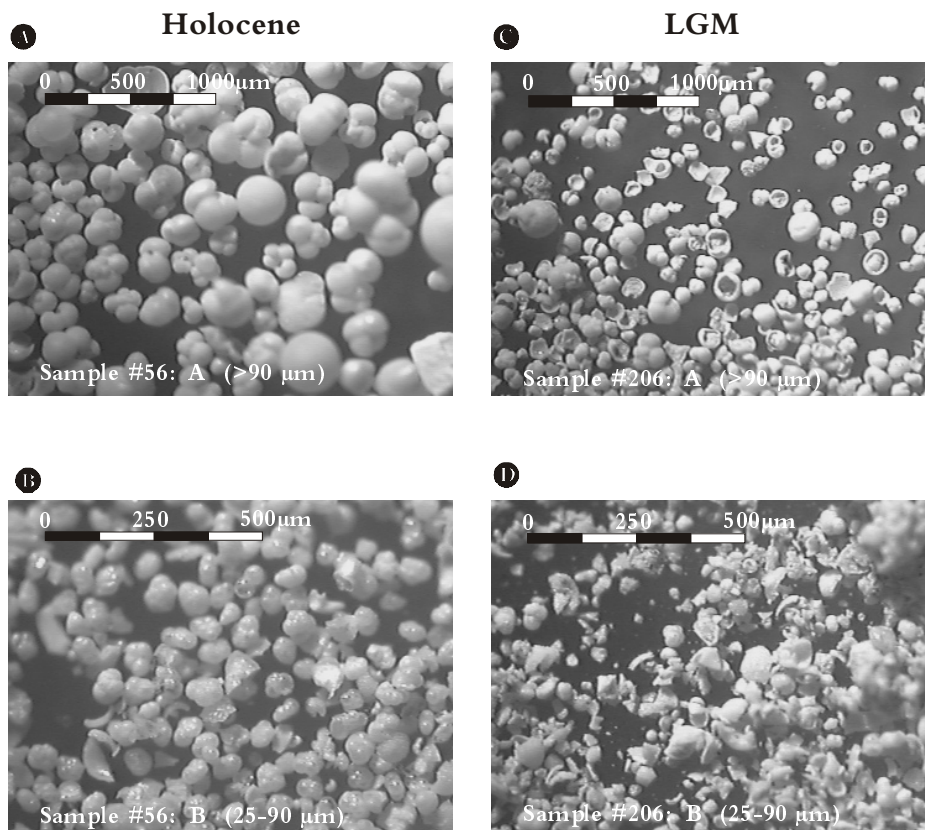


Figure 4.5. Light-microscope photographs. **A-B**) pictures of sample 56 (Holocene, 56 cm core depth). Samples were fractionated into the fractions of which modes are observed in the size distributions using sieves of 25 μm and 90 μm . **C-D**) pictures of sample 206 (Last Glacial Maximum, 206 cm core depth).

Carbonate fragmentation index

We defined a carbonate fragmentation index as the log-ratio of the relative abundances of the fractions A and B. The downcore fragmentation index is plotted versus age in Figure 4.6C. This figure shows that interglacial periods are marked by relatively high values of the index, indicating low fragmentation, and glacial periods are marked by relatively low values, indicating high fragmentation. Reproducibility of the fragmentation index could only be determined for sample #766 since sample #491 did not have size fractions >90 μm (Figure 4.2A). Multiple analysis ($n=9$) of the log-ratio determined in sample #766 resulted in an error bar of ± 0.25 , meaning that the variation observed in Figure 4.6C is significant.

The foraminiferal assemblages of Walvis Ridge sediments during the late Quaternary contain predominantly subtropical planktonic foraminifera with abrupt intervals of very high abundances of *Neoglobobulimina pachyderma* (s) attributed to periods of enhanced upwelling (Schmidt, 1992; Ufkes et al., 1998; Ufkes et al., 2000). Because *N. pachyderma* is a relatively small species, faunal changes might affect the carbonate fragmentation index. However, this is not the case since the average size of *N. pachyderma* is >200 μm (Peeters et al., 1999). We conclude that the log-ratio of the two coarsest fractions of the size distributions of the bulk sediments from core MD962094 can be interpreted as a carbonate fragmentation index.

Discussion

The photographs shown in Figure 4.5 clearly illustrate that the break-up of the foraminifera shells has occurred along the edges of the chambers. This can be ascribed to dissolution since this is the place where the shells are most vulnerable. (G-J Brummer pers comm).

The fragmentation curve of the nearby core GeoB 1028-5 was established using a ratio of the amount of fragments of foraminifera shells over whole foraminifera shells (Schmidt, 1992, Figure 4.6D). The two records (Figures 4.6C and D) show a good correlation one to another, which confirms our interpretation of the size distribution of the bulk sediments as a measure of fragmentation. The correlation of the two records could not be expressed in numbers owing to small differences in the age models of the two cores. The downcore variations in fragmentation of the foraminifera shells in core GeoB 1028-5 are attributed to changes in dissolution owing to changes in the trade-wind driven upwelling intensity (Schmidt 1992). The upwelling affects carbonate preservation in two ways: 1) The cold upwelling waters are strongly undersaturated in carbonate causing dissolution of the foraminifera shells settling through the water column and on the sea floor, 2) The nutrient-rich waters favour productivity in the surface waters, causing high fluxes of organic matter to the sea floor, resulting in reduced conditions in the deposited sediments, enhancing carbonate dissolution (Kucera et al., 1997). Although the effect of dissolution in the water column cannot be neglected, the larger part of dissolution probably takes place in the sediments (Conan et al., in prep.).

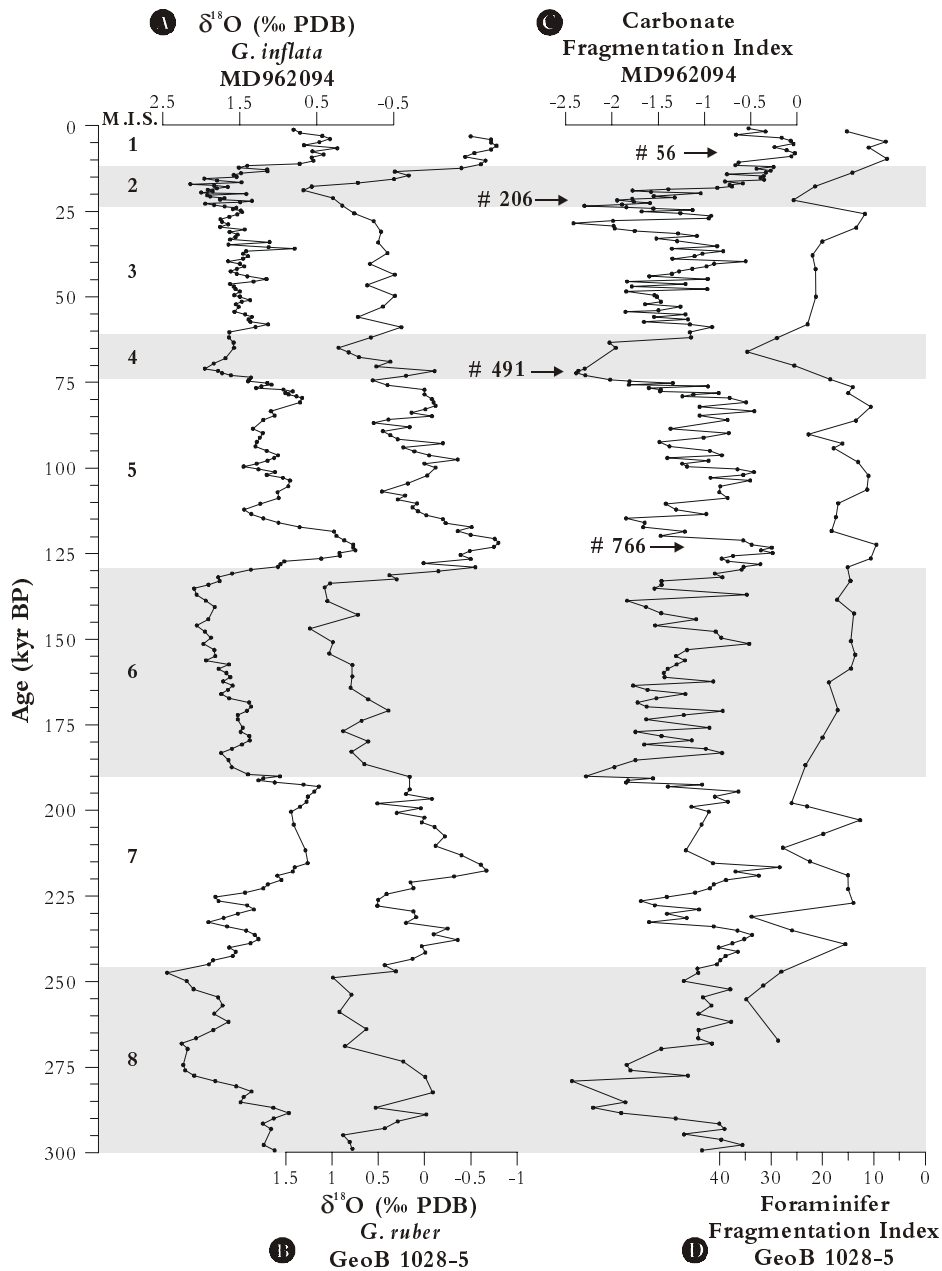


Figure 4.6. Age model and fragmentation curves. A) $\delta^{18}\text{O}$ -curve of *G. inflata* in core MD962094 (see Chapter 2), Marine Isotopic Stages (M.I.S.) after Martinson et al. (1987) are indicated. B) $\delta^{18}\text{O}$ -curve of *G. ruber* in core GeoB 1028-5 (from Schmidt, 1992). C) Log-ratio of the relative abundance of the coarsest two fractions of bulk sediments from core MD962094. Carbonate fragmentation increases to the left. Positions of the samples shown in Figures 4.2, 4.4 and 4.5 are indicated with arrows. D) Foraminifer Fragmentation Index (Schmidt, 1992) constructed from the ratio of fragments of foraminifera shells over whole foraminifera shells in core GeoB 1028-5. Fragmentation increases to the left.

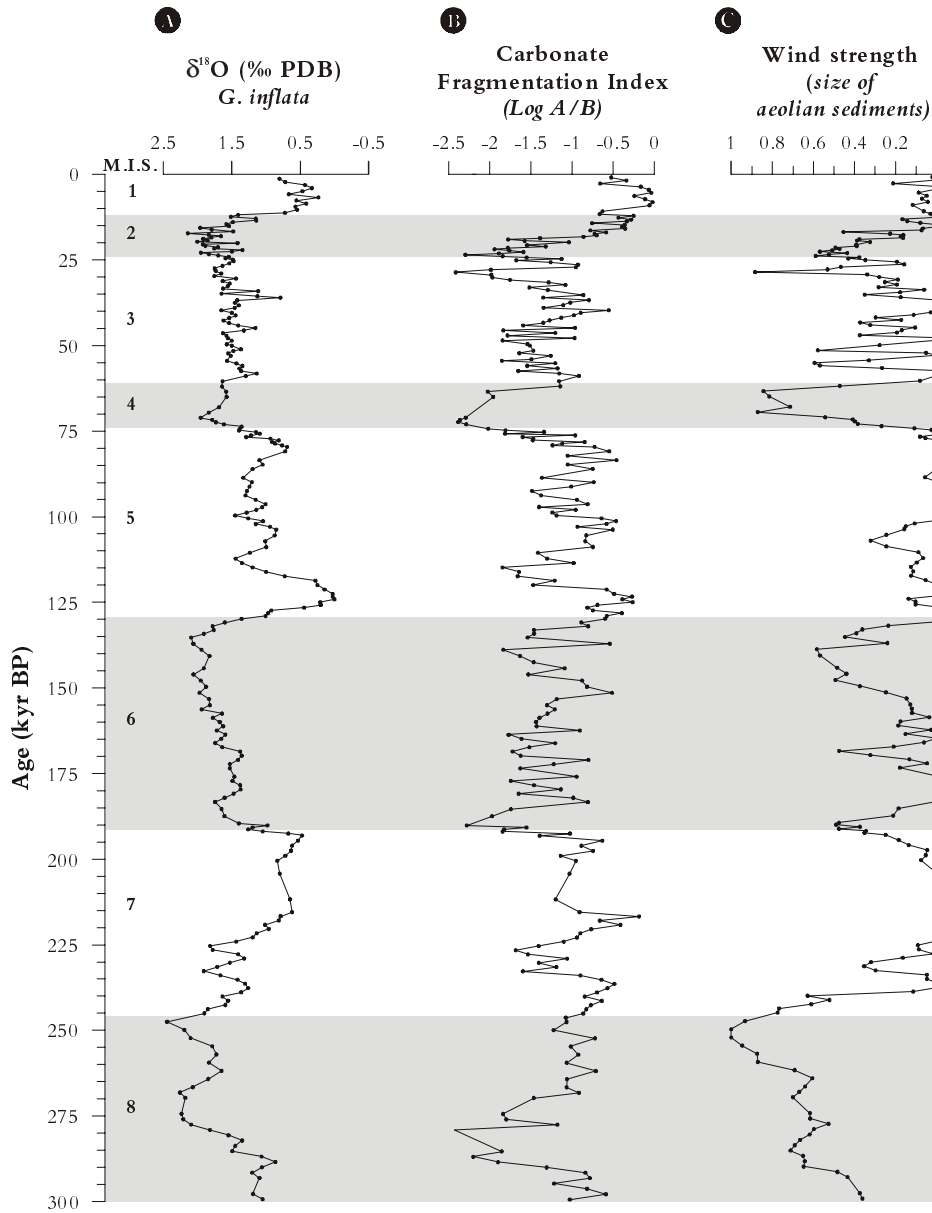


Figure 4.7. Wind-driven upwelling causes fragmentation. **A)** ^{18}O -curve of *G. inflata* in core MD962094 (Chapter 2), Marine Isotopic Stages (M.I.S.) after Martinson et al. (1987) are indicated. **B)** Log-ratio of the relative abundance of the coarsest two fractions of bulk sediments from core MD962094. Carbonate fragmentation increases to the left. **C)** Wind-strength curve derived from the grain size of wind-blown sediments.(Stuut et al., 2001, Chapter 5)

Carbonate dissolution, upwelling and trade-wind intensity

Stuut et al. (2001, Chapter 5) inferred changes in the trade-wind intensity from the grain size of eolian sediments in the same core (Figure 4.7C). The fragmentation index and the wind-strength record show a good correlation during the last 225 kyr, except in M.I.S. 5.4. Also M.I.S. 7 and 8 don't show a very good correlation. The good correlation supports the idea that carbonate fragmentation and dissolution are related to the trade-wind induced upwelling during the last 225 kyr in this area. The differences between the two records may result from the fact that upwelling is not always only wind induced (Ufkes et al., 2000). Besides, highest productivity and strongest upwelling do not always coincide, as was shown by comparison of proxies for palaeoproductivity and upwelling (Diester Haaß et al., 1985, Berger et al., 2001).

Summarising, the fragmentation of the foraminifera shells is caused by the dissolution of carbonate in the water column and on the seafloor. The dissolution is mirrored by the size distributions of the foraminifer nannofossil ooze and is described by the ratio of the coarsest two fractions. This ratio, or carbonate fragmentation index, can be constructed in a fast and reproducible way by analysing the size distribution of the bulk sediments. The carbonate dissolution is caused by trade-wind driven upwelling, and therefore, can be interpreted as an upwelling intensity record. This method may well be applicable in other areas in the world's oceans where sediments are carbonate rich.

Acknowledgements

We thank the crew and scientists aboard N.O. Marion Dufresne for their help with coring and sampling operations during IMAGES II. Geert-Jan Brummer and George Postma are thanked for their helpful suggestions to improve the manuscript. This work was financed by the NSG-NIOZ-Bremen co-operation.

5. A 300-kyr record of aridity and wind strength in southwestern Africa: inferences from grain-size distributions of sediments on Walvis Ridge, SE Atlantic.

Abstract

The terrigenous fraction of sediments recovered from Walvis Ridge, SE Atlantic Ocean, reveals a history of southwestern African climate of the last 300 kyr. End-member modelling of a data set of grain-size distributions (n=428) results in three end members. The two coarsest end members are interpreted as aeolian dust, the third end member as hemipelagic mud. The ratio of the two aeolian end members reflects the aeolian grain size and is attributed to the intensity of the SE trade winds. Trade winds were intensified during glacials compared to interglacials. Changes in the ratio of the two aeolian end members over the hemipelagic one are interpreted as variations in southwestern African aridity. Late Quaternary southwestern African climate was relatively arid during the interglacial stages and relatively humid during the glacial stages, owing to meridional shifts in the atmospheric circulation system. During glacials the polar front shifted equatorward, resulting in a northward displacement of the zone of westerlies, causing increased rainfall in southwestern Africa. The equatorward shift of the polar front is coupled with an increase of the meridional pressure gradient, leading to enhanced atmospheric circulation and increased trade-wind intensity.

Introduction

Terrigenous sediments deposited in the subtropical deep sea are a mixture of a pelagic component brought in by the wind and a hemipelagic component brought in by rivers and supplied from the shelf. Terrigenous sediments escaping from shelves are mainly deposited on the slope and rise by low-density turbidity currents and nepheloid-layer sedimentation. The flux of hemipelagic sediments is associated with continental runoff, thus providing a proxy for continental humidity (Prins & Weltje, 1999). The analysis of aeolian dust therefore, allows the estimation of aridity in aeolian source regions through flux determinations, and the intensity of the transporting winds through grain-size measurements (Rea, 1994). Aeolian sediments deposited in the deep sea close to the continent, are coarser grained than hemipelagic sediments (Koopmann, 1981; Sarnthein et al., 1981; Sirocko, 1991; Prins & Weltje, 1999). Thus, if the mixture of terrigenous sediments can be unmixed on the basis of the grain size of the different components, it can be used to reconstruct changes in continental climate.

In this study, we applied an inversion algorithm for end-member modelling of compositional data (Weltje, 1997) to the grain-size distributions from a core from Walvis Ridge. This method, developed for unmixing of multiple-sourced basin fills, is a powerful tool for the unmixing of grain-size distributions that are composed of sediment subpopulations, i.e. end members (Prins & Weltje, 1999; Prins et al., 2000b). Walvis Ridge is a NE-SW orientated volcanic ridge, extending from the North-Namibian coast to the Mid-Atlantic Ridge. Although the terrigenous sediment fraction makes up only a small part of the sediment that is dominantly composed of calcareous oozes, these land-derived components are likely to contain a significant proportion of aeolian dust owing to (1) the high altitude of the ridge relative to the surrounding sea floor (~2000 m) keeping off reworked sediments and turbidity currents from the continental slope, (2) its proximity to the Namib and Kalahari Deserts to the Southeast, and (3) the prevailing SE trade-wind system. Our objectives are (1) to unravel a late Quaternary (0–300 kyr) grain-size record of fine-grained terrigenous sediments from Walvis Ridge, (2) to attribute the reconstructed end members to the transport mechanisms of land-derived sediments, and (3) to use the results for the reconstruction of the paleoclimate evolution of southwestern Africa.

Previous reconstructions of southwestern African climate

There is a lack of knowledge on the nature of late Quaternary climate change within desert systems, which limits the knowledge of past environmental changes at low latitudes. Geomorphological studies have focussed on the origin of the Namib and Kalahari Deserts and their paleoclimate development through time, but continuous continental climate records from southwestern Africa are relatively scarce (Van Zinderen Bakker, 1976; Lancaster, 1984; Meadows, 1988; Rust & Vogel, 1988; Scott & Partridge, 1990; Heine, 1998; Stokes et al., 1998; Thomas et al., 2000). A number of proxies have been used to reconstruct climate history on the basis of terrestrial records: e.g. dune-crust orientation, speleothems, calcretes, fluvial and lake deposits, pollen and even molluscs (Van Zinderen Bakker, 1984b; Scott, 1989; Klein, 1991; Brook et al., 1996; Partridge et al., 1997; Partridge et al., 1999). Attempts were made to construct continuous records by stacking data from different sites and time intervals.

Unfortunately, owing to the effects of local conditions and dating uncertainties, records often contradict (Dreimanis et al., 1985; Shaw et al., 1988; Stokes et al., 1998; Thomas, 1999). In their compilation of southwestern African climate for the last 25 kyr, Cockcroft et al. (1987) conclude that the Last Glacial Maximum (LGM, ~18 kyr BP) in southern Africa was cooler and wetter than today. Brook et al. (1996) presented speleothem, tufa and sand-dune data that demonstrate the occurrence of several wet periods during the last 300 kyr. These wet periods occurred synchronously over the Southern African continent and show no clear glacial-interglacial pattern, in contrast to earlier findings by Cockcroft et al. (1987), Van Zinderen Bakker (1967) and Tyson (1986). A mechanism for increased humidity during glacials in southern Africa was presented by Van Zinderen Bakker (1967), and later corroborated by model studies of Tyson (1986). They concluded that the polar front must have been subject to N-S movements during the Late Quaternary. During glacials the front shifted equatorward, which resulted in a northward displacement of the climate zones, so that the zone of moist westerlies reached southwestern Africa, resulting in increased rainfall. During interglacial stages the polar front had shifted south, resulting in a poleward displacement of the climate zones.

The marine realm is favourable for the construction of uninterrupted paleoclimate records, since sedimentation is often continuous and age control can be obtained relatively easy using the oxygen-isotope composition of foraminifers (Imbrie et al., 1984; Martinson et al., 1987). A number of studies have concentrated on southwestern African paleoclimate by analysing fine-grained terrigenous sediments, pollen, freshwater diatoms and phytoliths transported to the ocean floor (Van Zinderen Bakker, 1984a; Diester-Haaf, 1985; Jansen & Van Iperen, 1991; Gingele, 1996; Shi & Dupont, 1997; Dupont et al., 1998; Shi et al., 1998; Shi et al., 2000). These studies showed that changes in the trade wind system and changes in southwestern African climate during the late Quaternary have had large effects on the transport of wind-blown and river-transported material to the SE Atlantic Ocean. However, there is no consensus on the southwestern African climate history. For example, Van Zinderen Bakker (1984b) concluded that no significant change in rainfall occurred in southwestern Africa during the last 18 kyr, whereas according to Shi et al. (1998) the LGM in this region was characterised by relatively cold and arid conditions. However, two years later the same authors (Shi et al., 2000) conclude that the region was influenced by northward movements of the winter-rain regime, causing increased rainfall during the LGM.

In summary, there is no consensus on the southwestern African climate history as yet, neither from land records, nor from marine records. In this study we evaluate the grain-size distributions of the terrigenous sediment fraction in Images II core MD962094 (Bertrand et al., 1996) from Walvis Ridge as a proxy for aridity and wind strength in southwestern Africa.

Materials and Methods

Core MD962094 was recovered from Walvis Ridge at 19°59,97 S / 9°15,87 E at 2280 m water depth (Figure 5.1). This 30.75 m long core fully covers the last ~650 kyr (Bertrand et al., 1996). The dominant lithology of the core is foraminifer nannofossil

ooze. The core was sampled at 2.5-cm intervals from the first 4.5 metres below sea floor (mbsf) and at 5-cm intervals from 4.5–14.7 mbsf, with two series of 10 ml syringes. These samples were used for stable oxygen-isotope analysis and for grain-size analysis.

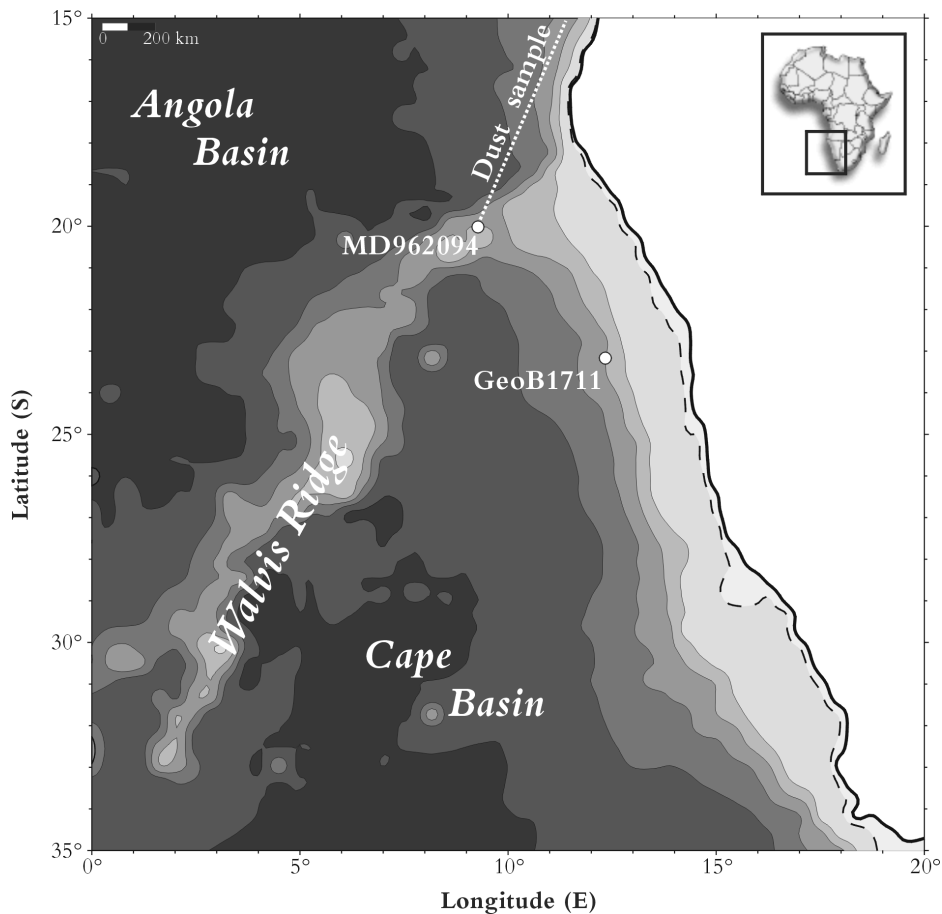


Figure 5.1. Locations of cores MD962094 and GeoB1711 (Little et al., 1997b) in the SE Atlantic Ocean. White dotted line: transect along which the present-day dust sample was collected. Bathymetry is shown in contour intervals of 1000 m. Annual rainfall is indicated in mm. Wavy lines: zone of wind driven coastal upwelling.

To separate the terrigenous sediment fraction for grain-size analysis, calcium carbonate, organic carbon and biogenic opal were carefully removed using repeatedly excess HAc-buffer (pH=4 at 20°C, see p 107 for a detailed description of this method), H₂O₂ (3% at 85°C) and NaOH (2M at 100°C for 25 minutes), respectively. Microscope analyses revealed that this method successfully removed all biogenic constituents. Grain-size analyses were carried out in the sedimentology laboratory, Utrecht University, on a

Malvern Instruments Mastersizer S using a lens with 300-mm focal length. This results in grain-size distributions from 0.05–814 μm in 64 size classes. Because the terrigenous sediment fraction from Walvis Ridge is fine-grained ($<100\ \mu\text{m}$, Figure 5.3A), the number of input variables for the end-member model is reduced from 64 to 34 size classes in the range 0.5–100 μm . To estimate the minimum number of end members required for a satisfactory approximation of the data, the coefficients of determination were calculated. The coefficient of determination represents the proportion of the variance of each grain-size class that can be reproduced by the approximated data. This proportion is equal to the squared correlation coefficient (r^2) of the input variables and their approximated values (Weltje, 1997; Prins & Weltje, 1999).

Present-day aeolian dust was collected along a transect (13°25'S / 12°04' E to 20°00'S / 09°15' E) off the Namibian coast (Figure 5.1) during the Images II expedition (Bertrand et al., 1996) using an Anderson dust sampler model GMWL 2000 which was located ~15 m above sea level. During the sampling period a SSW force 4Bft. wind prevailed. The dust was rinsed off the filter following the method described by Kiefert (1994) and Kiefert et al. (1996) using de-mineralised water instead of tri-Sodium orthophosphate (see p 109 for a detailed description of the method).

Eight to ten well-preserved and clean specimens of planktonic foraminifer *Globorotalia inflata* d'Orbigny were hand-picked under a binocular microscope from the 250–500 m fraction to achieve an analytical weight of 0.05 to 0.10 mg. The stable oxygen-isotope composition of *G. inflata* were measured with a Finnigan MAT 252 mass spectrometer at the Fachbereich Geowissenschaften in Bremen.

Age model

The oxygen-isotope record of *G. inflata* is correlated with the stacked record of Martinson et al. (1987) to obtain an age model for core MD962094 (Figures 5.2B and C). Correlation of the oxygen-isotope records was established using the software package Analyseries version 1.1 (Paillard et al., 1996). Twenty-two marine isotope events (MIE) were taken as calibration points for the age model. The final age model resulted from linear interpolation between the age-calibration points. The upper 14.7 m of the sediment record in core MD962094 appear to span the last ~300 kyr, i.e. marine isotope stages (MIS) 1 to 8. Assuming no hiatuses in sedimentation, the linear sedimentation rate varies between 2 and 12 cm/kyr (Figure 5.2D). MIE 7.5 was not recognised in the $\delta^{18}\text{O}$ curve as a single event. This phenomena is typical for the area (Schneider et al., 1996). Nevertheless, one isotope peak appears to coincide with MIE 7.5 in Martinson's curve (Figure 5.2C).

Results

The median grain-size record of the terrigenous fraction in core MD962094 is shown in Figure 5.3B. Median grain size varies between 3 and 7 μm . The grain-size record and the *G. inflata* $\delta^{18}\text{O}$ record show very similar patterns over time, albeit with a small phase difference, indicating relatively coarse-grained mud deposition during interglacial stages (MIS 1,3,5,7) and relatively fine-grained mud deposition during glacial stages (MIS 2,4,6,8).

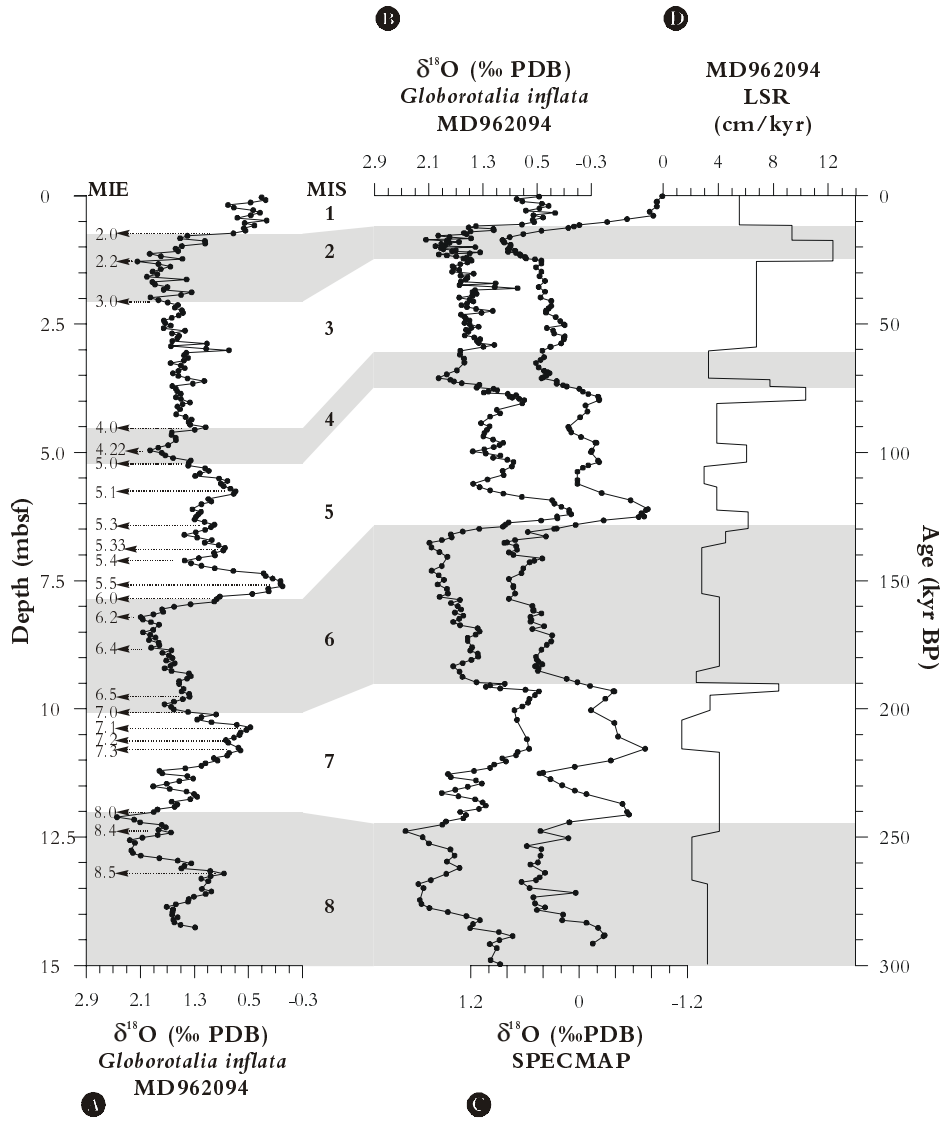


Figure 5.2. Age model. **A)** *Globorotalia inflata* $\delta^{18}\text{O}$ -record versus depth. Marine Isotopic Events (MIE) and Marine Isotopic Stages (MIS) after Martinson et al. (1987) are indicated. **B)** *Globorotalia inflata* $\delta^{18}\text{O}$ -record versus age. **C)** SPECMAP $\delta^{18}\text{O}$ -record after Martinson et al. (1987) **D)** Linear sedimentation rates (LSR).

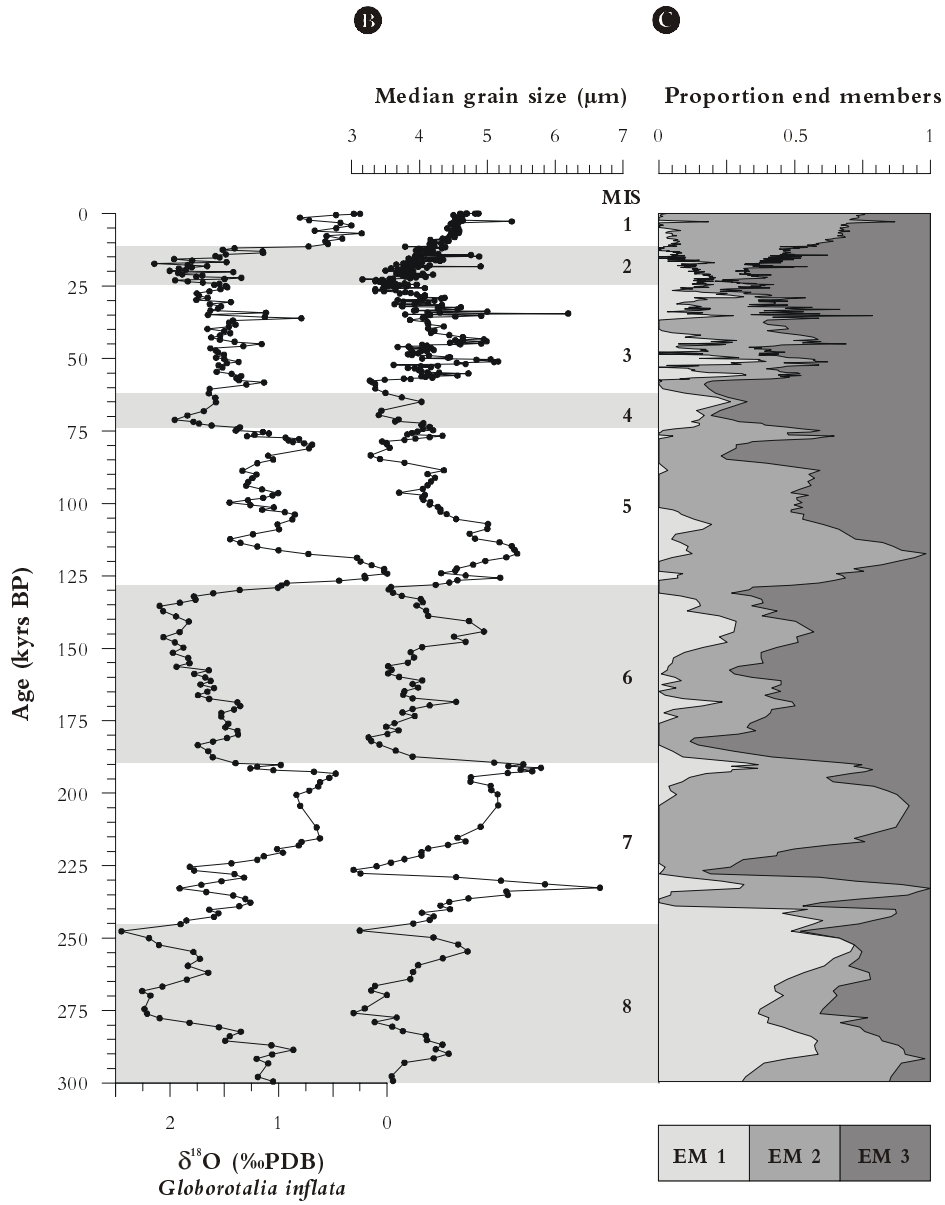


Figure 5.3. Time series of variations in median grain size and end member contributions of the terrigenous sediment fraction in core MD962094 compared with global climate. **A)** *Globorotalia inflata* $\delta^{18}\text{O}$ (‰ PDB). **B)** median grain size. **C)** End member contributions of the three end members.

The average grain-size distribution in core MD962094 has a modal grain size near 5 μm (Figure 5.4A). Figure 5.4B shows the coefficients of determination (r^2) plotted against grain size for models with 2 to 10 end members. The mean coefficient of determination of the grain-size classes increases when the number of end members increases (Figure 5.4C, page 73). The two end-member model ($r^2_{\text{mean}} = 0.62$) shows low r^2 (< 0.6) for the size ranges 4–8 μm and $>24 \mu\text{m}$. The three end-member model ($r^2_{\text{mean}} = 0.89$) shows low r^2 for the size range $>70 \mu\text{m}$ only. This coarse end is well reproduced by models with 5 or more end members only. For the choice of the number of end members, however, the coarse end ($>70 \mu\text{m}$) can be ignored because it comprises only less than 0.3% weight of the mass of the samples. The grain-size range $<10 \mu\text{m}$, on the contrary, should be well reproduced by the mixing model because this size range contains a considerable proportion of the sediment mass. The goodness-of-fit statistics thus demonstrate that the three-end-member model provides the best compromise between the number of end members and r^2 .

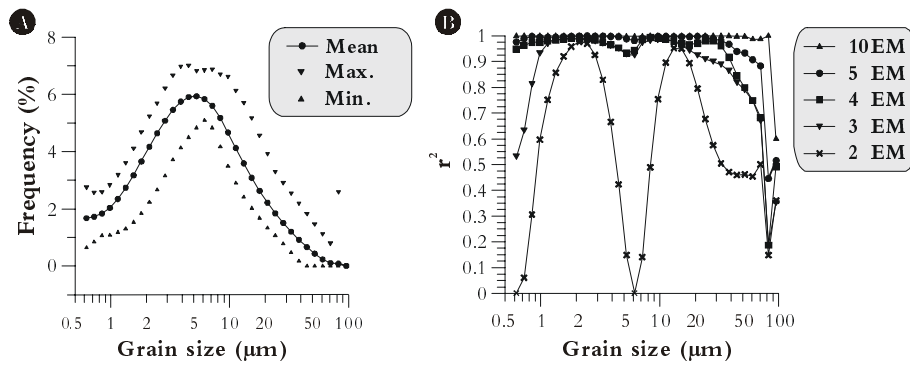


Figure 5.4. End-member modelling results of core MD962094. **A)** Summary statistics of input data (grain-size distributions, $n=428$); maximum, mean and minimum frequency recorded in each size class. **B)** Coefficients of determination (r^2) for each size class of models with 2–10 end members.

The grain-size distributions of the three end members are shown in Figure 5.4D. All end members have a clearly defined dominant mode. End member EM1 has a modal grain size of $\sim 13 \mu\text{m}$, end member EM2 of $\sim 7 \mu\text{m}$ and end member EM3 has a modal grain size of $\sim 4 \mu\text{m}$. The down-core record of the relative contributions of the end members is shown in Figure 5.3C. End member EM1 varies between 0–70 %, EM2 between 0–90 % and EM3 between 0–80%.

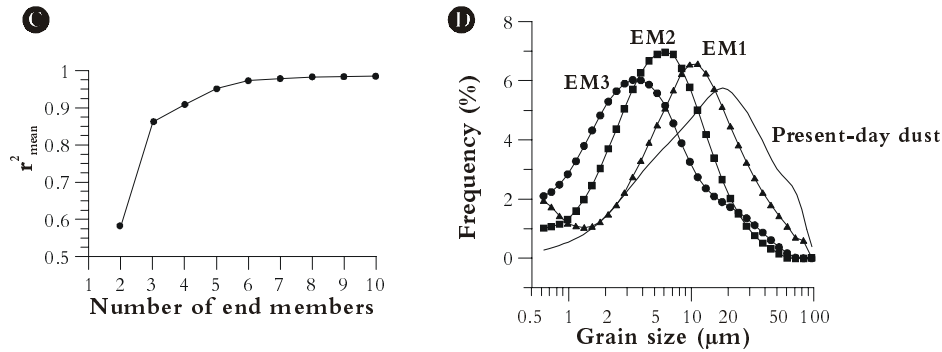


Figure 5.4 (continued). End-member modelling results of core MD962094. **C)** Mean coefficient of determination (r^2_{mean}) of all size classes for each end-member model. **D)** Modelled end members of the terrigenous sediment fraction of sediments from Walvis Ridge. For comparison the grain-size distribution of the present-day dust sample, collected along the transect shown in Figure 5.1, is plotted.

Late Quaternary southwestern African aridity and trade-wind intensity

Aeolian sediments deposited in the deep sea close to the continent, are coarser grained than hemipelagic sediments. Terrigenous sediments with median grain size larger than $6\mu\text{m}$ are generally attributed to aeolian transport, and smaller than $6\mu\text{m}$ to hemipelagic transport. This is based on deep-sea sediment studies (Koopmann, 1981; Sarnthein et al., 1981; Sirocko, 1991; Prins & Weltje, 1999; Prins et al., 2000a) as well as sediment-trap studies (Clemens, 1998; Ratmeyer et al., 1999). As a consequence, EM1 and EM2 are considered of aeolian, and EM3 of hemipelagic origin. The aeolian character of EM1 and EM2 is corroborated by the agreement of the grain-size distributions of EM1 and EM2 with the present-day aeolian dust sample (Figure 5.4D). The grain-size distribution of the present-day dust is somewhat coarser probably due to the fact that it was collected along a transect from the coast to core site (see Figure 5.1). End member EM3 is interpreted as hemipelagic mud, settled out of suspension from nepheloid layers. The nepheloid layers that produced EM3 may originate from the ephemeral rivers draining the Central Namib Desert or the Orange River, and be transported northward by the Benguela Current (Diester-Haas et al., 1988). We can not exclude potential nepheloid layers from the Cunene River that may be transported southward by tongues of the Angola-Benguela Front (Bremner & Willis, 1993). If nepheloid-layer formation is related to sea-level lowering, it may have an effect on the proportion of EM3 in the sediments. However, we assume that continental runoff dominates the supply of hemipelagic mud, and together with the flux of aeolian dust determines the aridity record.

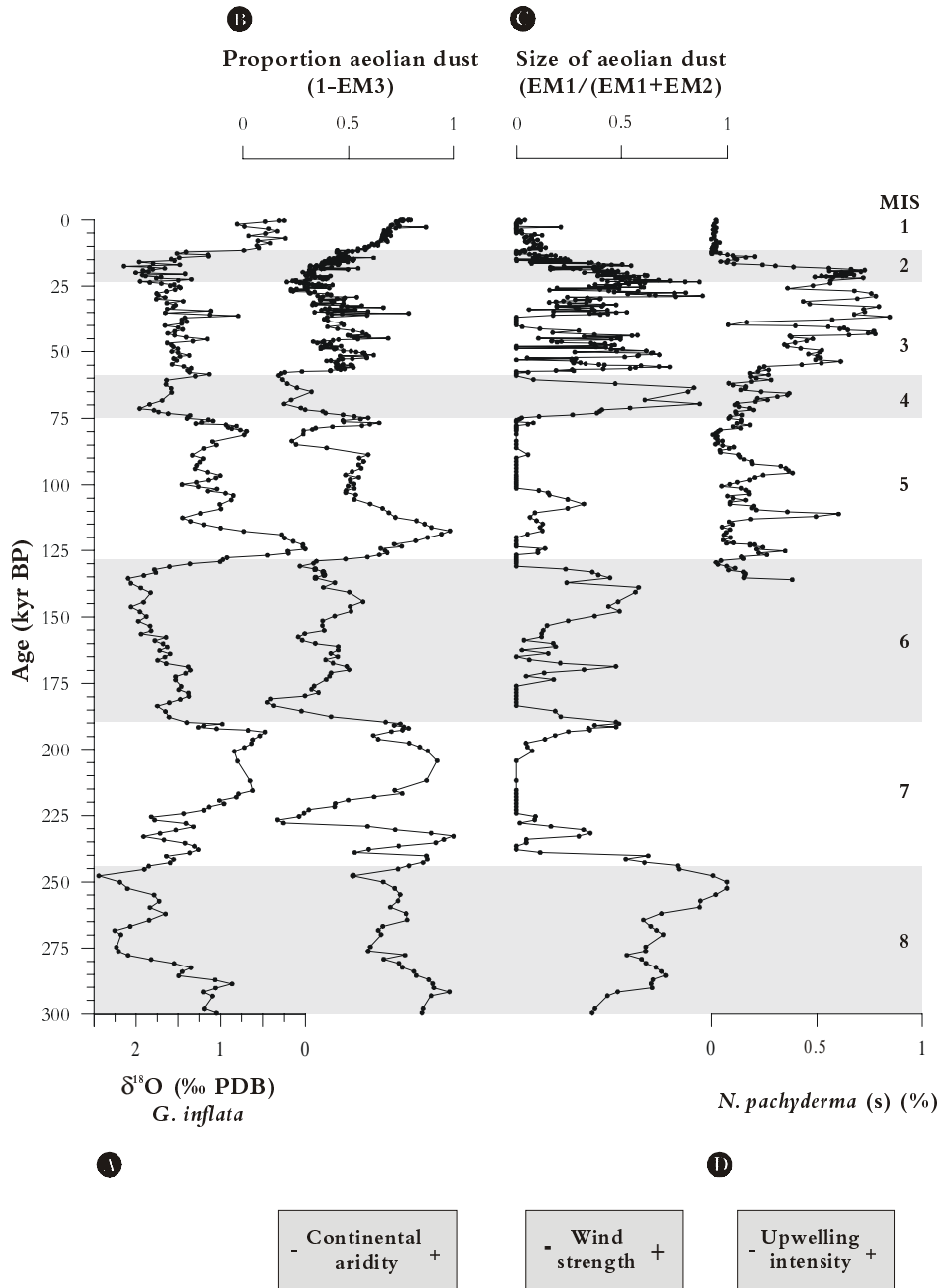


Figure 5.5. Reconstructions of Late Quaternary aridity and trade-wind strength in southwestern Africa. **A**) $\delta^{18}\text{O}$ record of *Globorotalia inflata*. **B**) The proportion of the aeolian end members are used as a proxy for continental aridity. **C**) The ratio of coarse over fine aeolian dust is used as a proxy for SE trade-wind intensity. **D**) Relative abundance of the planktonic foraminifer *Neogloboquadrina pachyderma* (s) in core GeoB 1711 reflects Benguela-upwelling intensity (Little et al., 1997b).

Considering the interpretation of the three-end-member model, changes in the ratios of the end members reflect paleoclimate variations in SW Africa. The proportion of the aeolian end members (1-EM3) is interpreted to represent continental aridity. The aridity record indicates relatively arid climate conditions during interglacials and relatively humid conditions during glacials (Figure 5.5B). The ratio of the coarse over the fine aeolian end member ($EM1/(EM1+EM2)$), reflecting the aeolian grain size, is interpreted as a measure of the intensity of the southeastern trade winds, that is the transport agent of the aeolian dust. The record indicates that the trade winds were intensified during glacials compared to interglacials (Figure 5.5C).

Partridge et al. (1997) reported an astronomical driving mechanism for South African climate. They constructed a 200-kyr southern-African rainfall record on the basis of textural and compositional changes of crater-lake sediments in northern South Africa. This rainfall record, predominated by the precessional cyclicity, correlates well with 30°S January insolation changes, and reflects humid monsoons during the periods with maximum austral summer insolation. In the western part of South Africa however, climate variability is regulated by the shifts of the climate belts connected to the movements of the polar front (Van Zinderen Bakker, 1967; Tyson, 1986). During glacial periods the polar front moved equatorward, resulting in a northward shift of the winter-rainfall belt, causing increased precipitation in southwestern Africa (Shi et al., 2000). The northward displacement of the polar front is coupled with an increase in the meridional pressure gradients, resulting in intensified SE trade winds. The apparent asynchrony of Late Quaternary aridity changes in the western and eastern part of southern Africa can be explained by regional variations in the aridity forcing mechanisms: precipitation in the western part is controlled by the winter rain regime associated with the westerlies, whereas precipitation in the eastern part is controlled by the summer monsoon system (Partridge et al., 1997). Our proxy records for continental aridity and trade-wind strength indeed show that glacial periods are characterised by increased wind strengths and decreased aridity. OIS 8 in particular shows a very high proportion of EM1. Whether this is caused by unusual windy conditions has to be proven by records from other cores.

The paleo-wind strength record of core MD962094 (Figure 5.5C) shows a similar variability compared to the record of the cold-water foraminifer *Neogloboquadrina pachyderma* (s) in core GeoB 1711 from the eastern Cape Basin (Little et al., 1997a, Figures 5.1 and 5.5D). The relative abundance of this species is considered a proxy for trade-wind induced upwelling (Little et al., 1997a; Little et al., 1997b; Ufkes et al., 2000). Although the correlation between the two high frequency records is not perfect, owing to imperfections in the age models of the two cores, it corroborates with the interpretation of end members EM1 and EM2. The differences between these records may also arise from the fact that peaks in the *N. pachyderma* (s) curve may be influenced by changes in the quality of the upwelled waters, not related to trade-wind intensity (Maslin et al., 2000).

Another possible transport mechanism for the aeolian dust deposited Walvis Ridge is the so-called berg winds. Berg winds are catabatic winds, generally blowing from the NE, supplying large amounts of aeolian dust into the SE Atlantic Ocean (Shannon &

Anderson, 1982). The possible interplay between berg winds and trade winds can not be discerned from our grain-size record. However, berg winds are local phenomena and are intermittent on an annual timescale. If they occur they blow for a few weeks only, whereas the SE trades are a year-round feature. Therefore, we assume that the aeolian dust deposited on Walvis Ridge has been supplied by the SE trade winds. Possible changes in trade wind zonality can not be derived from our proxy records either. Changes in the zonality of the SE trade winds could possibly result in changes in wind stress driving the Benguela upwelling system, as well as in changes in the composition of the wind-blown material transported to the Walvis Ridge. Thus, provenance studies of the aeolian sediments on Walvis Ridge are needed to reconstruct changes in the zonality of the SE trade winds and possible contributions of aeolian dust supplied by the berg winds.

Conclusions

- Three end members are recognised in the grain-size distributions of core MD962094 from Walvis Ridge, using an end-member modelling algorithm. The two coarsest end members are interpreted as ‘coarse’ and ‘fine’ aeolian dust, the third end member is interpreted as hemipelagic mud, deposited from nepheloid layers.
- Variations in the proportion of the aeolian end members reflect variations in aridity in southwestern Africa. The ratio of the two aeolian end members reflects the aeolian grain size. Changes in this ratio are interpreted to reflect changes in the intensity of the SE trade wind.
- The aridity record shows relatively arid climate conditions during interglacial stages and relatively humid climate conditions during glacial stages. The apparent asynchrony of Late Quaternary aridity changes in the western and eastern part of southern Africa can be explained by regional variations in the aridity forcing mechanisms: precipitation in the western part is controlled by the winter rain regime associated with the westerlies, whereas precipitation in the eastern part is controlled by the summer monsoon system (Partridge et al., 1997).
- The wind-strength record shows intensified trade winds during glacials compared to interglacials, and shows a similar variability compared to the upwelling-intensity record of Little et al. (1997b).

Acknowledgements

We thank the crew and scientists aboard N.O. Marion Dufresne for their help with coring and sampling operations during IMAGES II. We also thank M. Reith (Utrecht University) for analytical support, and M. Segl and B. Meyer-Schack (Universität Bremen) for carrying out the oxygen-isotope measurements. J. Compton, J. Giraudeau and an anonymous reviewer are thanked for their helpful suggestions to improve the manuscript. This work was financed by the NSG-NIOZ-Bremen co-operation. This is Netherlands Research School of Sedimentary Geology (NSG) publication number 20001105.

6. Palaeo- wind strength and aridity based on the terrigenous fraction of sediments from the continental margin offshore Walvis Bay, SE Atlantic.

Abstract

The grain-size distributions of the terrigenous sediment fraction from continental margin sediments offshore Walvis Bay (core MD962097) can be unmixed into three grain-size populations. These populations are interpreted as coarse- and fine aeolian dust and fluvial mud. The ratio of the proportion fluvial fraction and the aeolian fractions is taken as a measure for continental aridity. The ratio of the proportion coarse aeolian dust over fine aeolian dust is considered a measure of the aeolian sediment size, which is related to wind strength. The aeolian populations are compared with a present-day dust sample of the same locality. Downcore variation in aridity and wind strength has been studied in detail for three intervals in core MD962097: i.e. 236-198 kyr BP, 146-119 kyr BP and 36-18 kyr BP. The variation has been compared with similar records from Walvis Ridge (core MD962094) and with pollen data from core GeoB 1711. The aridity and wind strength records from the three cores are in good agreement with each other. The synchronous increased trade-wind intensities and increased precipitation during glacials in southwestern Africa are related to an equatorward shift of the zone of southern Westerlies during glacials.

Introduction

Analysis of the grain-size distributions of the terrigenous (CaCO_3 , C_{org} and biogenic opal-free) fraction of sediments from Walvis Ridge core MD962094 resulted in three end members that were interpreted as coarse- and fine aeolian dust and fluvial mud (Chapter 5). Although the sediments from this core were shown to be representative for the sediments in this part of the Southeastern Atlantic Ocean (Chapter 2), the interpretation of these end members suffers from a lack of spatial control. If the sediments on Walvis Ridge are a mixture of aeolian and fluvial sediments, the Cape-Basin sediment must also contain a record of temporal changes in continental aridity and wind strength, through changes in the contribution of aeolian and fluvial sediments. A downwind gradient in the size of the aeolian sediments is expected throughout the Cape Basin, owing to the efficient size selectivity of the wind (Hesse, 1994; Kiefert, 1994; McTainsh et al., 1997; Nickling et al., 1999). Therefore, lateral changes in the aeolian end members should be observed in cores throughout the Cape Basin parallel to the southeastern trade winds. The terrigenous sediment fraction of a sediment core (MD962097) from offshore Walvis Bay (Figure 6.1) was studied to test the interpretation of the end members.

Three time slices were sampled from core MD962097 (offshore Walvis Bay, Figure 6.1), on the basis of characteristic peaks in the aridity and wind-strength records from core MD962094. Due to the proximal position of this core relative to the source of aeolian dust, coarser aeolian end members are expected. Little change is expected for the fluvial end member.

Materials and Methods

Sediment cores

Core MD962094 was recovered from Walvis Ridge at 19°59,97 S / 9°15,87 E at 2280 m water depth (Figure 6.1). This 30.75 m long core fully covers the last ~650 kyr (Bertrand et al., 1996). The dominant lithology of the core is foraminifer nannofossil ooze. The upper 15 m of the core cover the last 300 kyr (Chapter 2). Core MD962097 was recovered from Walvis Slope at 23°23,17 S/11°58,60 E at 2662 m water depth (Figure 6.1). This 31.57 m long core fully covers the last ~500 kyr (Bertrand et al., 1996) except for a hiatus from 4.65 – 6.00 mbsf. The dominant lithology of the core is nannofossil ooze with some foraminifer ooze, containing variable amounts of biosiliceous components (radiolarians, diatoms and silicoflagellates).

Age models

The age model of core MD962094 is based on the correlation of the $\delta^{18}\text{O}$ curve of the planktonic foraminifer *Globorotalia inflata* and 5 additional AMS ^{14}C dates (Chapter 2). The age model of core MD962097 was constructed from correlation of the Fe records of this core with the one from core MD962094 (Chapter 2 and Figure 6.2).

Grain size

Core MD962094 was sampled at 2.5-cm intervals from the first 4.5 m and at 5-cm intervals from 4.5–14.7 metres below sea floor (mbsf), with two series of 10 ml syringes.

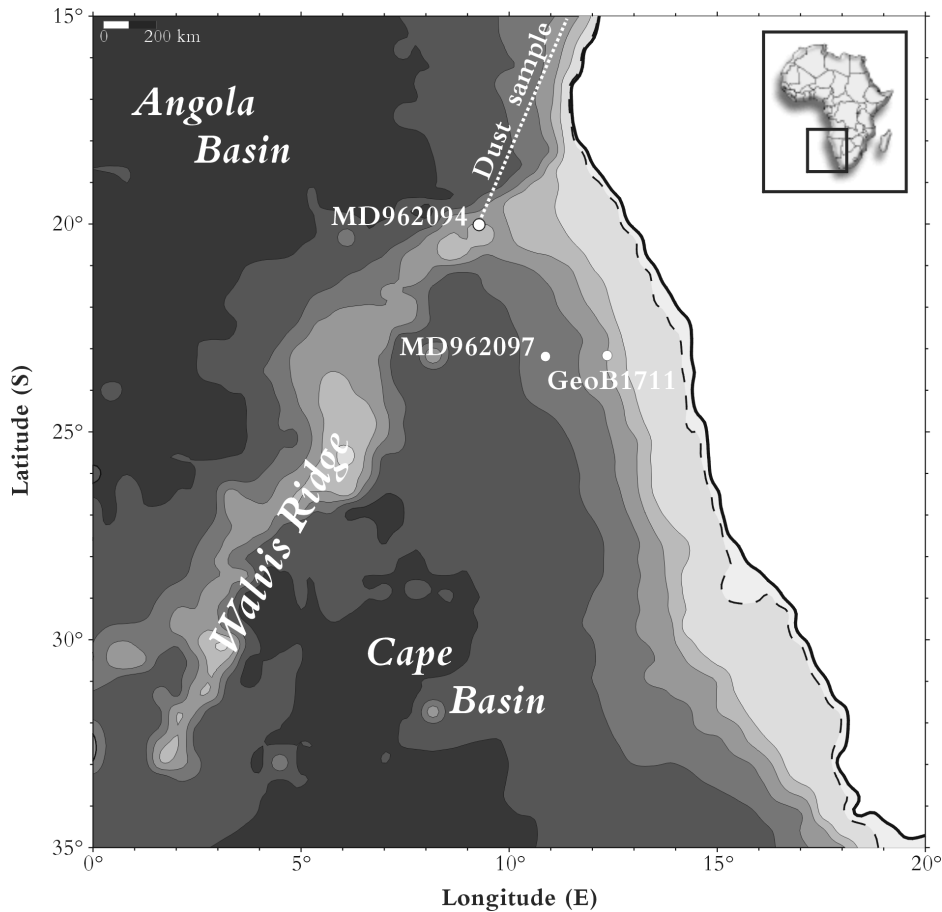


Figure 6.1. Location of cores MD962094, MD962097 and GeoB1711 in the SE Atlantic Ocean. White dotted line: transect along which the present-day dust sample was collected. Bathymetry is shown in contour intervals of 1000 m, the 125-m isobath is presented as a dotted line.

One series of samples was used for the stable oxygen-isotope analyses to construct the age model of the core (Chapter 2), the other series of samples was used for the grain-size analyses (Chapter 5). Three sections of core MD962097 from 153–349, 902–1046 and 1352–1452 cmbsf (indicated in Figure 6.2) were sampled at 4-cm intervals for the comparison with the grain-size results from core MD962094. These time slices were chosen for their characteristic high-amplitude peaks in the aridity and wind-strength records (Figure 6.4). To separate the terrigenous sediment fraction for further analysis, calcium carbonate, organic carbon and biogenic opal were carefully removed using repeatedly excess HAc-buffer (pH=4 at 20°C, see p 107 for a detailed description of this method), H₂O₂ (3% at 85°C) and NaOH (2M at 100°C for 25 minutes), respectively. Microscope analyses revealed that this method successfully removed all biogenic constituents from the Walvis Ridge sediments (Chapter 5). The sediments

from the Walvis Slope, however, contain more biosiliceous components so that the treatment with NaOH had to be extended to 45 minutes for four samples. Grain-size analyses were carried out in the sedimentology laboratory, Utrecht University, on a Malvern Instruments Mastersizer S using a lens with 300-mm focal length. This results in grain-size distributions from 0.05–814 μm in 64 size classes.

End-member model

The grain-size data from the three time slices from core MD962097 were combined to make one data set of 128 grain-size distributions, to which the end-member model (Weltje, 1997) was applied. The minimum number of end members required for a satisfactory approximation of the data is estimated through calculation of the coefficients of determination. The end-members that result from the three end-member model of the three time slices from core MD962097 are then compared with the end-member results of the complete record of core MD962094.

Results

End-member model

The average grain-size distribution of the terrigenous sediment fraction in core MD962097 has a modal grain size near 5 μm (Figure 6.3A). Because the terrigenous sediment fraction in the studied cores is fine-grained (<100 μm , Figure 6.3A), the number of input variables for the end-member model was reduced; we modelled 34 size classes in the range 0.5–100 μm . For end-member models consisting of two to ten end members, the coefficients of determination (r^2) per size class were calculated (Figure 6.3B). The mean coefficient of determination of the grain-size classes increases when the number of end members increases (Figure 6.3C). The inflection point of this curve (at $r^2_{\text{mean}}=0.88$) indicates the optimum combination of the number of end members and the goodness of fit of the data. Consequently, three end members are chosen to describe the variance in the data set (Figure 6.3D). Like in core MD962094, these end members are interpreted as coarse aeolian dust, fine aeolian dust and fluvial mud. The grain-size distributions of the two finest end members from core MD962097 have a clearly defined dominant mode. End member EM3 has a modal grain size of ~ 2.5 μm , and end member EM2 of ~ 7 μm . End member EM1 has a bimodal grain-size distribution with modes at ~ 3 and 27 μm . In core MD962094 the coarse aeolian and fluvial end members co-varied through the major part of the last 300 kyr (Figure 5.3C). This is also the case in the three time slices from core MD962097. However, because the coarsest and finest end members co-vary through the three time slices, the end-member model is not able to separate these end members adequately, which also explains why the coarse tail appears in the size distribution of the finest end member EM3 (Figure 6.3D). Comparison of the end members from the two cores (Figure 6.4A) shows similarity of the finest end members (EM3) and the intermediate end members (EM2) from the two cores. The coarsest end members (EM1) from the two cores differ significantly; the one from core MD962094 is a normal distribution whereas the one from core MD962097 is bimodal. Importantly, the coarsest end member in core MD962097 is also considerably coarser compared to the one in core MD962094.

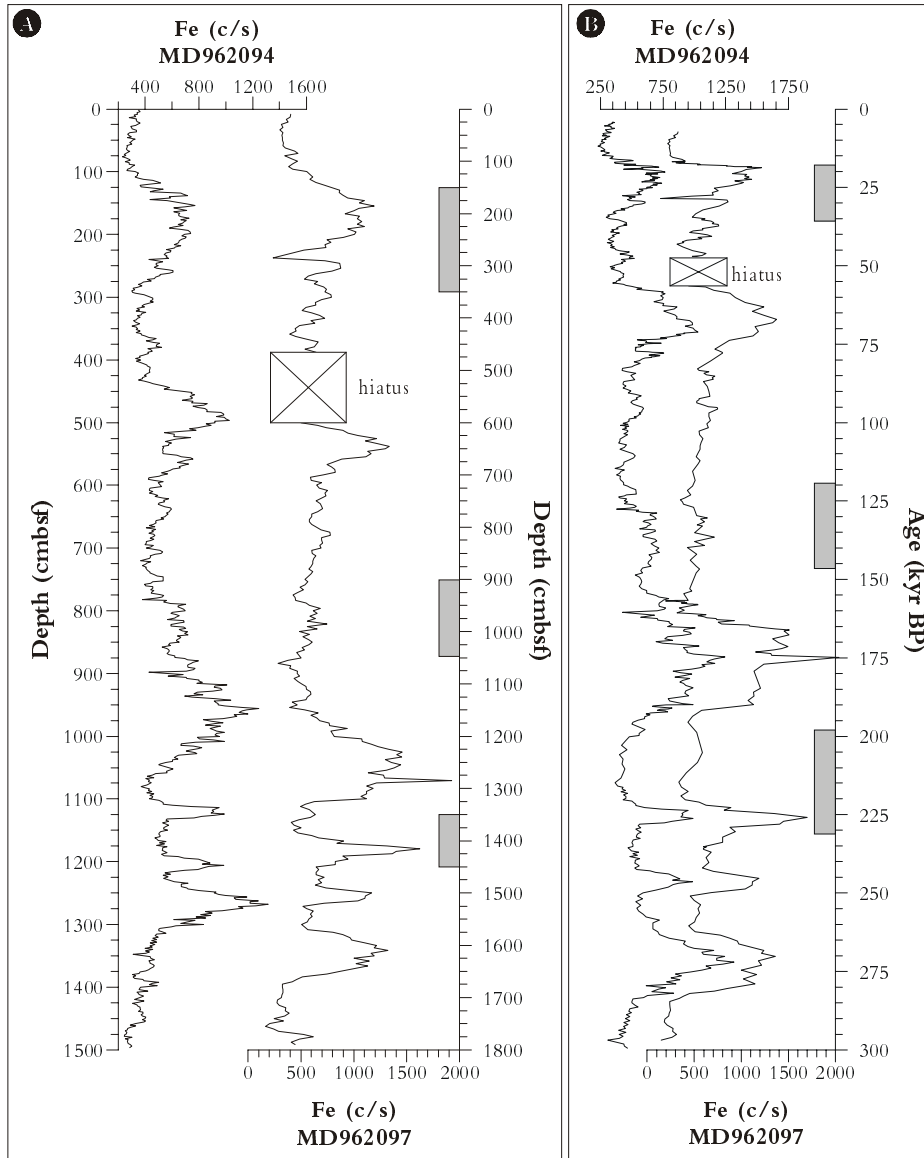


Figure 6.2. Age model of the last 300 kyr BP. **A**) Fe (c/s) records versus depth. **B**) Fe (c/s) records versus age. The age model of core MD962097 was established by correlation of the Fe records using the software package Analysis version 1.1 (Paillard et al., 1996). Sampled time slices are indicated with shaded bars.

Discussion

Interpretation of the end members

The bimodality of the coarsest end member in core MD962097 can have two different origins. It either represents a mix of both the coarsest and finest end members that was

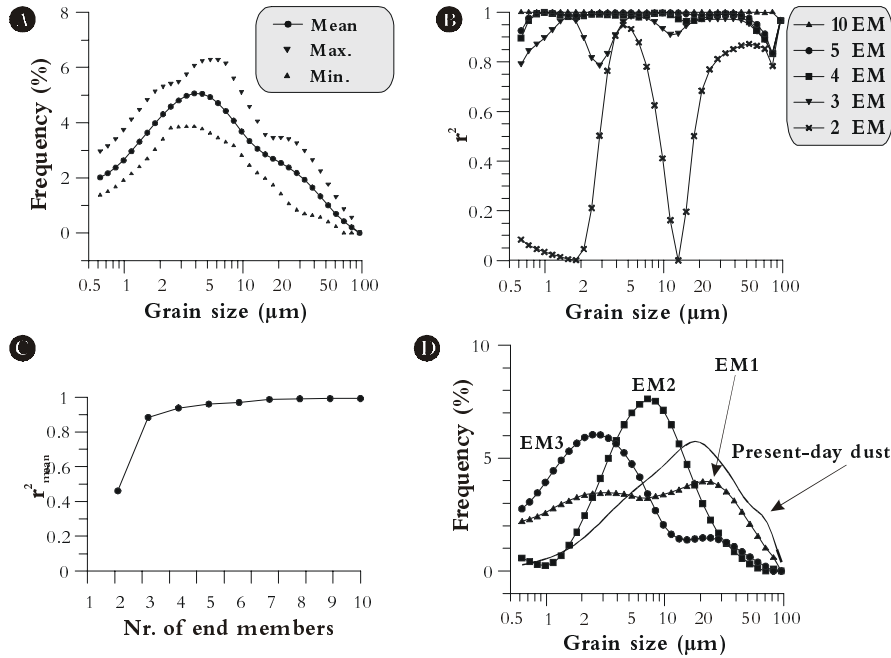


Figure 6.3. End-member modelling results of three time slices from core MD962097. **A)** Summary statistics of input data (grain-size distributions, $n=428$); maximum, mean and minimum frequency recorded in each size class. **B)** Coefficients of determination (r^2) for each size class of models with 2-10 end members. **C)** Mean coefficient of determination (r^2_{mean}) of all size classes for each end-member model. **D)** Modelled end members of the terrigenous sediment fraction of sediments from Walvis Slope. For comparison the grain-size distribution of the present-day dust sample, collected along the transect shown in Figure 5.6, is shown.

not separated well by the inverse model, or it is real and represents a bimodal aeolian fraction. We think the bimodality is best explained by the fact that the coarsest and finest end members occur simultaneously throughout the three time slices. This is also the case for the coarsest and finest end members in the same time slices in core MD962094 (Figure 5.3C), which however, could be distinguished on the basis of the rest of the core. To test if the synchronous occurrence of these two end members in the three time slices in both cores causes the bimodal coarsest end member, the end-member model was applied to a data set consisting of samples from the two cores in these particular time slices. This exercise resulted in three end members that are exactly the same as those modelled for the three time slices of core MD962097 separately (Figure 6.3D).

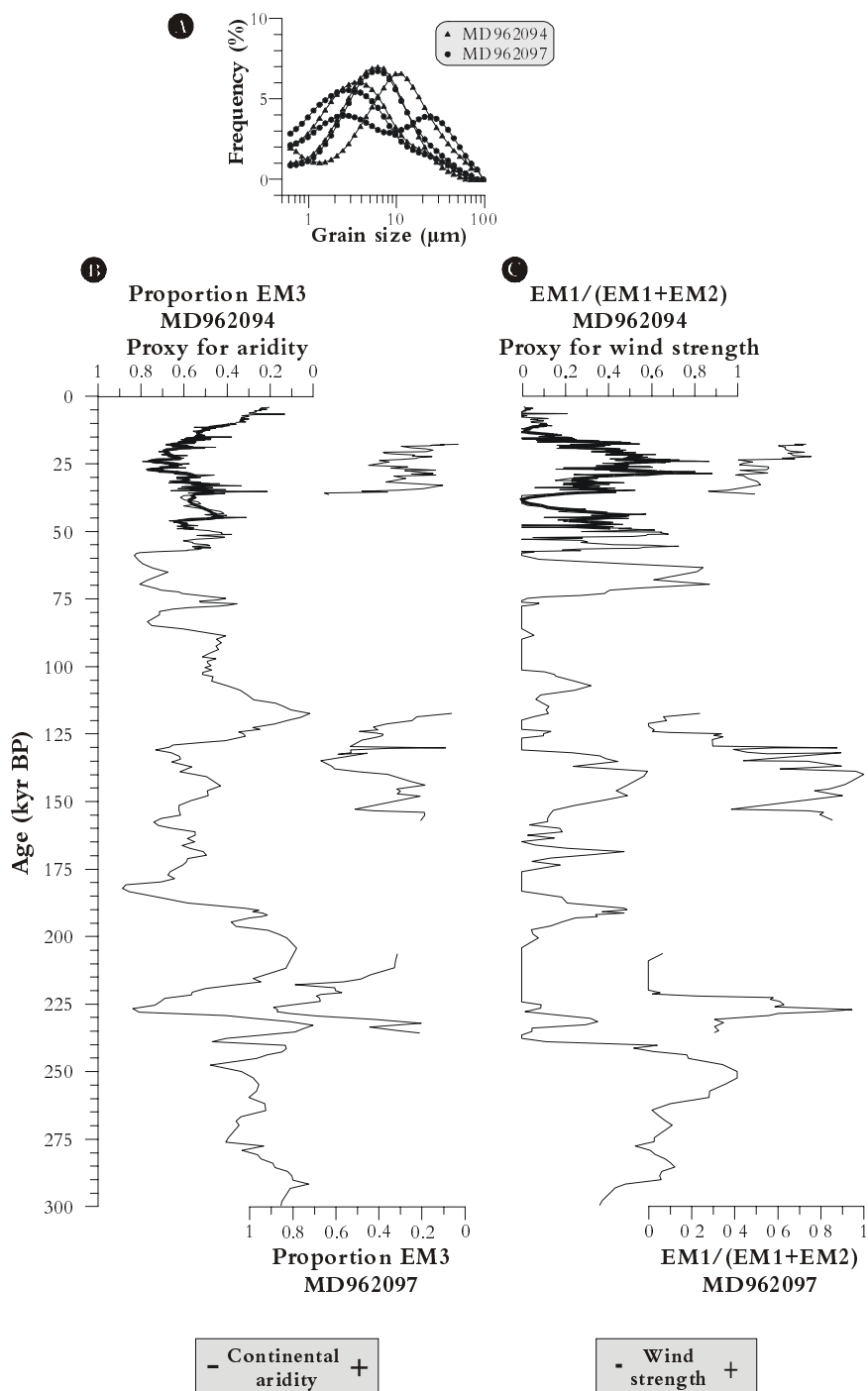
The fact that the coarsest end member is coarser in core MD962097 than in core MD962094 (Figure 6.4A) is attributed to the proximal position of this core relative to the source area of the dust and the dominant southeastern trade winds that carried the aeolian dust to the core site. In inferring wind strength from aeolian particle-size distributions it must be assumed that the dust is sorted by the transporting wind.

Therefore, the coarseness of the distribution is dependent on the distance from the source and the strength of the wind (Hesse, 1994). The interpretation of the end members is supported by the size distribution of the present-day dust sample (Figure 6.3D). This sample can be constructed by mixing the fine aeolian and coarse aeolian (without the fine mode) end members found in core MD962097. Due to the relatively low dust concentrations at the time of dust collection, the present-day dust sample was collected along a transect from the coast to the core site (see Figure 6.1). Therefore, it contains both the coarser fraction close to the source of dust and the finer fraction from more remote areas. During the sampling period a SSW force 4Bft. wind prevailed.

The ratio of the coarse over the fine aeolian end member ($EM1/(EM1+EM2)$) from core MD962097, is considered a measure of the intensity of the southeastern trade winds. The downcore ratio of the two aeolian end members over the fluvial one is considered a measure of continental aridity. The wind-strength and aridity records for the three time slices resemble those in the downcore record of core MD962094 (Figures 6.4B & C). Especially the lower two intervals of wind-strength and aridity appear to resemble those from core MD962094 well. The top interval of the MD962097 record (36–18 kyr) shows a less obvious correlation that could be caused by the large resolution differences between the two cores in both the CORTEX and grain-size results. A five-point moving average smoothing of the MD962094 records does not make the correlation more obvious either.

A 135-kyr wind strength record was presented by Shi et al. (2001). They interpreted the observed variations in the pollen fluxes in core GeoB 1711–4 (See Figure 6.1 for location) as changes in strength and zonality of the southeastern trade winds. Their pollen-flux record indicates relatively stronger wind intensities during glacials than during interglacials. During oxygen-isotope stage three however, there is a mismatch between the total pollen flux and upwelling (Shi et al., 2001, their figure 3). They used both a SST record (Kirst et al., 1999) and a left-coiling *N. pachyderma* record (Little et al., 1997) to deduce enhanced trade-wind driven upwelling, whereas the total pollen flux is low, indicating low trade-wind intensity. Shi et al. (2001) interpreted these discrepancies as a change in the zonality of the trade winds to a more southerly direction. During this period the winds simply wouldn't have blown over the Namib Desert, explaining the lack of pollen, but Ekman pumping would have caused intensified coastal upwelling. Our aridity record shows that this period is characterised by relatively humid intervals occurring synchronously with increased trade-wind intensities (Figure 6.4B). The pollen records of Shi et al. (2001) show that these events are also characterised by high influxes of *Restionaceae* (Shi et al., 2001, their figure 2), a pollen type that originates from the Fynbos vegetation, at present restricted to the winter-rain region of the Cape Province. This pollen type indicates increased precipitation (>200 mm/year, Shi et al., 2001). Hence, although they don't interpret them as such, the data presented by Shi et al. (2001) show that the periods that are characterised by increased pollen flux owing to increased wind intensities are also characterised by enhanced fluxes of pollen that indicate increased humidity. The synchronous occurrence of increased wind strengths and increased humidity was related to a shift in the latitudinal position of the zone of southern Westerlies (Stuut et al., 2001, Chapter 5). An equatorward shift of the frontal zones during glacials related to

Chapter 6



An equatorward shift of the frontal zones during glacials related to the expansion of the Antarctic ice sheet (Heusser, 1989; Brathauer & Abelmann, 1999; Kanfoush et al., 2000), would increase the latitudinal pressure gradients, leading to increased atmospheric circulation. Besides, the equatorward shift of the moisture-bearing Westerlies would enlarge the area of Southwestern Africa that is exposed to the winter rains. The synchronous increase of pressure gradients and equatorward shift of the southern Westerlies would also explain the increase of the total pollen flux and the increase of *Restionaceae*-flux during periods of intensified cooling in Antarctica (Shi et al., 2001). The relation between Antarctic cooling and atmospheric circulation in southwestern Africa will be discussed further in chapter 7.

Southeastern trades and Berg winds

At present, the trade winds carry large amounts of dust to the southeastern Atlantic Ocean (Figure 6.5A). Owing to the South Atlantic Anticyclone that is situated at 0–10°W/30–33°S during austral summer and at 5–15°W/25–30°S during austral winter (Tyson, 1986), the southeastern trade winds predominate throughout the year as the major feature of surface airflow over the southeastern Atlantic Ocean. However, at present the southeastern trade winds are not the only wind system that carries aeolian dust to the Atlantic Ocean. During austral winter, so called berg winds occasionally occur (Shannon & Anderson, 1982; Bremner & Willis, 1993). These katabatic winds, blowing from the northeast, carry sediments from the dry riverbeds into the Atlantic Ocean (Figure 6.5B). The interplay between berg winds and trade winds cannot be discerned from our grain-size record. We consider the importance of berg winds minor, because berg winds are local phenomena that are intermittent on an annual timescale. If they occur, they blow for a few weeks only, whereas the SE trades are a year-round feature. Another argument to disregard the influence of the berg winds is the coastal upwelling that occurs offshore Namibia. Therefore, we conclude that the bulk of the aeolian dust, recorded in cores MD962094 and MD962097 was transported by the southeastern trade winds. The downcore changes in the ratio of the aeolian end members thus reflect variation in the southeastern trade-wind intensity. Changes in the zonality of the trade winds cannot be derived from our proxy records. Changes in the zonality of the SE trade winds could possibly result in changes in wind stress driving the Benguela upwelling system (see for example Shi et al., 2001), as well as in changes in the composition of the wind-blown material transported to the Walvis Ridge. Thus, provenance studies of the aeolian sediments on Walvis Ridge are needed to reconstruct changes in the zonality of the SE trade winds and possible contributions of aeolian dust supplied by the berg winds.

(previous page) Figure 6.4. Reconstructions of Southwestern African aridity and trade-wind strength. The downcore 300 kyr records of core MD962094 are compared to the three time slices of core MD962097. **A)** Grain-size distributions of the three end members from the two cores. **B)** The ratio of the two aeolian end members over the fluvial one is used as a proxy for continental aridity. Thick line in the topmost interval of core MD962094 represents a five-point moving average. **C).** The ratio of coarse over fine aeolian dust is used as a proxy for SE trade-wind intensity. Thick line in the topmost interval of core MD962094 represents a five-point moving average.

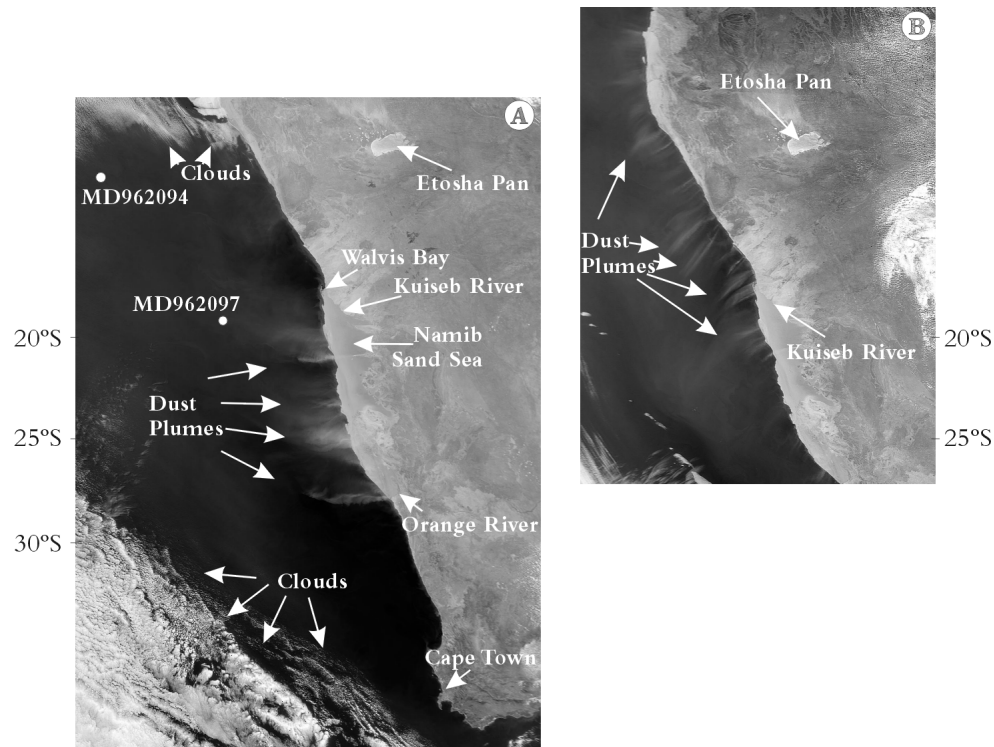


Figure 6.5. Satellite images of southwestern Africa, austral winter. © Orbital Imaging Corporation and processing by NASA Goddard Space Flight Center. **A)** Dust plumes carried to the Southeastern Atlantic Ocean by the southeastern trade winds. Dust originates from the Namib Sand Sea. (see front cover of this thesis for a colour image). **B)** Dust plumes caused by berg winds; eastern winds with a northern component. Dust is not only blown from the Namib Sand Sea but also from dry riverbeds north of the Kuiseb River.

Conclusions

- End-member modelling of the terrigenous sediment fraction from core MD962097 results in three end members that are interpreted as coarse and fine aeolian dust and fluvial mud. These end members resemble those from core MD962094 except for the coarse aeolian dust end member that is coarser in core MD962097 owing to its proximal location relative to the source of aeolian dust. In addition it is bimodal because the finest and coarsest end members occur simultaneously throughout the sampled time slices, so that the end-member model cannot discern them properly. The interpretation of the end members is supported by the size distribution of a present-day dust sample; it can theoretically be constructed by mixing of the two aeolian end members. Variations in the proportion of the fluvial and aeolian end members reflect aridity in southwestern Africa. The ratio of the two aeolian end members reflects the size of the aeolian fraction, attributed to changes in the intensity of the SE trade wind.
- The aridity and wind-strength records from the time slices from core MD962097 resemble those from core MD962094 and are supported by pollen records from core GeoB 1711.

Acknowledgements

We thank the crew and scientists aboard N.O. Marion Dufresne for their help with coring and sampling operations during IMAGES II. Julia Becker (Utrecht University) is thanked for assistance with the sampling of core MD962097. The work presented in this chapter are mainly results presented in the master's thesis by Rik Tjallingii.

7. Late Quaternary Southern-Hemisphere aridity signals in the grain-size distributions of deep-sea sediments.

Abstract

The grain-size distributions of the terrigenous fraction of sediments from the SE Atlantic (offshore Namibia) and the SE Pacific (offshore northern Chile) are unmixed into subpopulations and are interpreted as coarse aeolian dust, fine aeolian dust and fluvial mud. The ratio of the proportions aeolian dust and fluvial mud is interpreted as a palaeo-continental aridity record of southwestern Africa and northern Chile and shows a relatively wet last glacial compared to dry interglacials during the last 42 kyr BP. The changes in continental aridity in northern Chile and southwestern Africa are related to changes in the latitudinal position of the moisture-bearing Southern Westerlies. Time-series analysis of the 300-kyr records of southwestern African continental aridity, oxygen-isotope composition of the SE Atlantic Ocean, the oxygen-isotope composition of SPECMAP (Martinson et al., 1987), and temperature on Antarctica (Vostok ice core), shows a lead of the global ice volume of about 3.5 kyr relative to the southwestern African aridity. On the basis of the time-series analyses we infer that the waxing and waning of the Antarctic ice sheet and associated sea ice extent forced the zone of moisture-bearing Southern Westerlies to move equator- and poleward, respectively. The equatorward shift of the Southern Westerlies during glacials increased the area of winter rains on the southwestern part of the African continent and in northern Chile.

Introduction

The terrigenous fraction of deep-sea sediments provides a unique record of continental environments preserved within the framework of the marine palaeoclimatic record. The marine environment often offers continuity and chronological control through marine oxygen-isotope stratigraphy. Although the Southern Hemisphere contains a number of extreme arid environments, little is known about their evolution throughout the late Quaternary. Continental aridity records from the Southern Hemisphere are scarce and fragmented (Van Zinderen Bakker, 1984; Hesse, 1994; Lamy et al., 1998). This is in contrast with the lower-latitude northern hemisphere (Schütz & Jänicke, 1980; Sarnthein et al., 1982; Balsam et al., 1995; Guerzoni et al., 1996; Kiefert et al., 1996; Prins and Weltje, 1999; Guo et al., 2000; Moreno et al., 2001). Rea (1994) concluded that except for one location in northwestern South America, all of the late Quaternary northern-hemisphere aridity records showed the same pattern through time: arid climate conditions during glacial maxima compared to wet climate conditions during interglacials. Due to the monsoonal variation that dominates climate at the low-latitude northern hemisphere, the aridity records co-vary with changes in northern hemisphere summer (June) insolation resulting from orbital precession (McIntyre et al., 1989; deMenocal et al., 1993; Matthewson et al., 1995; Ruddiman, 1997; deMenocal et al., 2000). As a result, during glacial periods the amount of transported dust on the northern hemisphere was three to five times higher than the relatively wet interglacial periods (Rea, 1994).

Only a few southern hemisphere continental aridity records, based on sedimentological studies have been presented. Stuut et al. (2001, Chapter 5 and Chapter 6) argued that continental aridity in southwestern Africa increased during interglacials as a result of changes in the latitudinal position of the Southern Westerlies on a glacial-interglacial timescale. Owing to an equatorward movement of the Southern Westerlies and associated frontal zones during glacials, the part of southwestern Africa that was exposed to winter rains would have been enlarged. Contrary to aridity records from the northern hemisphere, this caused increased humidity during glacials relative to interglacials.

On the eastern side of the southern part of the African continent, Partridge and co-workers (1997) reconstructed a 200-kyr rainfall record for southern Africa, based on the mineralogical composition of crater-lake sediments. In contrast to the record reconstructed from Walvis Ridge sediments (Stuut et al., 2001, Chapter 5) and from sediments from the continental margin offshore Namibia (Chapter 6) they interpreted their aridity record as a summer rainfall record, which co-varied with precession controlled changes in southern hemisphere summer (January) insolation (Partridge et al., 1997).

Increased humidity on the southern hemisphere during glacials was also shown by two records from the equatorial Pacific (Boven & Rea, 1998), and southeastern Pacific (Lamy et al., 1998). Boven and Rea (1998) used a simple mixing model (Rea & Hovan, 1995) to distinguish between aeolian sediments with a mode at 2 μm and fluvial sediments with a mode at 4 μm . Lamy et al. (1998) interpreted variations in the median silt size and in the mineralogical composition of the terrigenous fraction of southeastern

Pacific sediments in terms of continental aridity, related to variations in the latitudinal position of the Southern Westerlies. Their 120-kyr record shows increased humidity during maxima in the precession index. The increased humidity during glacials was ascribed to an equatorward displacement of the Southern Westerlies causing increased precipitation in the dry climate of northern Chile. Iriondo (1999a) made a sub division of the South American continent distinguishing a northern part (North of $\sim 10^{\circ}\text{S}$) that was characterised by relatively humid glacials relative to interglacials and a southern part (South of $\sim 10^{\circ}\text{S}$) characterised by relatively dry glacials compared to interglacials. Glaciological and oceanographic studies led Iriondo (1999b) to conclude that the Antarctic Anticyclone covered an area during the LGM that was double the area covered during the Hypsithermal. This produced a consequent shifting of the climatic belts of about 10° latitude in an equatorward direction during the LGM, provoking generalised droughts on the entire Southern Hemisphere during the LGM relative to the Hypsithermal. Evidence for the increased aridity during the LGM was found by studying geological and geomorphological features, such as dunefields, paleosols, fluvial terraces and lake levels (Iriondo 1999b).

Hesse (1994) used the flux of terrigenous sediments in the Tasman Sea (east of Australia) to reconstruct fluxes in the aeolian dust coming from the Australian continent. Fluxes appeared to have increased during glacials, possibly related to increased atmospheric circulation. However, Hesse and McTainsh (1999) concluded that these increased fluxes were more likely the result of an expansion of the source areas of the dust, and hence increased aridity, rather than increased wind strengths.

In summary, there is no consensus on the effects of the southern hemisphere atmospheric circulation as reflected in the climate history of the continents on this hemisphere during the Late Quaternary. Here we will evaluate different climate proxy records from the southern hemisphere in terms of changes in the atmospheric circulation throughout the late Quaternary. The end-member algorithm, which was used to unmix the grain-size distributions of the terrigenous-sediment fraction of Walvis Ridge sediments (Chapter 5), was applied to grain-size distributions of the terrigenous sediment fractions from core GeoB 3375-1 (offshore northern Chile, SE Pacific Ocean, Prins et al. 1999). Here we compare the end-member results of the two cores offshore Namibia and Chile to see if sedimentation processes and changes in continental aridity occurred synchronously in the two areas. The two cores are situated at about the same latitude (Figure 7.1), and in comparable climatological settings. Therefore, if the hypotheses of Lamy et al. (1998) and Stuut et al. (2001) are correct, they are expected to show comparable palaeoclimate signals, in response to changes in the southern-hemisphere atmospheric circulation. The 300-kyr continental aridity record from southwestern Africa and proxies for both global ice volume and Antarctic ice volume are compared to see if there is a connection between the latter two and southwestern African climate through the southern-hemisphere atmospheric circulation.

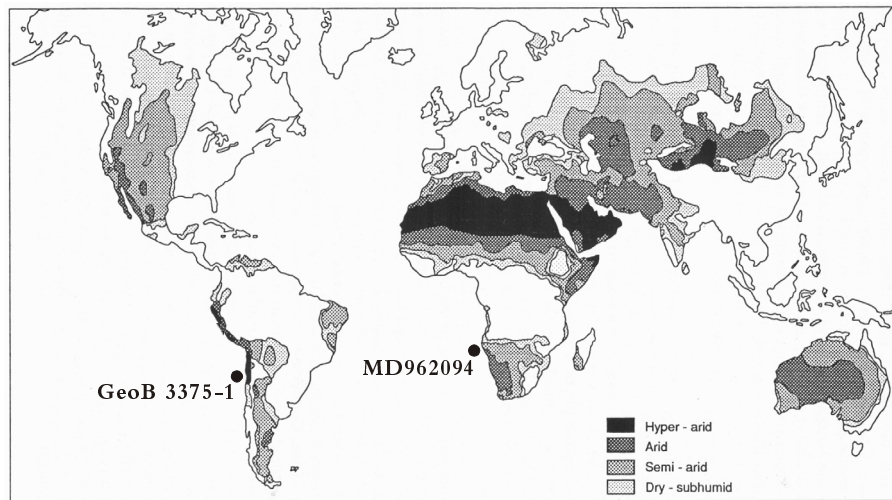


Figure 7.1. World map showing dry areas in the world (from Thomas & Middleton, 1994). Locations of cores MD962094 and GeoB 3375-1 are indicated.

Present-day climate models

Tyson (1986), Goudie (1996), and Nicholson (2000) presented climate models for the African continent showing that at present, the ITCZ plays a major role in the separation of wind fields over the African continent (Figure 7.2). During the northern hemisphere winter (January) the ITCZ is situated near the equator and runs parallel to it in the western part of Africa. In the middle and eastern part of Africa however, the ITCZ is orientated North-South until $\sim 20^{\circ}\text{S}$ from where it runs parallel to the equator again (Figure 7.2A). The position of the ITCZ thus ensures that the North African winter monsoon, characterized by northeasterly winds, influences almost the entire East coast of the African continent. During northern hemisphere summer (July) the ITCZ is situated $10\text{--}15^{\circ}$ North of the equator and runs parallel to it (Figure 7.2B). The South Atlantic high-pressure cell is shifted equatorward and the moisture-bearing southwesterly winds blow over the southwestern tip of the African continent, causing rain. The eastern part of southern Africa remains relatively dry owing to the eastern circulation around the high-pressure cell in the Southwestern Indian Ocean.

Southwestern African aridity record (Walvis Ridge)

Stuut et al. (2001, Chapter 5) showed that the grain-size distributions of the terrigenous part of Walvis Ridge sediments contain detailed information about the climate conditions in southwestern Africa. Using the end-member algorithm of Weltje (1997), they unravelled the grain-size distributions of the terrigenous fraction of deep-sea sediments from Walvis Ridge into subpopulations that were interpreted in terms of transport mechanisms of the terrigenous material. Three subpopulations were modelled that adequately describe the variance in the data set of grain-size distributions: coarse aeolian dust, fine aeolian dust and fluvial mud (Figure 5.4D, p 73). The end members from core MD962094 were interpreted in terms of transport mechanisms of the sediments: fluvial transport by low-density turbidity currents and aeolian transport by

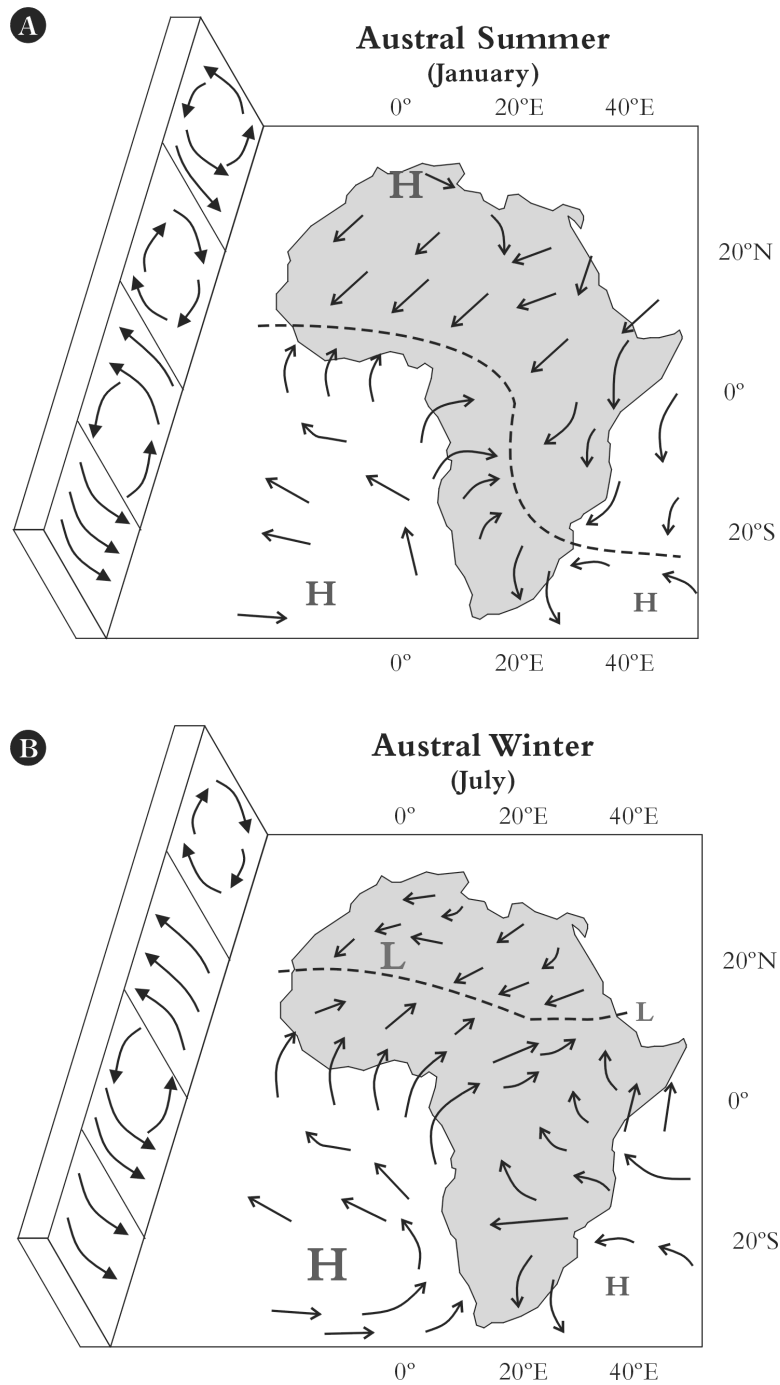


Figure 7.2. Climate models. Schematic representation of the general patterns of winds, pressure and convergence over Africa, modified after Goudie 1996 and Nicholson, 2000. Dashed lines indicate the ITCZ. **A)** Austral summer situation (January). **B)** Austral winter situation (July).

the southeastern trade winds. Since the fluvial end member eventually originates from fluvial runoff, the downcore proportion of fluvial mud results in a late Quaternary aridity record of southwestern Africa. The resulting aridity record (Figure 5.5B, p 74), shows a glacial-interglacial pattern with relatively dry interglacials and wet glacials.

Materials and Methods

Sediment core

Gravity core GeoB 3375-1 was recovered from the Chilean continental margin at 27°28'S / 71°15'W, 1947 m water depth (Figure 7.1) during the CHIPAL-Expedition of R/V Sonne (Hebbeln et al., 1995). The dominant lithology of the core is clayey silt to silty clay with < 20% CaCO₃. This 4.89 m long core fully covers the last ~116 kyr (Lamy et al., 1998).

Age model

The age model of core GeoB 3375-1 is based on tuning of the clay-mineral record to the precession index and seven additional AMS ¹⁴C dates (Lamy et al., 1998 and 2000). Lamy et al. (1998) did not use a correlation of their $\delta^{18}\text{O}$ record of the planktonic foraminifer *Neogloboquadrina pachyderma* (s) to a standard $\delta^{18}\text{O}$ curve because their record does not show a clear enough pattern. For this reason we consider only the AMS-¹⁴C dated part (the upper 42 kyr) of this core.

End-member model

An end-member model (Weltje, 1997) was applied to the grain-size data from core GeoB 3375-1 as measured with a Micromeritics Sedigraph 5100 (see Lamy et al., 1998 for a detailed description of the method). The Sedigraph considers the silt fraction (2–63 μm) and determines grain size on the basis of the hydrodynamic size of the sediments (see Syvitski 1991 for a detailed discussion of the Sedigraph). The data set was reduced from 51 to 47 size classes by combining size classes at grain sizes <4 μm . The minimum number of end members required for a satisfactory approximation of the data is estimated through calculation of the coefficients of determination.

Time-series analysis

Spectral- and cross-spectral analyses were carried out on records of continental aridity (MD962094), the $\delta^{18}\text{O}$ curve of the planktonic foraminifera *Globorotalia inflata* (MD962094), a standard $\delta^{18}\text{O}$ curve (Martinson et al., 1987), and the Vostok ice core delta-Temperature (δT) record (Petit et al., 2000), using the software package Analyseries (Paillard et al., 1996). The proxy records were compared to the 65°N summer (average of 21 May until 20 July) insolation curve (W/m^2) for solution La90 (Laskar et al., 1993), including the present-day values for tidal dissipation and dynamical ellipticity (Lourens et al., 1996). Cross-spectral estimates are based on 1-kyr linear interpolated time series for the time interval between 0 and 300 ka. We used a Parzen smoothing-window with 232 lags, which resulted in a bandwidth of 0.0077910. Lower and upper confidence limits at the 95% level are given by: $0.381976 < P$ (95 %) / $P < 6.466908$.

Results and Interpretation

South-American aridity record (offshore northern Chile)

The average grain-size distribution of the terrigenous sediment fraction in core GeoB 3375-1 has a modal grain size near 32 μm (Figure 7.3A). For end-member models consisting of two to ten end members, the coefficients of determination (r^2) per size class were calculated (Figure 7.3B). The mean coefficient of determination of the grain-size classes increases when the number of end members increases (Figure 7.3C). The inflection point of this curve (at $r^2_{\text{mean}}=0.95$) indicates the optimum combination of the number of end members and the goodness of fit of the data. Consequently, three end members are chosen to describe the variance in the data set (Figure 7.3D). The grain-size distributions of the three end members from core GeoB 3375-1 all have a clearly defined dominant mode, the shoulder observed at 2.9 μm , also present in the original grain-size data (Figure 7.3A), results from the reduction of the number of size classes.

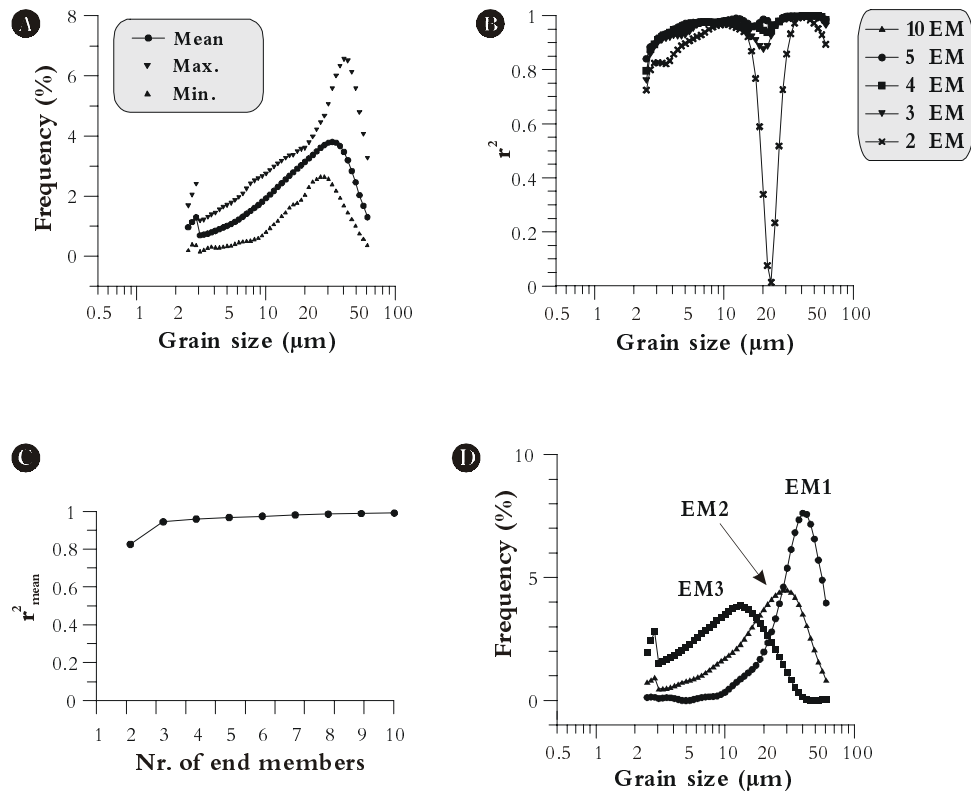


Figure 7.3. End-member modelling results of core GeoB 3375-1.

A) Summary statistics of input data (grain-size distributions, $n=97$); maximum, mean and minimum frequency recorded in each size class. **B)** Coefficients of determination (r^2) for each size class of models with 2-10 end members. **C)** Mean coefficient of determination (r^2_{mean}) of all size classes for each end-member model. **D)** Modelled end members of the terrigenous sediment fraction of sediments from offshore Northern Chile.

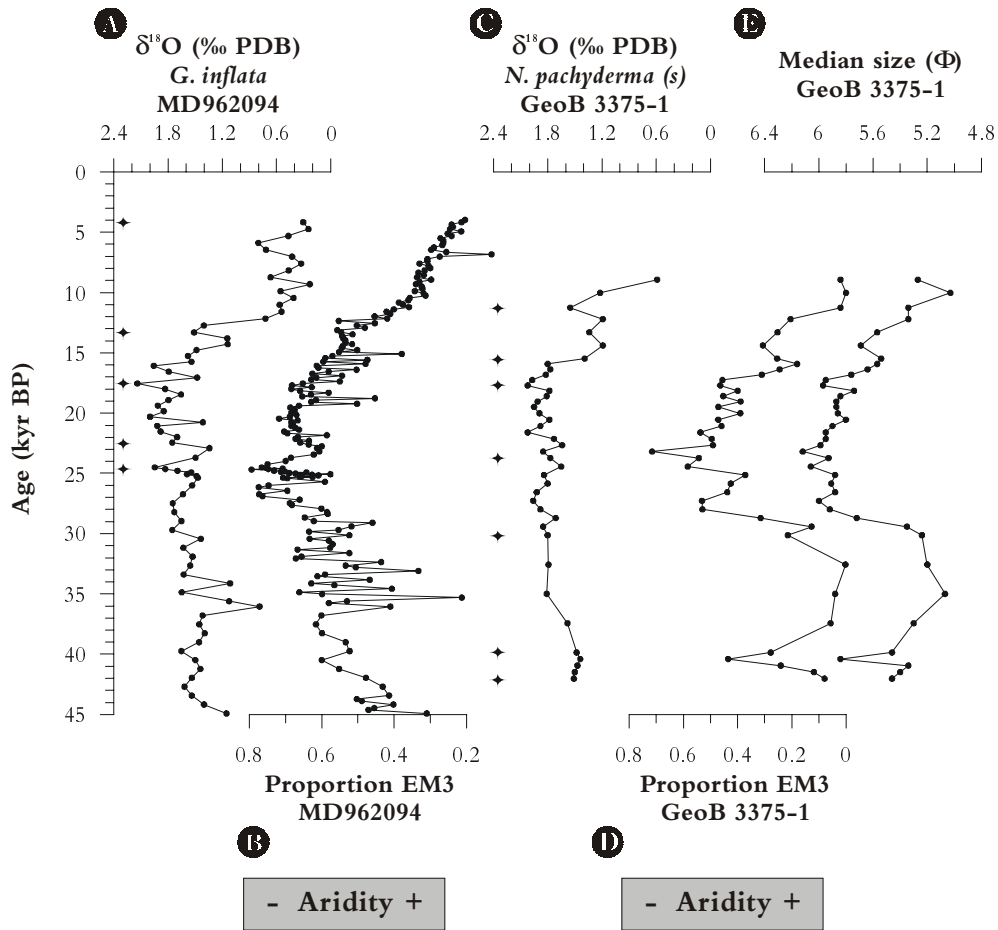


Figure 7.4. 45-kyr palaeoclimate time series. **A)** MD962094 *Globorotalia inflata* $\delta^{18}\text{O}$ -record. **B)** MD962094, continental aridity record derived from the ratio of aeolian and fluvial subpopulations. **C)** GeoB 3375-1 *Neogloboquadrina pachyderma* (s) $\delta^{18}\text{O}$ -record (from Lamy et al. 1998). **D)** GeoB 3375-1, continental aridity record derived from the ratio of aeolian and fluvial subpopulations **E)** GeoB 3375-1 median silt size record (in Φ , from Lamy et al. 1998).

End member EM1 has a modal grain size of $\sim 40\ \mu\text{m}$, end member EM2 of $\sim 29\ \mu\text{m}$, and end member EM3 of $\sim 12\ \mu\text{m}$. Like in core MD962094, these end members are interpreted as coarse aeolian dust, fine aeolian dust and fluvial mud.

The northern Chilean aridity record that results from the proportion of the fluvial end member, shows exactly the same pattern as the median silt size record presented by Lamy et al. (1998, See Figure 7.4E). This record was shown to co-vary with the changes in the precession index; relatively humid conditions prevailed during maxima of the precession index (Lamy et al., 1998). The continental aridity record from Walvis Ridge core MD962094 shows a similar pattern: dry interglacials and wet interglacials. Time-series analysis of the latter record shows that southwestern African continental

aridity is not only influenced by precession but also by other orbital parameters like eccentricity and obliquity (Figure 7.6A). If the two records were caused by the same mechanism, they are expected to record the same orbital frequencies. Here we only consider the ^{14}C -dated part (the last 42 kyr) of the Chile-core, which is too short to show the obliquity and eccentricity frequencies of 41 and 100 kyr, respectively.

Time-series analysis

The 300-kyr southwestern African aridity record appears to contain strong eccentricity (100 kyr), obliquity (41 kyr) and precession (23 kyr) signals, as well as minor signals at 30 kyr, 14 kyr and 11kyr (Figure 7.6A). The $\delta^{18}\text{O}$ record of core MD962094 and the δT record of the Vostok ice core respond in phase to orbital precession and obliquity. Since the latter two are tuned to the SPECMAP $\delta^{18}\text{O}$ record, these three records are expected to respond in phase. However, the SPECMAP $\delta^{18}\text{O}$ record shows a small lag relative to the Walvis Ridge $\delta^{18}\text{O}$ and the Vostok δT records. The aridity record of core MD962094 lags the $\delta^{18}\text{O}$ and δT records by ~ 3.5 kyr (Table 7.1 and Figures 7.6B and C).

Table 7.1 Coherencies and phase lags between proxies and precession and obliquity

Proxy record	Precession			Obliquity		
	Phase (kyr)	Coherency	Error	Phase (kyr)	Coherency	Error
δT Vostok (Petit <i>et al.</i> 2000)	3.68	0.74	0.75	5.54	0.80	0.87
$\delta^{18}\text{O}$ SPECMAP (Martinson <i>et al.</i> '87)	4.95	0.94	0.34	7.10	0.96	0.51
$\delta^{18}\text{O}$ Walvis Ridge	3.78	0.97	0.24	5.79	0.93	0.68
SW African aridity	7.20	0.96	0.26	8.34	0.87	0.93

Discussion

Late Quaternary climate models

The role of the tropics for global climate is still the subject of debate (e.g. Clemens *et al.*, 1996). Are the insolation changes at the lower latitudes the main cause of the existence of monsoonal systems, or is it the interplay with insolation changes at the higher latitudes that cause monsoons (e.g. Clemens *et al.*, 1996; Reichert, 1997, chapter 6)? Here we take the model of the present-day distribution of High and Low pressure cells and the ITCZ throughout the year as examples for the position of these characteristic atmospheric features during glacials and interglacials. Thus, the position of the ITCZ appears crucial to the southwestern part of Africa due to its influence on the latitudinal position of the South Atlantic High pressure belt (Figure 7.2).

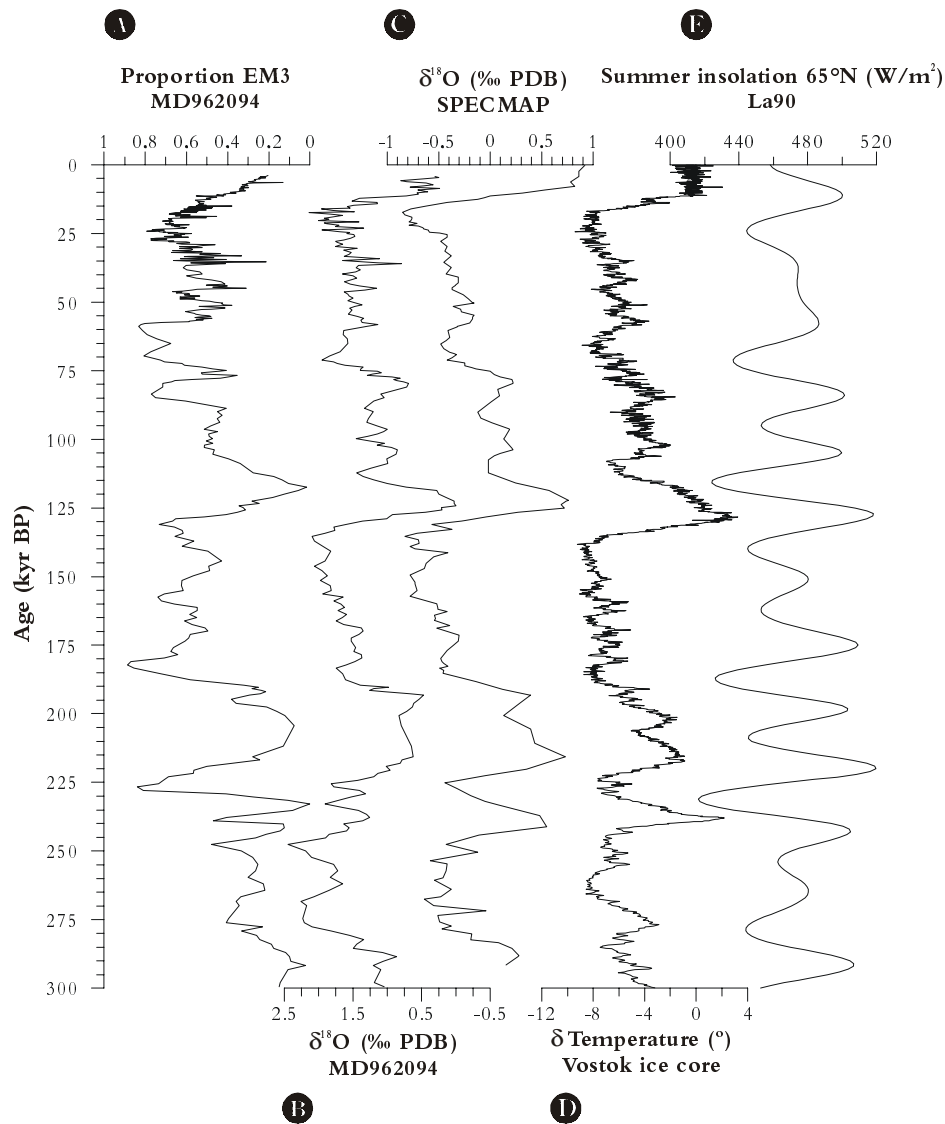


Figure 7.5. 300-kyr palaeoclimate records. **A)** MD962094, continental aridity record derived from the ratio of aeolian and fluvial subpopulations. **B)** MD962094 *Globorotalia inflata* $\delta^{18}\text{O}$ -record. **C)** SPECMAP $\delta^{18}\text{O}$ -record (Martinson et al. 1987). **D)** $\delta\text{Temperature}$ record from the Vostok ice core, Antarctica (Petit et al. 2000). **E)** Summer insolation record (65°N, average of 21 May until 20 July, from Laskar et al., 1993)

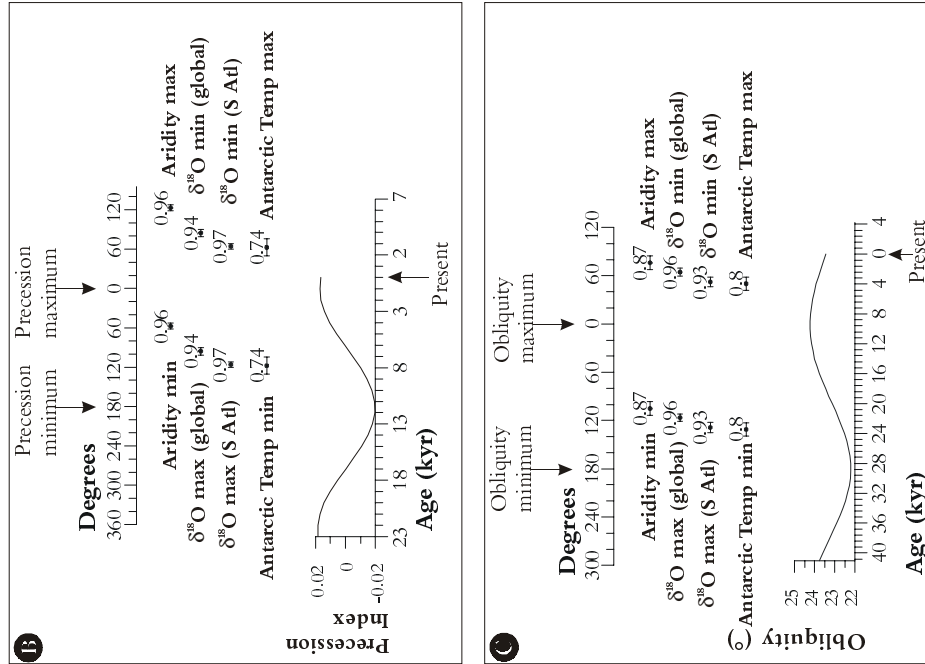


Figure 7.6. Time-series analysis. **A** Power spectra for MD962094. Main orbital frequencies are indicated. **B** Phase relationships between proxies for global ice volume (Vostok δT and MD962094 $\delta^{18}O$) and southwestern African continental aridity and precession. Numbers represent coherency, error bars mark 95% confidence interval. **C** Phase relationships between proxies for global ice volume (Vostok δT and MD962094 $\delta^{18}O$) and southwestern African continental aridity and obliquity.

Antarctic Ice regulates the Southern Hemisphere atmospheric circulation?

The southwestern African continental aridity record contains strong signals of both eccentricity and obliquity, and, to a lesser extent, precession (Figure 7.5A). Therefore, this record cannot be explained by the precession-dominated lower latitude insolation alone. We think that precipitation in this part of Southwestern Africa is dominated by a process that is the result of a forcing mechanism on a larger scale, like the latitudinal position of frontal zones. The position of the Polar Front and associated frontal zones is related to the extension of the Antarctic ice sheet (Heusser, 1989; Brathauer & Abelmann, 1999; Kanfoush et al., 2000). Estimates of the equatorward displacement of the Polar Front and associated frontal zones during glacial periods vary from 2-4° (Brathauer & Abelmann, 1999) to 12° latitude (Van Zinderen Bakker, 1976). Van Zinderen Bakker (1976; 1984) argued that the equatorward displacement of the zone of moisture-bearing Southern Westerlies during glacial periods caused increased humidity in southwestern Africa. The same mechanism of latitudinal shifts in the position of the westerly circulation was suggested to cause the glacial increase in humidity in northern Chile but was predominantly related to orbital precession (Lamy et al, 1998).

The sediments originating from the southwestern part of the African continent are influenced by the changes in the latitudinal position of the Southern Westerlies. At present, these moisture-bearing winds only bring winter rains to the southwestern tip of the African continent (e.g. Nicholson, 2000). During glacial times the Southern Westerlies intensified and shifted equatorward causing increased precipitation in southwestern Africa. In the southeastern part of the Pacific Ocean, the latitudinal position of the Southern Westerlies influences precipitation in the western part of South America in the same way. A possible mechanism for the glacial shift of the latitudinal position of the Southern Westerlies is presented schematically in Figure 7.7. The glacial increase of the Antarctic ice sheet causes frontal zones in the ocean and atmosphere to move equatorward. The equatorward shift of the Southern Westerlies causes larger parts of Africa and South America to get exposed to these moisture-bearing winds, thus increasing the amount of winter precipitation in those areas.

Since there are no proxies for Antarctic ice volume yet, we chose to compare our aridity record with proxies for global ice volume ($\delta^{18}\text{O}$ records of SPECMAP and core MD962094) and with the changes in Antarctic air temperature (Petit et al., 2000), which is also tuned to the SPECMAP curve. The exact age model of the Vostok ice core and the timing of the behaviour of the Antarctic ice sheet relative to the global oxygen-isotope records (Imbrie et al., 1984, Martinson et al., 1987) is still under debate due to the lack of a good Antarctic ice-volume proxy (Shackleton, 2000; Blunier & Brook, 2001; Mudelsee, 2001). However, the southwestern African aridity record shows a phase lag of ~3-3.5 kyr relative to the δT and $\delta^{18}\text{O}$ records in both the precession and obliquity frequencies (Table 7.1 and Figures 7.6 B and C). The potential connection between the Antarctic air temperature and southwestern African aridity could be established through the latitudinal shifts of the frontal zones, related to the waxing and waning of the Antarctic ice sheet.

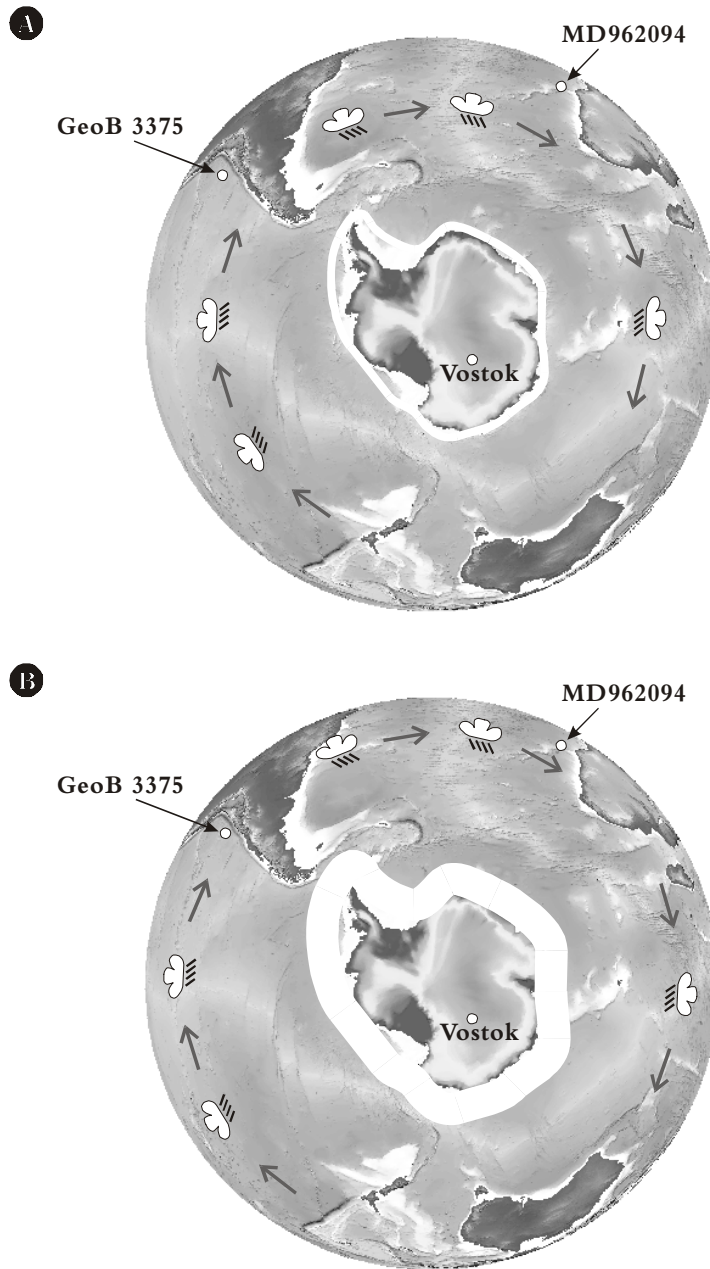


Figure 7.7. Schematic representation of the Antarctic ice-volume related shifts in the latitudinal position of the Southern Westerlies. **A)** Interglacial situation. **B)** Glacial situation.

Mudelsee (2001) showed that global ice volume lags Antarctic air temperature by ~ 4 kyr. However, his estimates are based on the average phase lags of the three dominant insolation parameters. Our estimates show that global ice volume, as reflected by the stable-oxygen isotope records from core MD962094 (SE Atlantic) and from Martinson (1987), show a very small phase lag relative to Antarctic air temperature for both the precession and the obliquity frequencies (Table 7.1 and Figures 7.6 B and C). Since our record is 300 kyr long, we did not consider the eccentricity frequency of 100 kyr. Hence, the large differences with the estimates by Mudelsee (2000) can be explained by a large phase lag in the 100-kyr frequency.

Apart from the discussion whether the Antarctic ice sheet leads or lags global ice volume we observe that the southwestern African aridity record lags the proxies for Antarctic air temperature by ~ 3 – 3.5 kyr. We think that changes in the Antarctic ice volume and sea-ice extent may determine continental aridity in southwestern Africa through changes in the latitudinal position of the Southern Westerlies. During glacial, when the Antarctic ice sheet expands, the Southern Westerlies are pushed equatorward. During interglacials, when the Antarctic ice sheet decreases in volume, the Southern Westerlies shift poleward again. The observed lag of ~ 3.5 kyr is possibly caused by delays in for example the vegetation and runoff. The latitudinal shifts of the Southern Westerlies strongly influence regional climate in northern Chile and southwestern Africa and, possibly, also northwestern Australia. The apparent opposite behaviour of continental aridity in these two regions on the southern hemisphere relative to the well-known aridity records from the lower-latitude northern hemisphere, therefore, could mean a regional sensitivity to changes in Antarctic ice volume rather than an opposite behaviour of the two hemispheres.

Conclusions

- End-member modelling of the terrigenous silt fraction of core GeoB 3375-1 (offshore northern Chile) results in three end members that are interpreted as coarse aeolian dust, fine aeolian dust and fluvial mud. These results are very similar to those from core MD962094 (offshore southwestern Africa).
- The ratio of the proportions fluvial mud and aeolian dust is interpreted as a palaeo-continental aridity record of northern Chile and shows a relatively dry Holocene compared to a wet last glacial. Changes in the aridity record occur simultaneously with changes in the aridity record from southwestern Africa.
- The late Quaternary northern Chilean and southwestern African aridity changes are inferred to be caused by shifts in the latitudinal position of the moisture-bearing Southern Westerlies. These aridity changes are related to changes in the Antarctic ice volume through shifts in the latitudinal position of the frontal zones in the Southern Hemisphere Oceans and Atmosphere. The waxing and waning of the Antarctic ice sheet may have forced the zone of moisture-bearing Southern Westerlies to move equator- and poleward, respectively, influencing regional climate in a large part of the southern hemisphere.

Acknowledgments

Gert Jan Weltje (Technical University Delft) is thanked for providing the end-member algorithm.

8. Concluding remarks

Two subjects that received abundant attention in literature over the last few years are: 1) the hypothesis that iron may be the key to the onset of glacial periods during the late Quaternary (e.g. Martin, 1990; Berger & Wefer, 1991; Kumar et al., 1995), and 2) the asynchrony of the two hemispheres (e.g. Partridge et al., 1997; White & Steig, 1998; Vidal et al., 1999; Blunier & Brook, 2001). These two topics are closely related to the subject of my thesis. Therefore I wish to briefly comment on these hypotheses from the perspective of the data presented in this thesis.

Iron and the ice ages

Iron, present as a coating around aeolian grains, has been related to the development of the ice ages (e.g. Martin, 1990; Berger & Wefer, 1991; Kumar et al., 1995). According to these authors, the observed drop in atmospheric CO₂ during glacials would have been caused by increased primary productivity of marine algae, fertilised by increased dust fluxes. The iron detected in the Walvis Ridge sediments (Chapter 2) can potentially be used to test this hypothesis. However, comparison of the three proxy records, that have been related in this thesis to the intensity of the Southern African trade-wind system (Fe content from CORTEX, carbonate dissolution from the size of foraminifers, and the size of aeolian dust), shows that during glacial times the amount of iron in the sediments is high, fragmentation of the foraminifers is high, and the size of the aeolian sediments is increased relative to interglacials (Figure 8.1). Hence, the variations in the Fe record are due to the combined effect of variations in terrigenous supply of iron (both by aeolian and fluvial transport mechanisms), and the relative enrichment of Fe in the bulk sediments through dissolution of calcium carbonate.

If the iron, supposed to be present around aeolian grains, would have helped decrease the atmospheric CO₂ through fertilisation of the oceans, there should be a correlation between the record of atmospheric CO₂ content (Barnola et al., 1999) and the aeolian dust flux in the southeastern Atlantic Ocean. To examine this potential relationship, the aeolian flux in core MD962094 was calculated using the sedimentation rates between the tie points used for the correlation of the *G. inflata* $\delta^{18}\text{O}$ curve with the $\delta^{18}\text{O}$ curve of Martinson (1987, see Chapter 2) and the five additional AMS-¹⁴C dates (Figure 2.2). Multiplication with the dry bulk density and the proportion aeolian dust in the sediments produced the aeolian flux record (Figure 8.2F). However, the exact biogenic opal and C_{org} content (both ~1% in core GeoB 1028-5, Schmidt, 1992). are unknown for these sediments. Therefore, the flux record (Figure 8.2) is not exact. Besides, it is based on the relative proportions of the aeolian end members (Chapter 5), assuming that all the iron is present as a coating around the aeolian particles and does not depend on the size or composition of the aeolian dust. The relation between the approximated aeolian flux in core MD962094 and the Antarctic CO₂ content in the Vostok ice core (Barnola et al., 1999) may, therefore, be not so obvious. Hence, on the basis of our data we cannot confirm nor reject the hypothesis of iron fluxes being related to ice ages. High-resolution aeolian flux records and detailed analysis of the iron content of the dust would need to be constructed to test this hypothesis.

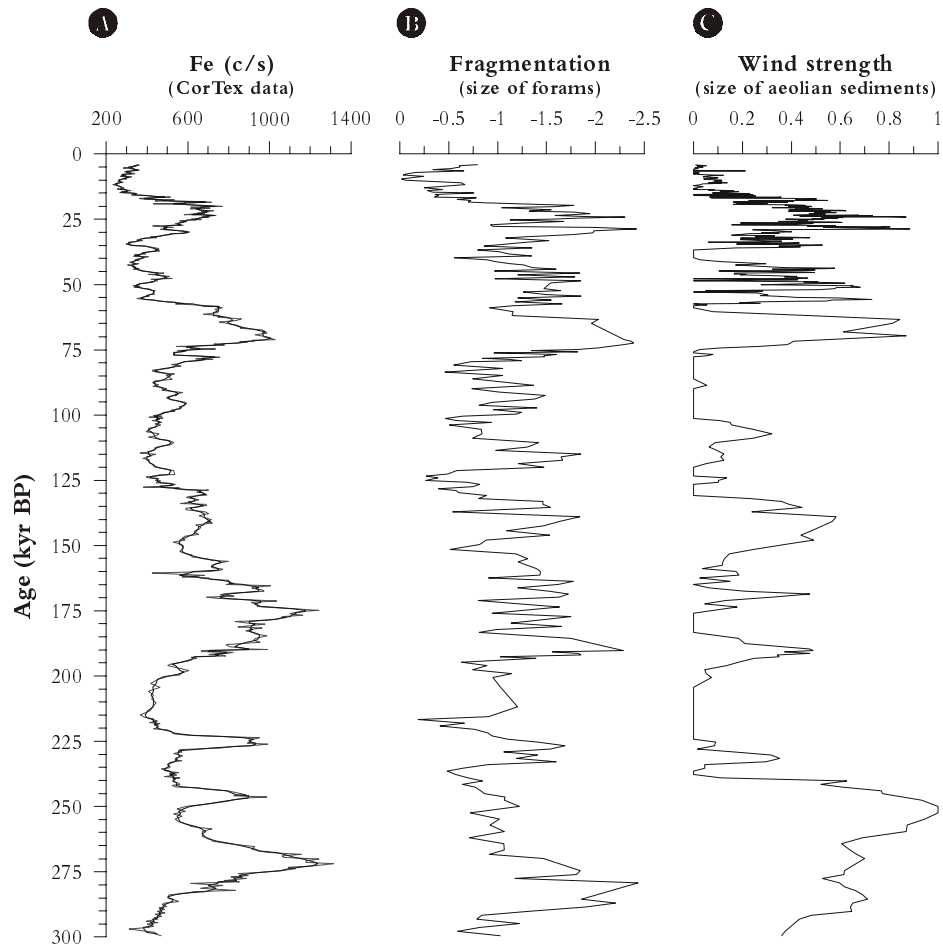


Figure 8.1. Proxies for southwestern African climate derived from sediments from core MD962094 recovered from Walvis Ridge, southeastern Atlantic Ocean. **A)** CORTEX data of bulk sediments of the element Fe in counts per second. A Five-point moving average was applied. **B)** Calcium carbonate dissolution record derived from the fragmentation of foraminifer shells. **C)** Southeastern trade-wind strength derived from the grain size of aeolian sediments.

In addition, the dust flux on Antarctica, available for the last 186 kyr BP (Vostok ice core, Petit et al., 1990; Jouzel et al., 1993) was compared to the proxies for wind strength and continental aridity from core MD962094 (Figure 8.2). In general the dust flux (Figure 8.2 E) shows increased values during glacial times, which compares well to the wind-strength record from Southwestern Africa. In detail however, the correlation is not so obvious. This may be related to differences in the age models used but could also have to do with the fact that the aeolian dust blown to Antarctica during glacials predominantly originates from Patagonia (Basile et al., 1997).

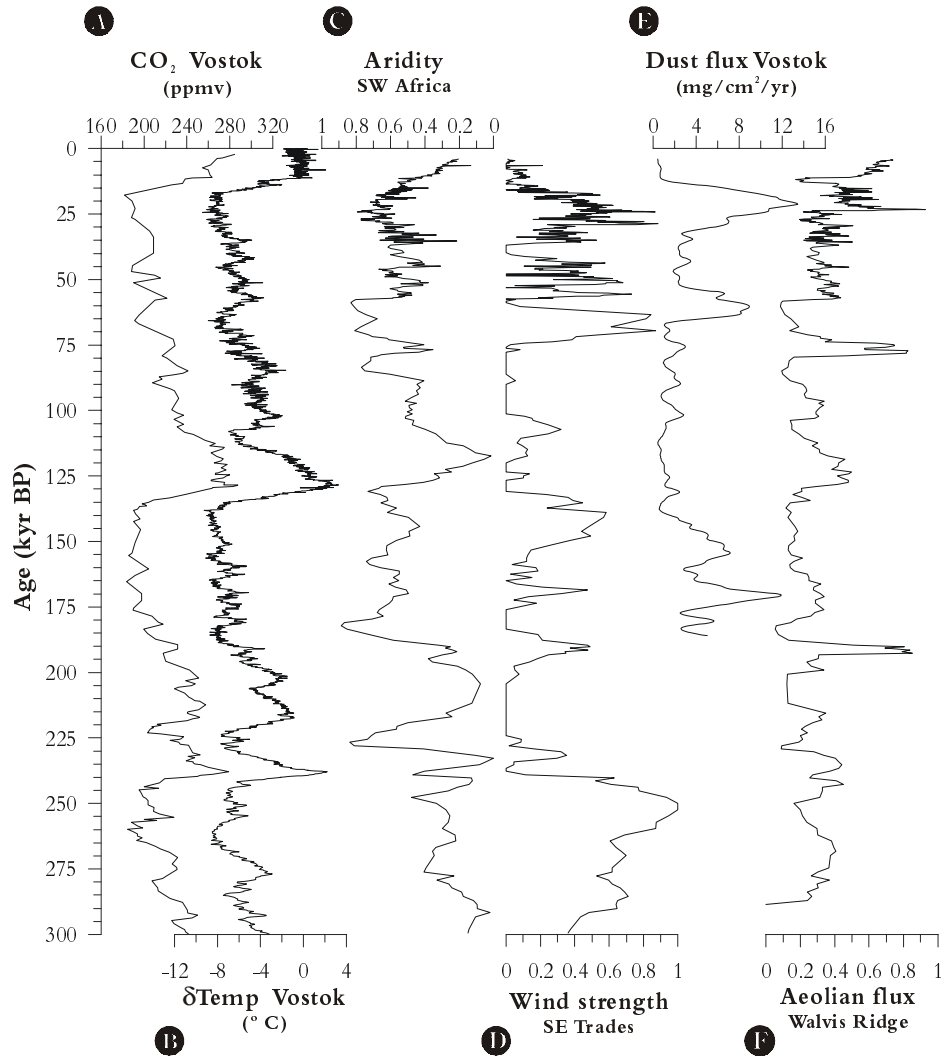


Figure 8.2. Proxy records for atmospheric circulation on the Southern Hemisphere. **A)** CO₂ record of the Vostok ice core (Barnola et al. 1999) **B)** δTemperature record of the Vostok ice core (Petit et al. 2000) **C)** Southwestern African continental aridity record derived from the grain size of aeolian and fluvial sediments. **D)** Southeastern trade-wind strength derived from the grain size of aeolian sediments. **E)** Dust-flux record of the Vostok ice core (Jouzel et al. 1987). **F)** Aeolian flux record derived from the grain size of aeolian sediments.

Asynchronous behaviour of the two hemispheres

Many authors considered the 65°N summer insolation as the motor behind the formation of the ice ages (e.g. Imbrie et al., 1984; Martinson et al., 1987) although it is also thought that the onset of glaciations may have started on the Southern Hemisphere (Charles et al., 1996; Broecker & Henderson, 1998). The latter hypothesis was fed by the observations that changes in the Arctic ice sheet lagged those in the Antarctic one (Bender et al., 1994; Blunier

et al., 1998; Shackleton et al., 2000). To check if the southwestern African aridity record could be used to solve the observed asynchrony between the two hemispheres, it was compared to the Antarctic air temperature record (Petit et al., 2000) and proxies for global ice volume (Chapter 7).

It appears that the southwestern African aridity record lags the Antarctic air temperature record by ~ 3.5 kyr (Figure 7.5). This lag is larger than the ~ 1.3 kyr lag of the CO_2 record relative to Antarctic air temperature (Mudelsee, 2001), which indicates that aeolian dust from southwestern Africa cannot be the cause of the decrease in atmospheric CO_2 . However, there is still a lot of debate going on about the tuning of the age models used for the ice cores (Shackleton, 2000; Blunier & Brook, 2001; Mudelsee, 2001). The southwestern African continental aridity record was related to the shifts in the latitudinal position of the southern Westerlies (Chapter 7, Figure 7.7), which could be forced by the waxing and waning of the Antarctic ice sheet. Expansion of the Antarctic ice sheet would have caused an equatorward shift of the oceanic and atmospheric frontal zones, thus enlarging the parts of southwestern Africa that are susceptible to the winter-rain regime. The same increase in precipitation during glacials is observed in an aridity record from northwestern South America (Chapter 7). This is in contrast to aridity records from the Northern Hemisphere that show relatively dry glacials and wet interglacials (Schütz & Jänicke, 1980; Sarnthein et al., 1982; Balsam et al., 1995; Guo et al., 2000; Moreno et al., 2001). Variations in atmospheric circulation (wind strength) appear to have occurred synchronously on the two hemispheres, caused by the increase in the meridional atmospheric pressure gradients that results from the equatorward displacement of the frontal zones during glacials relative to interglacials.

Hence, the observed asynchrony between the southern-hemispheric records and those from the low-latitude Northern Hemisphere reflects a regional sensitivity to changes in oceanic and atmospheric frontal zones of the regions on the Southern Hemisphere, rather than an opposite behaviour of two hemispheres.

9. Analytical methods

Sediment core MD962094 (19°59.97'S/9°15.87'E, see Figure 1.1), collected at Walvis Ridge during cruise Images II (Bertrand et al., 1996) was sampled at 5-cm intervals, with three series of 10 ml syringes. The first and second series were used for stable oxygen-isotope analyses and dry-bulk density measurements, respectively; the third series was used for grain-size studies. To obtain a higher resolution, the upper 4.5 m of the core were sampled at two cm intervals, later during the study.

Removal of calcium carbonate

The Walvis Ridge sediments are very rich in calcium carbonate (70–95%, see Chapter 2). To isolate the terrigenous fraction of these sediments, these carbonates had to be removed, next to the C_{org} and biogenic opal. The standard routine to remove calcium carbonate in the sedimentology laboratory of the Utrecht University was by treatment with excess of 3% HCl solution (e.g. Prins & Weltje, 1999). Another standard routine, is the treatment with the ‘milder’ acetic acid (e.g. McCave et al., 1995). The 3% HCl treatment was compared with treatment with excess buffered HAc (pH=4, at room temperature) to Walvis Ridge sediments. A carbonate-rich sample from boxcore T89-40 (see Figure 2.1 for location of the core) was split in two fractions and measured with a Malvern 2600 before and after treatment (Figure 9.1). It appeared that treatment with HCl caused the fine fraction of the sediments to decrease. Most probably the clay fraction was damaged by the treatment with HCl, causing the grain-size distribution to get skewed toward the coarse side.

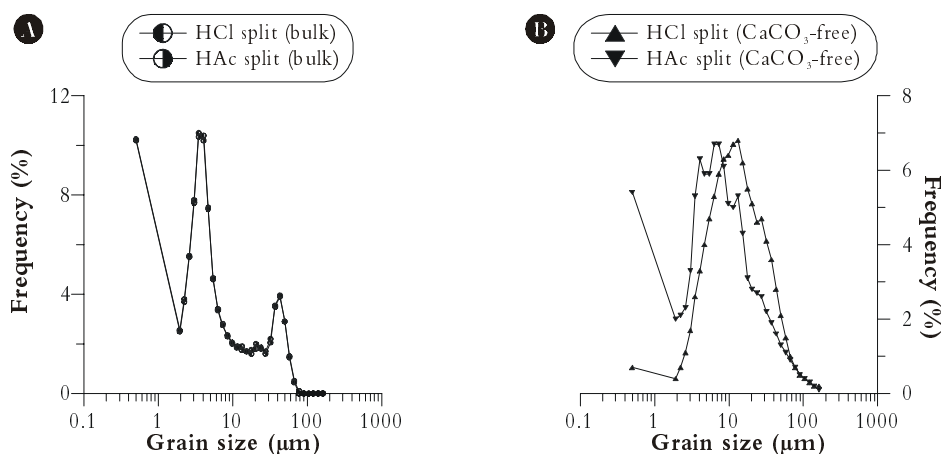


Figure 9.1. Grain-size results of Walvis Ridge sediments after removal of $CaCO_3$ by two different chemical treatments. **A)** Bulk sample, split into two identical samples. **B)** The two splits, after removal of $CaCO_3$ by the two different chemical treatments.

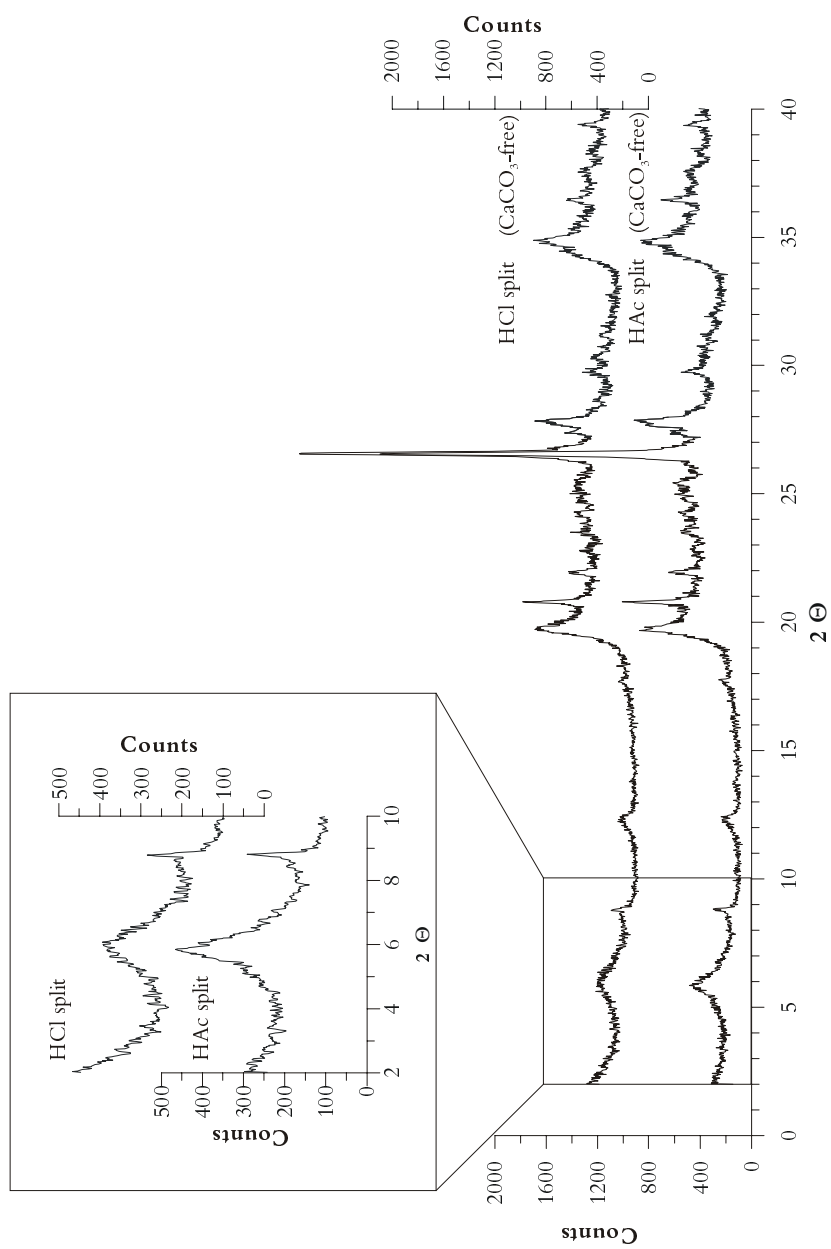


Figure 9.2. XRD results of Walvis Ridge sediments after removal of CaCO_3 by two different chemical treatments.

To study the results for the clay-mineralogical content, XRD spectra were made of the two splits after treatment with the two acids (Figure 9.2). The damage caused by the HCl can clearly be seen in the crystallinity of the clay minerals at $\sim 6^\circ 2\Theta$. This is caused by the relatively low pH of the 3% HCl (pers comm. S. van de Gaast). For this reason we chose to apply acetic acid to remove calcium carbonate from the Walvis Ridge sediments.

Removal of C_{org}

The standard routines of McCave et al. (1995) and Prins & Weltje (1999) to remove C_{org} (6% H_2O_2 at $100^\circ C$) from the sediments were applied to the Walvis Ridge sediments, but with a lower concentration H_2O_2 (3%) to avoid a low pH.

Removal of biogenic opal

The standard routine of McCave et al (1995) to remove biogenic opal (0.1 M calgon solution for 12 hrs) was evaluated by Stuut (1996) and by Prins et al. (in prep). From the results of these studies we chose to apply a 2M NaOH solution at $100^\circ C$ to the sediments from core MD962094 and check the time needed to remove all the biogenic opal. Every five minutes a subsample was taken and studied with an optical microscope to check for opal fragments. It appeared that all biogenic opal was removed after 25 minutes.

Present-day aeolian dust

The present-day dust samples collected during Images II (Bertrand et al., 1996), were rinsed off the filter following the method described by Kiefert (1994) and Kiefert et al. (1996). Tests were carried out using powdered FeO_2 and muscovite. To examine the amount of material that could be retrieved from the filter, a precisely measured amount of FeO_2 was sucked on the filter using a hose and funnel. The FeO_2 then was rinsed off the filter, dried and weighed. This was repeated with three filters. The average recovery of FeO_2 was 61%.

To check if a particular grain-size fraction would be left on the filter, powdered muscovite was measured with a Coulter LS 2300 before and after it was sampled by the dust collectors. The grain-size distributions are identical, showing that no particular size fraction is left behind on the filter (Figure 9.3).

Appendix A

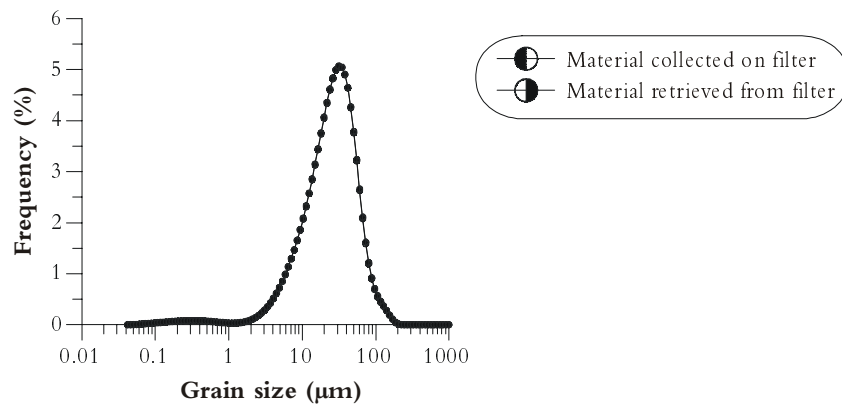


Figure 9.3. Grain-size results after the retrieval of the artificial sediments from the dust filters.

10. References

- Agrawal, Y.C., McCave, I.N., Riley, J.B., 1991. Laser diffraction size analysis. In: J.P.M. Syvitsky (Editor), *Principles, methods and application of particle size analysis*. Cambridge University Press, Cambridge, pp. 119-128.
- An, Z., Kukla, G.J., Porter, S., C., Xiao, J., 1991. Magnetic susceptibility evidence of monsoon variation on the Loess Plateau of central China during the last 130,000 years. *Quaternary Research*, 36: 29-36.
- Arz, H.W., Pätzold, J., Wefer, G., 1998. Correlated Millennial-scale changes in surface Hydrography and terrigenous sediment yield inferred from Last-Glacial marine deposits off NE Brazil. *Quaternary Research*, 50(2): 157-166.
- Arz, H., Pätzold, J., Wefer, G., 1999. Climatic changes during the last deglaciation recorded in sediment cores from the northeastern Brazilian Continental Margin. *Geo-Marine Letters*, 19(3): 209-218.
- Balsam, W.L., Otto-Bliesner, B.L., Deaton, B.C., 1995. Modern and last glacial maximum eolian sedimentation patterns in the Atlantic Ocean interpreted from sediment iron oxide content. *Paleoceanography*, 10(3): 493-507.
- Bard, E., 1988. Correction of accelerator mass spectrometry ^{14}C ages measured in planktonic foraminifera: paleoceanographic implications. *Paleoceanography*, 3(6): 635-645.
- Basile, I., Grousset, F.E., Revel, M., Petit, J.R., Biscaye, P., Barkov, N.I. (1997). Patagonian origin of glacial dust deposited in East Antarctica (Vostok and Dome C) during glacial stages 2,4, and 6. *Earth and Planetary Science Letters*, 146: 573-589.
- Bassinot, F.C., Beaufort, L., Vincent, E., Labeyrie, L.D., Rostek, F., Müller, P., J., Quidelleur, X., Lancelot, Y., 1994. Coarse fraction fluctuation in pelagic carbonate sediments from the tropical Indian Ocean: A 1500 kyr record of carbonate dissolution. *Paleoceanography*, 9(4): 579-600.
- Berger, A., Imbrie, J., Hays, J., Kukla, G., Saltzman, B., 1982. *Milankovitch and Climate: Understanding the Response to Astronomical forcing*, NATO advanced research workshop on Milankovitch and climate. NATO ASI series C. Reidel, New York.
- Berger, A., Loutre, M.F., 1991. Insolation values for the climate of the last 10 million years. *Quaternary Science Reviews*, 10: 297-317.
- Berger, W.H., Wefer, G. (1996). Expeditions into the Past: Paleocceanographic studies in the South Atlantic. In: *The South Atlantic: present and past circulation*. G. Wefer, W.H. Berger, G. Siedler & D. Webb (eds.). p 363-410.
- Bertrand, P., Balut, Y., Schneider, R., Chen, M.T., Rogers, J., and shipboard scientific party, 1996. Scientific report of the NAUSICAA-IMAGES II coring cruise. Les rapports de campagne à la mer à bord du Marion-Dufresne, URA CNRS 197. Université Bordeaux-1, Département de Géologie et Oceanographie, Talence cédex, France, 382 pp.
- Best, A.I., Gunn, D.E., 1999. Calibration of marine sediment core loggers for quantitative acoustic impedance studies. *Marine Geology*, 160: 137-146.
- Beuselinck, L., Govers, G., Poesen, J., Degraer, G., Froyen, L., 1998. Grain-size analysis by laser diffractometry: comparison with the sieve-pipette method. *Catena*, 32: 193-208.
- Bickert, T., Wefer, G., 1996. Late Quaternary Deep Water circulation in the South Atlantic: Reconstruction from carbonate dissolution and benthic stable isotopes. In: *The South Atlantic: present and past circulation*. G. Wefer, W.H. Berger, G. Siedler & D. Webb (eds.). p 599-620.
- Blunier, T., Brook, E., 2001. Timing of millennial-scale climate change in Antarctica and Greenland during the last glacial period. *Science*, 291(5 January): 109-112.
- Boven, K.L., Rea, D.K., 1998. Partitioning of eolian and hemipelagic sediment in eastern equatorial Pacific core TR 163-31B and the late Quaternary paleoclimate of the Northern Andes. *Journal of Sedimentary Research*, 68(5): 850-855.
- Brathauer, U., Abelmann, A., 1999. Late Quaternary variations in sea surface temperatures and their relationship to orbital forcing recorded in the Southern Ocean (Atlantic sector). *Paleoceanography*, 14(2): 135-148.
- Bremner, J.M., Willis, J.P., 1993. Mineralogy and geochemistry of the clay fraction of sediments from the Namibian continental margin and the adjacent hinterland. *Marine Geology*, 115: 85-116.

References

- Broecker, W.S., Takahashi, T., 1980. Hydrography of the Central Atlantic-III. The North Atlantic deep-water complex. *Deep-Sea Research*, 27A: 591-613.
- Broecker, W.S., Peng, T.-H., 1982. Tracers in the sea. Lamont-Doherty Geological Observatory, Columbia University, New York, 690 pp.
- Broecker, W.S., Henderson, G.M., 1998. The sequence of events surrounding Termination II and their implications for the cause of glacial-interglacial CO₂ changes. *Paleoceanography*, 13(4): 352-364.
- Broecker, W.S., Clark, E., 1999. CaCO₃ size distribution: A paleocarbonate ion proxy? *Paleoceanography*, 14(5): 596-604.
- Brook, G.A., Cowart, J.B., Marais, E., 1996. Wet and dry periods in the southern African summer rainfall zone during the last 300 kyr from speleothem, tufa and sand dune age data. *Palaeoecology of Africa* 24: 147-158.
- Coakley, J.P., Syvitski, J.P.M., 1991. SediGraph technique. In: J.P.M. Syvitski (Editor), *Principles, methods, and application of particle size analysis*. Cambridge University Press, Cambridge, pp. 129-142.
- Cockcroft, M.J., Wilkinson, M.J., Tyson, P.D., 1987. The application of a present-day climate model to the late Quaternary in Southern Africa. *Climatic Change*, 10: 161-181.
- Davis, J.C., 1973. *Statistics and data analysis in geology*. John Wiley & Sons, Inc., Singapore, 646 pp.
- deMenocal, P.B., Ortiz, J., Guilderson, T., Adkins, J., Sarnthein, M., Baker, L., Yarusinsky, M., 2000. Abrupt onset and termination of the African Humid Period: rapid climate responses to gradual insolation forcing. *Quaternary Science Reviews*, 19: 347-361.
- deMenocal, P.B., Ruddiman, W.F., Pokras, E.M., 1993. Influences of high- and low-latitude processes on african terrestrial climate: Pleistocene eolian records from equatorial atlantic Ocean Drilling Program site 663. *Paleoceanography*, 8(2): 209-242.
- Diester-Haaf, L., 1985. Late Quaternary sedimentation on the Eastern Walvis Ridge, SE Atlantic. *Marine Geology*, 65(1/2): 145-189.
- Diester-Haaf, L., Heine, K., Rothe, P., Schrader, H., 1988. Late Quaternary history of continental climate and the Benguela current off South West Africa. *Paleoceanography*, 65: 81-91.
- Dittert, N., Henrich, R., 2000. Carbonate dissolution in the South Atlantic Ocean: evidence from ultrastructure breakdown in *Globigerina bulloides*. *Deep-Sea Research I*, 47: 603-620.
- Dreimanis, A., Hütt, G., Raukas, A., Whippley, P.W., 1985. Dating methods of Pleistocene deposits and their problems: Thermoluminescence dating. In: N.W. Rutter (Editor), *Dating methods of Pleistocene deposits and their problems*. Geological Association of Canada, pp. 1-7.
- Dupont, L.M., Marret, F., Winn, K., 1998. Land-sea correlation by means of terrestrial and marine palynomorphs from the equatorial East Atlantic: phasing of SE trade winds and the oceanic productivity. *Palaeogeography, Palaeoclimatology, Palaeoecology*, 142: 51-84.
- Emerson, S., Bender, M., 1981. Carbon fluxes at the sediment-water interface of the deep-sea: calcium carbonate preservation. *Journal of Marine Research*, 39: 139-162.
- Farrell, J.W., Prell, W.L., 1991. Pacific CaCO₃ preservation and $\delta^{18}\text{O}$ since 4 Ma: Paleoceanic and paleoclimatic implications. *Paleoceanography*, 6(4): 485-498.
- Farrell, J.W., Prell, W.L., 1989. Climatic change and CaCO₃ preservation: an 800,000 year bathymetric reconstruction from the central equatorial Pacific ocean. *Paleoceanography*, 4(4): 447-466.
- Fischer, G., Wefer, G. (Editors), 1999. *Use of proxies in paleoceanography*. Springer Verlag, Berlin Heidelberg New York, 735 pp.
- Fossing, H., Ferdelman, T.G., Berg, P., 2000. Sulfate reduction and methane oxidation in continental margin sediments influenced by irrigation (South-East Atlantic off Namibia). *Geochimica et Cosmochimica Acta*, 64(5): 897-910.
- Frederichs, T., Bleil, U., Däumler, K., Von Döbeneck, T., Schmidt, A., 1999. The magnetic view on the Marine Paleoenvironment: parameters, techniques and potentials of rock magnetic studies as a key to Paleoclimatic and Paleoceanographic changes. In: G. Fischer and G. Wefer (Editors), *Use of proxies in paleoceanography*. Springer Verlag, Berlin Heidelberg New York, pp. 575-599.
- Gingele, F., X., 1996. Holocene climatic optimum in Southwest Africa-evidence from the marine clay mineral record. *Palaeogeography, Palaeoclimatology, Palaeoecology*, 122: 77-87.

References

- Goudie, A.S., 1996. Climate: Past and Present. In: W.M. Adams, A.S. Goudie and A.R. Orme (Editors), *The physical geography of Africa*. Oxford University Press, New York, pp. 34-59.
- Guerzoni, S., Quarantotto, G., Cesari, G., Molinaroli, E., Rampazzo, G., Le Bolloch, O., 1996. Trace metal composition and grain size of particulates in aerosols and precipitation collected in nw mediterranean (39N, 9E) a multivariate analysis. *The Impact of desert dust across the mediterranean*, (Guerzoni & Chester): 333-338.
- Guo, Z., Petit-Maire, N., Kröpelin, S., 2000. Holocene non-orbital climatic events in present-day arid areas of northern Africa and China. *Global and Planetary Change*, 26(1-3): 97-103.
- Hay, W.W., Brock, J.C., 1992. Temporal variation in intensity of upwelling off southwest Africa. Summerhayes, C.P., Prell, W.L. & Emeis, K.C. (eds.) *Upwelling Systems: Evolution since the early Miocene*, Geological Society Special Publication(63): 463-497.
- Heine, K., 1998. Climate change over the past 135,000 years in the Namib Desert (Namibia) derived from proxy data. *Palaeoecology of Africa* 25: 171-198.
- Huber, R., Meggers, H., Baumann, K.-H., R., H., 2000. Recent and Pleistocene carbonate dissolution in sediments of the Norwegian-Greenland Sea. *Marine Geology*, 165: 123-136.
- Imbrie, J., Hays, J.D., Martinson, D.G., McIntyre, A., Mix, A.C., Morley, J.J., Pisias, N.G., Prell, W.L., Shackleton, N.J., 1984. The orbital theory of Pleistocene climate: support from a revised chronology of the marine $\delta^{18}\text{O}$ record. In: A. Berger, J. Imbrie, J. Hays, G. Kukla and B. Saltzman (Editors), *Milankovitch and Climate, understanding the response to astronomical forcing*. NATO Advanced Science Institute Series. D. Reidel Publishing Company, Dordrecht / Boston / Lancaster, pp. 510.
- Iriondo, M.H., 1999a. Climatic changes in the South American plains: records of a continent-scale oscillation. *Quaternary International* 57/58: 93-112.
- Iriondo, M.H., 1999b. Last Glacial Maximum and Hypsithermal in the Southern Hemisphere. *Quaternary International* 62: 11-19.
- Jansen, J.H.F., 1985. Middle and Late Quaternary carbonate production and dissolution, and paleoceanography of the eastern Angola Basin, South Atlantic Ocean. In: K.J. Hsü and H.J. Weissert (Editors), *South Atlantic Paleoceanography*. Cambridge University Press, Cambridge, pp. 25-46.
- Jansen, J.H.F., Van Iperen, J.M., 1991. A 220,000-year climatic record for the east equatorial Atlantic ocean and equatorial Africa: evidence from diatoms and opal phytoliths in the Zaire (Congo) deep-sea fan. *Paleoceanography*, 6(5): 573-591.
- Jansen, J.H.F., Ufkes, E., Schneider, R.R., 1996. Late Quaternary movements of the Angola-Benguela Front, SE Atlantic, and implications for advection in the equatorial ocean. *The South Atlantic: present and past circulation*. G. Wefer, W.H. Berger, G. Siedler & D. Webb (eds.). p 553-575.
- Jansen, J.H.F., Van der Gaast, S.J., Koster, B., Vaars, A.J., 1998. CORTEX, a shipboard XRF-scanner for element analyses in split sediment cores. *Marine Geology*, 151(1-4): 143-153.
- Jenkins, R., 1976. *An introduction to X-ray spectrometry*. Heiden en Son, London - New York - Rheine, 163 pp.
- Jouzel, J., Barkov, N.I., Barnola, J.M., Bender, M., Chappelaz, J., Genthon, C., Kotlyakov, V.M., Lipenkov, V., Lorius, C., Petit, J.R., Raynaud, D., Raisbeck, G., Ritz, C., Sowers, T., Stievenard, M., Yiou, F., Yiou, P. (1993). Extending the Vostok ice-core record of paleoclimate to the penultimate glacial period. *Nature*, 364: 407-412.
- Kanfoush, S.L., Hodell, D.A., Charles, C.D., Guilderson, T.P., Mortyn, P.G., Ninnemann, U.S., 2000. Millennial-scale instability of the Antarctic ice sheet during the last glaciation. *Science*, 288(June 2000): 1815-1818.
- Kennedy, S.K., Mazzullo, J., 1991. Image analysis method of grain size measurement. In: J.P.M. Syvitski (Editor), *Principles, methods, and application of particle size analysis*. Cambridge University Press, Cambridge, pp. 76-87.
- Kiefert, L., 1994. *Characteristics of wind transported dust in Eastern Australia*, Griffith University, Brisbane, 340 pp.
- Kiefert, L., McTainsh, G.H., Nickling, W.G., 1996. Sedimentological characteristics of Saharan and Australian dusts. In: S. Guerzoni and R. Chester (Editors), *The Impact of desert dust across the mediterranean*. Kluwer Academic Publishers, Dordrecht, pp. 183-190.

References

- Kirst, G.J., Schneider, R.R., Müller, P., Von Storch, I., Wefer, G., 1999. Late Quaternary temperature variability in the Benguela Current system derived from alkenones. *Quaternary Research*, 52: 92-103.
- Klein, R.G., 1991. Size variation in the Cape Dune Molerat (*Bathergues suillus*) and Late Quaternary Climatic Change in the Southwestern Cape Province, South Africa. *Quaternary Research*, 36: 243-256.
- Konert, M., Vandenbergh, J., 1997. Comparison of laser grain size analysis with pipette and sieve analysis: a solution for the underestimation of the clay fraction. *Sedimentology*, 44: 13 p.
- Koopmann, B., 1981. Sedimentation von Saharastaub im subtropischen Nordatlantik während der letzten 25.000 Jahre. *Meteor Forschungsergebnisse C*, 35: 23-59.
- Kucera, M., Malmgren, B.A., Sturesson, U., 1997. Foraminiferal dissolution at shallow depths of the Walvis Ridge and Rio Grand Rise during the latest Cretaceous: Inferences for deep-water circulation in the South Atlantic. *Palaeogeography, Palaeoclimatology, Palaeoecology*, 129: 195-212.
- Laberey, L., Labracherie, M., Gorfti, N., Pichon, J.J., Vautravers, M., Arnold, M., Duplessy, J.-C., Paterne, M., Michel, E., Duprat, J., Caralp, M., Turon, J.-L., 1996. Hydrographic changes of the Southern Ocean (southeast Indian sector) over the last 230 kyr. *Paleoceanography*, 11(1): 57-76.
- Lamy, F., Hebbeln, D., Wefer, G., 1998. Late Quaternary precessional cycles of terrigenous sediment input off the Norte Chico, Chile (27.5° S) and paleoclimatic implications. *Palaeogeography, Palaeoclimatology, Palaeoecology*, 141(3-4): 233-251.
- Lamy, F., Klump, J., Hebbeln, D., Wefer, G., 2000. Late Quaternary rapid climate change in northern Chile. *Terra Nova* 12: 8-13.
- Lamy, F., Hebbeln, D., Röhl, U., Wefer, G., 2001. Holocene rainfall variability in southern Chile: a marine record of latitudinal shifts of the Southern Westerlies. *Earth and Planetary Science Letters*, 185: 369-382.
- Lancaster, N., 1984. Palaeoenvironments in the Tsonab valley, central Namib Desert. *Palaeoecology of Africa* 16: 411-419.
- Le, J., Shackleton, N.J., 1992. Carbonate dissolution fluctuations in the western equatorial Pacific during the Late Quaternary. *Paleoceanography*, 7(1): 21-42.
- Lea, D.W., Mashiotta, T.A., Spero, H.J., 1999. Controls on magnesium and strontium uptake in planktonic foraminifera determined by live culturing. *Geochimica et Cosmochimica Acta*, 63(16): 2369-2379.
- Little, M.G., Schneider, R.R., Kroon, D., Price, B., Bickert, T., Wefer, G., 1997a. Rapid paleoceanographic changes in the Benguela Upwelling System for the last 160,000 years as indicated by abundances of planktonic foraminifera. *Palaeogeography, Palaeoclimatology, Palaeoecology*, 130: 135-161.
- Little, M.G., Schneider, R.R., Kroon, D., Price, B., Summerhayes, C.P., Segl, M., 1997b. Trade wind forcing of upwelling, seasonality, and Heinrich events as a response to sub-Milankovitch climate variability. *Paleoceanography*, 12(4): 568-576.
- Lohmann, G.P., Rosenthal, Y., McCorkle, D., 1999. Evidence for changes in ocean carbonate ion concentration and foraminiferal calcite solubility during the last glaciation, AGU Fall meeting. *Eos Trans.*, San Francisco.
- Martinson, D.G., Pisias, N.G., Hays, J.D., Imbrie, J., Moore, T.C., Shackleton, N.J., 1987. Age dating and the orbital theory of the Ice Ages: development of a high-resolution 0 to 300,000-year chronostratigraphy. *Quaternary Research*, 27: 1-29.
- Matthewson, A.P., Shimmield, G.B., Kroon, D., 1995. A 300 kyr high-resolution aridity record of the North-African continent. *Paleoceanography*, 10(3): 677-692.
- McCave, I.N., Bryant, R.S., Cook, H.F., Coughanowr, C.A., 1986. Evaluation of a laser-diffraction-size analyser for use with natural sediments. *Journal of Sedimentary Petrology*, 56: 561-564.
- McIntyre, A., Ruddiman, W.F., Karlin, K., Mix, A.C., 1989. Surface water response of the equatorial Atlantic ocean to orbital forcing. *Paleoceanography*, 4(February 1989): 19-55.
- McTainsh, G.H., Nickling, W.G., Lynch, A.W., 1997. Dust deposition and particle size in Mali, West Africa. *Catena*, 29: 307-322.
- Meadows, M.E., 1988. Vlei sediments and sedimentology: A tool in the reconstruction of palaeoenvironments of southern Africa. *Palaeoecology of Africa* 19: 249-260.

References

- Milligan, T.G., Kranck, K., 1991. Electroresistance particles size analysers. In: J.P.M. Syvitski (Editor), Principles, methods, and application of particle size analysis. Cambridge University Press, Cambridge, pp. 109-118.
- Mix, A.C., Rugh, W., Pisias, N.G., Veirs, S., Sedimentologists, L.-S., Party, L.-S.S., 1992. Color reflectance spectroscopy: a tool for rapid characterization of deep-sea sediments. *Proceedings of the Ocean Drilling Program, Initial Reports*, 138: 67-77.
- Moreno, A., Targarona, J., Henderiks, J., Canals, M., Freudenthal, T., Meggers, H., 2001. Orbital forcing of dust supply to the North Canary Basin over the last 250 kyr. *Quaternary Science Reviews*, 20: 1327-1339.
- Mudelsee, M., 2001. The phase relations among atmospheric CO₂ content, temperature and global ice volume over the past 420 ka. *Quaternary Science Reviews*, 20: 583-589.
- Nickling, W.G., McTainsh, G.H., Leys, J.F., 1999. Dust emissions from the Channel Country of western Queensland, Australia. *Zeitschrift für Geomorphologie*, 116: 1-17.
- Paillard, D., Labeyrie, L., Yiou, P., 1996. Macintosh Program Performs Time-Series Analysis. *Eos Trans. AGU*, 77: 379.
- Partridge, T.C., Demenocal, P.B., Lorentz, S.A., Paiker, M.J., Vogel, J.C., 1997. Orbital forcing of climate over South Africa: a 200,000 year rainfall record from the Pretoria Saltpan. *Quaternary Science Reviews*, 16: 1125-1133.
- Partridge, T.C., Scott, L., Hamilton, J.E., 1999. Synthetic reconstructions of southern African environments during the Last Glacial Maximum (21-18 kyr) and the Holocene Altithermal (8-6 kyr). *Quaternary International*, 57/58: 207-214.
- Peeters, F.J.C., Ivanova, E.M., Conan, S.M.-H., Brummer, G.J.A., Ganssen, G.M., Troelstra, S.R., Van Hinte, J.E., 1999. A size analysis of planktic foraminifera from the Arabian Sea. *Marine Micropaleontology*, 36(1): 31-63.
- Peterson, L.C., Prell, W.L., 1985. Carbonate dissolution in recent sediments of the eastern equatorial Indian Ocean: preservation patterns and carbonate loss above the lysocline. *Marine Geology*, 64: 259-290.
- Petit, J.R., Mounier, L., Jouzel, J., Korotkevitch, V., Kotlyakov, V., Lorius, C. (1990). Paleoclimatological implications of the Vostok core dust record. *Nature*, 343: 56-68.
- Prins, M.A., 1999. Pelagic, Hemipelagic and Turbidite Deposition in the Arabian Sea during the Late Quaternary. Ph.D. Thesis, Utrecht University, Utrecht, 192 pp.
- Prins, M.A., Stuut, J.-B.W., Lamy, F., Weltje, G.J., 1999. End-member modelling of grain-size distributions of deep-sea detrital sediments and its palaeoclimatic significance: examples from the NW Indian, E Atlantic and SE Pacific oceans: *Geophysical Research Abstracts*, v. 1, p. 564.
- Prins, M.A., Weltje, G.J., 1999. End-member modelling of siliciclastic grain-size distributions: the Late Quaternary record of eolian and fluvial sediment supply to the Arabian Sea and its paleoclimatic significance. In: J. Harbaugh et al. (Editors), *Numerical experiments in stratigraphy: Recent advances in stratigraphic and sedimentologic computer simulations*. SEPM Special Publication 62. Society for Sedimentary Geology, pp. 91-111.
- Prins, M.A., Postma, G., Cleveringa, J., Cramp, A., Kenyon, N.H., 2000a. Controls on terrigenous sediment supply to the Arabian Sea during the late Quaternary: the Indus Fan. *Marine Geology*, 169: 327-349.
- Prins, M.A., Postma, G., Weltje, G.J., 2000b. Controls on terrigenous sediment supply to the Arabian Sea during the late Quaternary: the Makran continental slope. *Marine Geology*, 169: 351-371.
- Rea, D.K., 1994. The paleoclimatic record provided by eolian deposition in the deep sea: the geologic history of wind. *Reviews of Geophysics*, 32: 159-195.
- Rea, D.K., Hovan, S.A., 1995. Grain size distribution and depositional processes of the mineral component of abyssal sediments: lessons from the North Pacific. *Paleoceanography*, 10(2): 251-258.
- Reichart, G.J., 1997. Late Quaternary variability of the Arabian Sea monsoon and oxygen minimum zone. Ph.D. Thesis, Utrecht University, Utrecht, 174 pp.
- Richter, T.O., Lassen, S., van Weering, T.C.E., de Haas, H., 2001. Magnetic susceptibility patterns and provenance of ice-rafted material at Feni Drift, Rockall Trough: implications for the history of the British-Irish ice sheet. *Marine Geology*, 173: 37-54.
- Ruddiman, W.F., 1997. Tropical Atlantic terrigenous fluxes since 25,000 yrs BP. *Marine Geology*, 136: 189-207.

References

- Rühlemann, C., Müller, P.J., Schneider, R.R., 1999. Organic carbon and carbonate as paleoproductivity proxies: examples from high and low productivity areas of the tropical Atlantic. In: G. Fischer and G. Wefer (Editors), *Use of proxies in paleoceanography*. Springer Verlag, Berlin, pp. 315-344.
- Rust, U., Vogel, J.C., 1988. Late Quaternary environmental changes in the northern Namib Desert as evidenced by fluvial landforms. *Palaeoecology of Africa* 19: 127-138.
- Sarnthein, M., Tetzlaff, G., Koopmann, B., Wolter, K., Pflaumann, U., 1981. Glacial and interglacial wind regimes over the eastern subtropical Atlantic and North-West Africa. *Nature*, 293: 193-196.
- Sarnthein, M., Thiede, J., Pflaumann, U., Erlenkeuser, H., Fütterer, D., Koopmann, B., Lange, H., Seibold, E., 1982. Atmospheric and oceanic circulation patterns off northwest Africa during the past 25 million years. In: U. Von Rad, K. Hinz, M. Sarnthein and E. Seibold (Editors), *Geology of the northwest African continental margin*. Springer Verlag, Berlin, pp. 545-604.
- Schenau, S., Prins, M.A., de Lange, G.J., Monnin, C., 2001. Barium accumulation in the Arabian Sea: controls on barite preservation in marine sediments. *Geochimica et Cosmochimica Acta*, 65(10): 1545-1556.
- Schmidt, H., 1992. *Der Benguelastrom im Bereich des Walfisch-Rückens im Spätquartär*. Ph.D. Thesis, Bremen University, Bremen, 172 pp.
- Schmiedl, G., Mackensen, A., 1997. Late Quaternary paleoproductivity and deep water circulation in the eastern South Atlantic Ocean: Evidence from benthic foraminifera. *Palaeogeography, Palaeoclimatology, Palaeoecology*, 130: 43-80.
- Schneider, R.R., Müller, P.J., Ruhland, G., 1995. Late Quaternary surface circulation in the east equatorial South Atlantic: Evidence from alkenone sea surface temperatures. *Paleoceanography*, 10(2): 197-219.
- Schneider, R.R., Müller, P.J., Ruhland, G., Meinecke, G., Schmidt, H., Wefer, G., 1996. Late Quaternary surface temperatures and productivity in the East-equatorial South Atlantic: Response to changes in Trade/Monsoon wind forcing and surface water advection. In: G. Wefer, W.H. Berger, G. Siedler and W. D.J. (Editors), *The South Atlantic: Present and past circulation*. Springer Verlag, Berlin, pp. 527 - 551.
- Schütz, L., Jaenicke, R., 1980. Eolian dust from the Sahara Desert. *Palaeoecology of Africa* 12: 97-98.
- Scott, L., 1989. Climatic conditions in southern Africa since the Last Glacial Maximum, inferred from pollen analysis. *Palaeogeography, Palaeoclimatology, Palaeoecology*, 70: 345-353.
- Scott, L., Partridge, T.C., 1990. Some manifestations of Pliocene warming in Southern Africa.
- Shackleton, N., Backman, J., Zimmerman, H., Kent, D.V., Hall, M.A., Robers, D.G., Schnitker, D., Baldauf, J., 1984. Oxygen isotope calibration of the onset of ice-rafting and history of glaciation in the North Atlantic region. *Nature*, 307: 620-623.
- Shannon, L.V., Anderson, P.P., 1982. Applications of satellite ocean colour imagery in the study of the Benguela current system. *South African Journal of Photogrammetry*, 13(3): 153-169.
- Shaw, P.A., Cooke, H.J., Thomas, D.S.G., 1988. Recent advances in the study of Quaternary landforms in Botswana. *Palaeoecology of Africa* 19: 15-26.
- Shi, N., Dupont, L., 1997. Vegetation and climatic history of southwest Africa: a marine palynological record of the last 300,000 years. *Vegetation history and Archaeobotany*, 6: 117-131.
- Shi, N., Dupont, L.M., Beug, H.-J., Schneider, R., 1998. Vegetation and climate changes during the last 21 kys in SW Africa based on a marine pollen record. *Vegetation history and Archaeobotany*, 7: 127-140.
- Shi, N., Dupont, L.M., Beug, H.-J., Schneider, R., 2000. Correlation between vegetation in Southwestern Africa and Oceanic Upwelling in the past 21,000 years. *Quaternary Research*, 54: 72-80.
- Shi, N., Schneider, R., Beug, H.-J., Dupont, L.M., 2001. Southeast trade wind variations during the last 125 kyr: evidence from pollen spectra in eastern South Atlantic sediments. *Earth and Planetary Science Letters*, 187: 311-321.
- Sirocko, F., 1991. Deep-sea sediments of the Arabian Sea: a paleoclimatic record of the Southwest-Asian monsoon. *Geologische Rundschau*, 80: 557-566.
- Soft Imaging System GmbH, 1999. *AnalySIS v3.0 User's Guide*, Münster, 572 pp.

References

- Stokes, S., Haynes, G., Thomas, D.S.G., Horrocks, J.L., Higginson, M., Malifa, M., 1998. Punctuated aridity in southern Africa during the last glacial cycle: The chronology of linear dune construction in the northeastern Kalahari. *Palaeogeography Palaeoclimatology Palaeoecology*, 137: 305-322.
- Stuiver, M., Reimer, P.J., 1993. Extended ^{14}C database and revised CALIB radiocarbon calibration program. *Radiocarbon*, 35: 215-230.
- Stuut, J.-B.W., Prins, M.A., Schneider, R.R., Weltje, G.J., Jansen, J.H.F., Postma, G., 2001. A 300 kyr record of aridity and wind strength in southwestern Africa: evidence from grain-size distributions of sediments on Walvis Ridge, SE Atlantic. *Marine Geology* 180(1-2).
- Syvitski, J.P.M., 1991. Principles, methods and application of particle size analysis. Cambridge University Press, Cambridge, 368 pp.
- Syvitski, J.P.M., Asprey, K.W., Clattenburg, D.A., 1991. Principles, design, and calibration of settling tubes. In: J.P.M. Syvitski (Editor), Principles, methods, and application of particle size analysis. Cambridge University Press, Cambridge, pp. 45-63.
- Thomas, D.S.G., 1999. 160 ka record of aeolian activity in central southern Africa: links to aridity and subregional variations., INQUA XV International Congress, Durban, South Africa, pp. 178.
- Thomas, D.S.G., O' Connor, P.W., Bateman, M.D., Shaw, P.A., Stokes, S., Nash, D.J., 2000. Dune activity as a record of late Quaternary aridity in the Northern Kalahari: new evidence from northern Namibia interpreted in the context of regional arid and humid chronologies. *Palaeogeography, Palaeoclimatology, Palaeoecology*, 156: 243-259.
- Tomczak, M., Godfrey, J.S., 1994. Regional Oceanography. Pergamon, Oxford, 422 pp.
- Tyson, P.D., 1986. Climatic change and variability in Southern Africa. Oxford University Press, Cape Town, 220 pp.
- Ufkes, E., Jansen, J.H.F., Schneider, R.R., 2000. Anomalous occurrences of *Neogloboquadrina pachyderma* (left) in a 420-ky upwelling record from Walvis Ridge (SE Atlantic). *Marine Micropaleontology*, 40: 23-42.
- Van Dam, J.A., Weltje, G.J., 1999. Reconstruction of the Late Miocene climate of Spain using rodent palaeocommunity successions: an application of end-member modelling. *Palaeogeography, Palaeoclimatology, Palaeoecology*, 151: 267-305.
- Van Zinderen Bakker, E.M., 1967. Upper Pleistocene and Holocene stratigraphy and ecology on the basis of vegetation changes in sub-Saharan Africa. In: W.W. Bishop and J.D. Clark (Editors), Background to Evolution in Africa. University of Chicago, Chicago, pp. 125-147.
- Van Zinderen Bakker, E.M.S., 1976. The evolution of Late Quaternary paleoclimates of Southern Africa. *Palaeoecology of Africa* 9: 160-202.
- Van Zinderen Bakker, E.M., 1984a. Aridity along the Namibian coast. *Palaeoecology of Africa* 16: 149-160.
- Van Zinderen Bakker, E.M., 1984b. A Late- and Post-glacial pollen record from the Namib Desert. *Palaeoecology of Africa* 16: 421-428.
- Vidal, L., Brüchert, V., Shipboard Scientific Party, 1998. Regional and stratigraphic patterns in color reflectance of sediments from leg 175. In: G. Wefer, W.H. Berger and C. Richter (Editors), Proceedings of the Ocean Drilling Program, Initial Reports. The Ocean Drilling Program, pp. 1-9.
- Weber, M., Niessen, F., Kuhn, G., Wiedicke, M., 1997. Calibration and application of marine sedimentary physical properties using a multi-sensor core logger. *Marine Geology* 136: 151-172.
- Weber, M.E., Pisias, N.G., 1999. Spatial and temporal distribution of biogenic carbonate and opal in deep-sea sediments from the eastern equatorial Pacific: implications for ocean history since 1.3 Ma. *Earth and Planetary Science Letters*, 174: 59-73.
- Wefer, G., Berger, W.H., Siedler, G., Webb, D.J. (Editors), 1996. The South Atlantic, Present and Past Circulation. Springer Verlag, Berlin Heidelberg New York, 644 pp.
- Wefer, G., Berger, W.H., Richter, C. (Editors), 2001. Proceedings of the Ocean Drilling Program, Scientific Results Volume 175.
- Weltje, G., 1997. End-member modelling of compositional data: Numerical-statistical algorithms for solving the explicit mixing problem. *Journal of Mathematical Geology*, 29: 503-549.
- White, J.C., Steig, E.J., 1998. Timing is everything in a game of two hemispheres. *Nature*, 394(August 1998): 717-718.

References

- Zachariasse, W.J., Schmidt, R.R., Van Leeuwen, R.J.W., 1984. Distribution of foraminifera and calcareous nannoplankton in Quaternary sediments of the eastern Angola Basin in response to climatic and oceanic fluctuations. *Netherlands Journal of Sea Research*, 17(2-4): 250-275.
- Zinck, J.A., Sayago, J.M., 2001. Climatic periodicity during the late Pleistocene from a loess-paleosol sequence in northwest Argentina. *Quaternary International*, 78: 11-16.

11. Samenvatting

De eerste op schrift vastgelegde waarnemingen van windgeblazen stof over de open oceaan dateren waarschijnlijk uit de 12^e eeuw toen de beroemde zeevaarder Edrisi (1100-1166) tijdens zijn ontdekkingsreizen stof vond op zijn schip. Ruim 7 eeuwen later publiceerde Charles Darwin, naar aanleiding van zijn beroemde reizen met de “Beagle”, één van de eerste verhalen over Sahara-stof voor de kust van West Afrika, getiteld: “An account of the fine dust which often falls on vessels in the Atlantic Ocean”. Inmiddels zijn er legio publicaties over windgeblazen stof en is het zelfs een ‘hot topic’ geworden nu wordt gedacht dat ijzerrijk stof, uit bijvoorbeeld de Sahara en de Namibische Woestijn, wel eens mede de oorzaak zou kunnen zijn van de ontwikkeling van ijsstijden door ‘bemesting’ van de oceaan. Algen die in zee leven maken namelijk gebruik van ijzer en verlagen het gehalte aan CO₂ in de atmosfeer wanneer het door hun geproduceerde organisch materiaal in het sediment wordt opgeslagen.

Dit proefschrift gaat voor een groot deel over windgeblazen stof. Dit stof werd gevonden in diepzee sedimenten voor de kust van zuidwestelijk Afrika en is afkomstig uit de grote woestijnen op het zuidelijk deel van het Afrikaanse continent. Hoofddoel van het onderzoek was om te kijken of de klimaatgeschiedenis van de laatste 300.000 jaar van dit deel van Afrika kan worden gereconstrueerd aan de hand van de fysische eigenschappen van het terrigene (van het land afkomstige) deel van de sedimenten in het zuidoostelijk deel van de Atlantische Oceaan. Windgeblazen stof is uiteraard maar één van de componenten die vanaf land naar zee worden getransporteerd. Naast wind transporteren ook rivieren en gletsjers sediment naar zee. In het bestudeerde gebied zijn en waren er echter geen gletsjers en stromen maar weinig grote rivieren.

Het idee achter het reconstrueren van een klimaatgeschiedenis aan de hand van diepzee sedimenten is dat in de diepe delen van de oceaan de depositie van sediment continu is. Daardoor ontstaat een opeenstapeling die grootschalige variaties in samenstelling en hoeveelheid van aangevoerde terrigene sedimenten door de tijd heen registreert. Veranderingen in de hoeveelheid en compositie van het terrigene materiaal vertellen iets over klimaatontwikkelingen op land. In het algemeen wordt namelijk de aanvoer van terrigene sedimenten naar de open oceaan bepaald door tektoniek (blootstelling van gesteente aan erosie), klimaat en veranderingen daarvan (verwering en transport van erosieprodukten) en zeespiegel en zeespiegelveranderingen (erosie- en transport competentie van rivieren). Vooral de laatste twee mechanismen bepaalden in het Laat Kwartair de hoogfrequente veranderingen in mariene sedimentaire opeenvolgingen.

Door doorlopende veranderingen in de positie en oriëntatie van de aarde ten opzichte van de zon veranderde de hoeveelheid en de ruimtelijke verdeling van warmte die de aarde van buitenaf ontving. Door de grote temperatuurschommelingen die dit tot gevolg had konden onder andere de ijskappen op de Noord- en Zuidpool en in de bergen over de hele aarde aangroeien en weer afsmelten. Dit aan- en afsmelten is wereldwijd goed te herkennen aan de hand van de onderlinge verhouding van stabiele zuurstofisotopen die in de oceanen voorkomen. De verhouding van zuurstofisotopen in

Samenvatting

de oceanen verandert voornamelijk onder de invloed van de hoeveelheid water die als sneeuw en ijs wordt opgeslagen in de ijskappen. In de waterkolom levende organismen die calcium carbonaat produceren, bewaren in de door hun gemaakte kalkskeletjes de zuurstofisotopenverhouding in de oceaan van dat moment. De kalkskeletjes komen uiteindelijk in het sediment terecht waar ze worden opgeslagen. Door achteraf de zuurstofisotopenverhouding van het calcium carbonaat te meten kunnen we de hoeveelheid ijs in het verleden reconstrueren en hebben we een indicatie voor het klimaat van dat moment.

De grote temperatuursverschillen op aarde hadden onder andere tot gevolg dat er grote variaties in de circulatiepatronen in de oceanen en in de atmosfeer optraden. Dit leidde tot veranderingen in neerslagpatronen, die uiteraard ook weer grote gevolgen hadden voor het klimaat op aarde. Grote verschillen tussen droge en natte klimaatcondities op land vinden hun weerslag op transportmechanismen van terrigene sedimenten naar de open oceaan. Een relatief nat klimaat zal bijvoorbeeld resulteren in verhoogde afvoer van sediment door rivieren, terwijl een relatief droog klimaat woestijnvorming en daarmee samenhangend transport van eolisch (windgeblazen) sediment zal bevorderen. Het vóórkomen van de transportmechanismen behorende bij deze 'klimaatuitersten' (rivier transport versus eolisch transport) is te herkennen in het terrigene deel van diepmariene sedimenten. Variaties hierin kunnen worden vertaald in veranderingen van de relatieve klimaatcondities in het brongebied van de sedimenten. Dit laatste is het hoofdthema van dit proefschrift.

Het nut van klimaatreconstructies op lange tijdsschalen is duidelijk: als we geen gedegen kennis hebben van het 'hoe en waarom' van klimaatveranderingen in het verleden, kunnen we bijvoorbeeld de dramatische stijging van atmosferisch CO₂ sinds de industriële revolutie ook niet in het juiste perspectief plaatsen. Het is daarom van groot belang dat er meer gereedschappen worden ontwikkeld die zijn te gebruiken om klimaatvariaties van ver vóór het bereik van de moderne meteorologische waarnemingen te begrijpen. In dit proefschrift wordt zo'n gereedschap besproken: de korrelgrootte van diep-mariene sedimenten.

Korrelgrootte

Rode draad in dit onderzoek is de korrelgrootte van het sediment. Zowel de korrelgrootte van kalkskeletjes van plankton dat in de waterkolom leeft, als die van de terrigene componenten in het sediment blijken een schat aan informatie te bevatten. Met de informatie uit de korrelgroottes van het plankton werd een windsterkte curve gereconstrueerd voor Zuidwestelijk Afrika voor de laatste 300.000 jaar. De wind is namelijk van invloed op de oceaanstromingen, die op hun beurt zorgen voor oplossing van kalkskeletjes van plankton. Deze oplossing laat de kalkskeletjes uit elkaar vallen en dat is te herkennen in de korrelgrootte van de kalkdeeltjes (hoofdstuk 4). Daarnaast transporteert de wind natuurlijk ook grote hoeveelheden stof naar de oceaan en dat is terug te vinden op bijvoorbeeld de Walvis Rug (Zuidoost Atlantische Oceaan, zie Figuur 11.1). Uit de korrelgroottes van het terrigene deel van de sedimenten die werden afgezet op Walvis Rug werd een klimaatreconstructie gemaakt voor Zuidwestelijk Afrika in termen van continentale ariditeit en ook weer (passaat-) windsterkte gedurende de afgelopen 300.000 jaar (hoofdstuk 5). De

korrelgrootteverdelingen van sedimenten van Walvis Rug geven een zelfde beeld als die van de continentale helling voor de kust van Walvis Baai (hoofdstuk 6).

Zuidoost Atlantische Oceaan

Het bestudeerde gebied beslaat een deel van het Angola Bekken en het Kaap Bekken in de Zuidoost Atlantische Oceaan (Figuur 11.1). De twee bekkens worden van elkaar gescheiden door de Noordoost-Zuidwest georiënteerde Walvis Rug, een vulkanisch gevormde onderzeese bergrug ontstaan tijdens de opening van het zuidelijk deel van de Atlantische Oceaan in het Late Krijt. De Walvis Rug is bedekt met voornamelijk kalkhoudende mariene sedimenten. De oceanografie van het gebied wordt gekenmerkt door twee stromingen: de zuidwaartse Angola Stroom en de noordwaartse Benguela Stroom. Op de plaats waar deze beide stromen elkaar ontmoeten vormt zich het Angola-Benguela Front, op dit moment een paar honderd kilometer ten noorden van de Walvis Rug. De expressie van het Angola-Benguela Front op land is de grens tussen het aride gebied in Namibië en het (sub)tropisch regenwoud in Angola. Het Kaap Bekken wordt verder gekarakteriseerd door kustopwelling: onder invloed van de Zuidoost passaatwinden wordt oppervlaktewater oceanwaarts geblazen en vervangen door dieper (en koud en voedselrijk) water. Deze opwelling vindt plaats in, door de topografie van het continentale plat bepaalde, 'cellen' en zorgt voor een hoge biogene productie in de kustwateren van Namibië en Zuid Afrika.

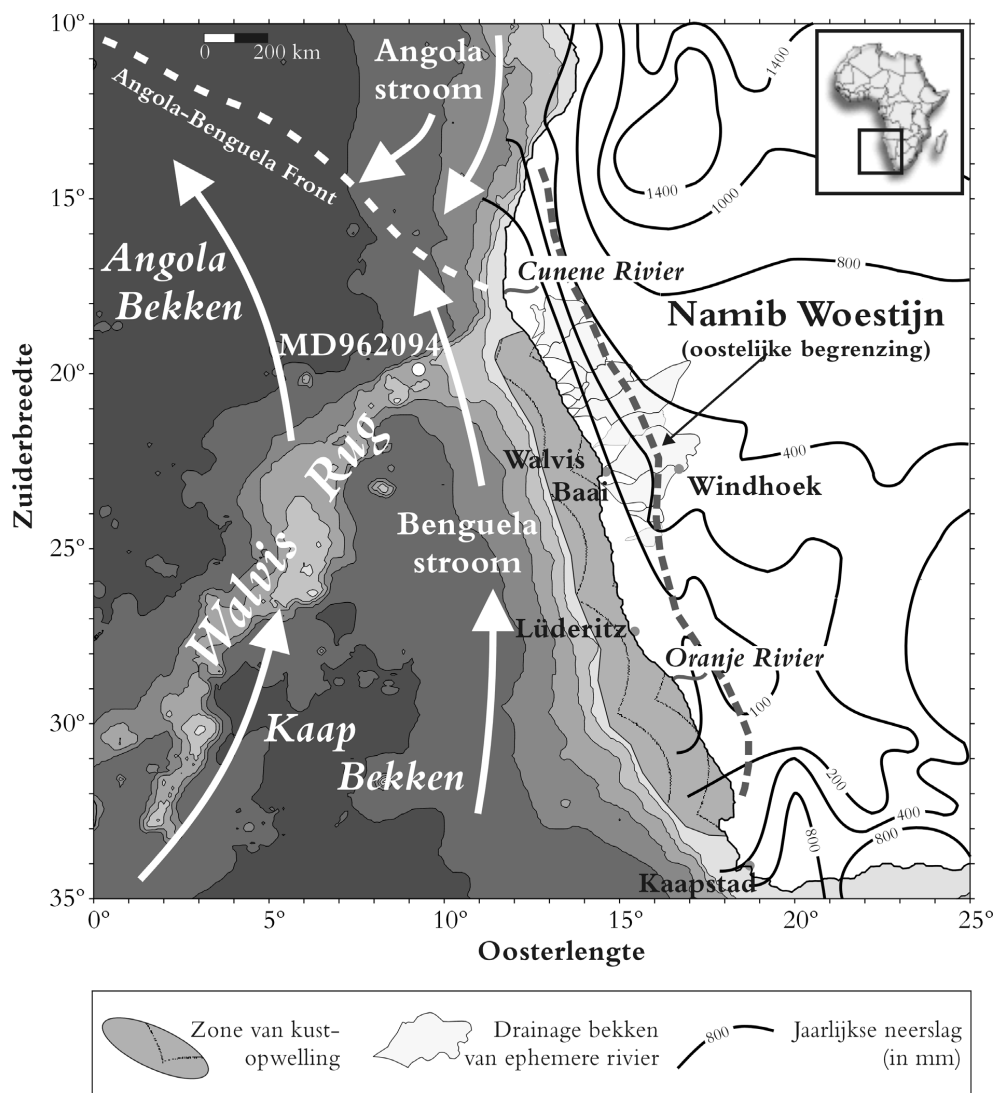
Door de opwelling van koud en voedselrijk water bestaat het sediment, dat uiteindelijk bewaard blijft op en in de zeebodem, hoofdzakelijk uit skeletjes van foraminiferen (ééncellige organismen die voornamelijk in het bovenste deel van de waterkolom leven en een kalkskeletje maken van ongeveer 20 μm tot 1 mm) en skeletjes van diatomeeën (ééncellige plantjes die in de waterkolom leven en silica-skeletjes maken van ongeveer 2–200 μm).

De grootste bron van terrigeen materiaal is de Namibische kustwoestijn (~ 140.000 km²) die, in combinatie met de zuidoost passaat winden, grote hoeveelheden eolisch sediment levert. Daarnaast zijn er twee grote continu stromende rivieren; de Cunene Rivier in het Noorden en de Oranje Rivier in het Zuiden. De Oranje Rivier draineert vrijwel geheel Zuid Afrika ten westen van de Drakensbergen en een groot deel van Namibië en is daarmee de grootste leverancier van fluviatiel (rivier getransporteerd) materiaal. Een aantal efemere rivieren (bevatten slechts nu en dan water) leveren tegenwoordig slechts eens in de 10 à 15 jaar sediment aan de kust. Gedurende het Laat Kwartair hebben de hoeveelheden fluviatiel en eolisch sediment die naar de Zuidoost Atlantische Oceaan werden vervoerd gevarieerd. De relatieve variaties van deze twee componenten zijn dus te gebruiken als proxies (indicaties) voor het klimaat. Om de variaties in de aanvoer van de terrigene componenten te bestuderen werden monsters genomen van de Walvis Rug en de continentale helling voor de kust van Walvis Baai door middel van sediment kernen (Figuur 11.1).

De Walvis Rug steekt gemiddeld ongeveer 2000 m boven de omgevende zeebodem uit en is daardoor zeer geschikt voor het construeren van een continue Laat Kwartaire opeenvolging vanwege de zeer geringe kans op verstoringen door massatransport van sediment vanaf het continentale plat. Daarnaast ligt de Walvis Rug zeer gunstig ten opzichte van de Namibische woestijn vanwege de Zuidoost passaat winden die sedimenten uit deze woestijn richting de Atlantische Oceaan blazen.

Samenvatting

Met name kern MD962094 (Figuur 11.1) werd in detail bestudeerd. Deze 30.68 m lange kern werd genomen op een diepte van 2281 m. Met behulp van stabiele zuurstofisotopen en ^{14}C -dateringen werden de sedimenten precies gedateerd. Het accent van deze studie lag op de laatste 300.000 jaar, dat wil zeggen: de bovenste 15 m van de kern.



Figuur 11.1. Overzichtskarta van het studiegebied met daarin de meest kenmerkende eigenschappen. Bathymetrie is gegeven in 1000-meter intervallen.

Indeling van dit proefschrift

Uit de chemische analyses van een transect van zeven kernen door de Zuidoost Atlantische Oceaan werd vastgesteld dat de variaties in de sedimenten van kern MD962094 representatief zijn voor dit deel van de Oceaan (hoofdstuk 2). Vóórdat verder wordt gekeken naar de korrelgrootte verdelingen van het sediment wordt de kwaliteit van het nieuwe laser deeltjesgrootte apparaat *Malvern Mastersizer S* onder de loep genomen. Een test met een eindlid model laat zien dat de metingen van dit apparaat zeer toepasbaar zijn voor het kwantitatief ontmengen van mengsels (hoofdstuk 3). De korrelgrootte van de bulk sedimenten (voornamelijk bestaande uit calcium carbonaat) is een goede maat voor de carbonaatpreservatie op Walvis Rug (hoofdstuk 4). De interpretatie van de tijdserie van carbonaatpreservatie als maat voor opwelling correleert zeer goed met de tijdserie van de windsterkte die is gebaseerd op de korrelgroottemetingen van het terrigene materiaal (hoofdstukken 5 en 6). De tijdserie van continentale ariditeit die ook in dit hoofdstuk wordt beschreven, is geen lokaal verschijnsel maar valt te correleren met andere klimaattijdseries op het Zuidelijk Halfrond (hoofdstuk 7). De chemische en fysische eigenschappen van het sediment uit de Zuidoost Atlantische Oceaan blijken nauw met elkaar samen te hangen. Dit wordt beschreven in de het laatste hoofdstuk (hoofdstuk 8). Hier blijkt dat de interpretatie van afzonderlijke tijdseries tot de verkeerde conclusies kan leiden maar dat juist de combinatie van verschillende proxies leidt tot de beste interpretatie van de meetgegevens.

Hoofdstuk 2

CORTEX

De chemische samenstelling van zeven sedimentkernen over een transect van offshore Walvis Baai tot op het distale deel van de Walvis Rug werd bestudeerd om na te gaan of een bepaalde locatie representatief is voor de samenstelling van de sedimenten in de Zuidoost Atlantische Oceaan. Met de CORTEX (CoreScanner Texel) werd de downcore distributie van zeven chemische elementen geanalyseerd. De duidelijke variatie die de verschillende elementen in alle kernen laten zien, weerspiegelen processen van sedimentatie, preservatie en diagenese. De resultaten van de CORTEX zijn kwantitatief te gebruiken, zo blijkt uit de correlatie met de resultaten van andere analyse methoden. Daarnaast blijkt dat met behulp van de CORTEX data de verschillende kernen goed met elkaar kunnen worden gecorreleerd. Uit de goede correlatie van de verschillende kernen wordt geconcludeerd dat de in de sedimenten van kern MD962094 geobserveerde variaties representatief zijn voor de hele Zuidoost Atlantische Oceaan.

Hoofdstuk 3

‘Malvern Mastersizer S’

Vrijwel alle sedimenten zijn mengsels van verschillende componenten. Die componenten verschillen van elkaar –onder meer qua korrelgrootte– doordat ze bijvoorbeeld op verschillende manieren werden geproduceerd (bijvoorbeeld foraminiferen versus diatomeeën) of door verschillende transportmechanismen naar de gekozen locatie zijn getransporteerd. In dit hoofdstuk wordt gekeken naar de kwaliteit van het nieuwe laser deeltjesgrootte apparaat *Malvern Mastersizer S*. Aan de hand van synthetische mengsels van glasparels wordt gekeken naar de precisie (hoe reproduceerbaar zijn de metingen?), de accuraatheid (hoe goed wordt de werkelijke korrelgrootte weergegeven?) en de resolutie (hoe goed kan het apparaat de

Samenvatting

mengverhoudingen van de componenten in de mengsels onderscheiden?). Daarnaast wordt gekeken of de dataset van korrelgrootte metingen te ont mengen is met een eindlid model. Immers, in tegenstelling tot de natuurlijke situatie, zijn nu de subpopulaties die samen de matrix van korrelgroottes vormen wél bekend. De resultaten laten duidelijk zien dat de combinatie van de korrelgroottemetingen en een eindlid model een zeer goede methode is voor het onderscheiden van subpopulaties in mengsels van glasparsels.

Hoofdstuk 4

Korrelgrootte van bulk sediment

In de korrelgrootteverdelingen van de sedimenten van Walvis Rug blijken drie hoofdpijken voor te komen. Deze zijn toe te schrijven aan de kalkskeletjes van verschillende organismen die leven in de waterkolom. Aangezien 70-95 % van deze sedimenten uit calcium carbonaat bestaat, worden de bulk korrelgrootte verdelingen representatief geacht voor de compositie van het calcium carbonaat. De twee grofkorrelige pieken worden voornamelijk veroorzaakt door foraminiferen (één cellige organismen die een kalkskeletje produceren) en fragmenten daarvan, de fijnkorrelige piek bestaat voornamelijk uit coccosferen (één cellige algen die een kalkskeletje produceren) en fragmenten daarvan. Uit microscoopbeelden van het sediment blijkt dat er door de tijd heen intervallen zijn waarin de kalkskeletjes van de foraminiferen goed bewaard zijn gebleven tegenover intervallen waarin de meeste kalkskeletjes zijn beschadigd. Omdat de beschadigingen plaats hebben gevonden op de grenzen van de kamertjes in de skeletjes van de één celligen, zijn ze hoogstwaarschijnlijk veroorzaakt door oplossing van calcium carbonaat. De meeste oplossing heeft plaatsgevonden in de monsters waarbij de grofstkorrelige piek in de korrelgrootteverdelingen laag is. De verhouding tussen de twee grofkorrelige pieken in de korrelgrootteverdelingen blijkt goed de mate van fragmentatie weer te geven welke is veroorzaakt door oplossing van calcium carbonaat. In het geval van de Zuidoost Atlantische Oceaan is de oplossing van calcium carbonaat te relateren aan de mate van windgedreven opwelling, welke verder zal worden bestudeerd in hoofdstuk 5.

Hoofdstuk 5

Korrelgrootte van terrigeen sediment

Variaties in de korrelgrootteverdelingen van het terrigene deel van de sedimenten op Walvis Rug geven een beeld van de transportmechanismen die het materiaal daarheen hebben vervoerd. Deze variaties staan in nauw verband met de klimaatcondities op land. De korrelgrootteverdelingen van het terrigene deel (na verwijdering van calcium carbonaat, organisch materiaal en opaal) van de sedimenten uit kern MD962094 van Walvis Rug (Figuur 11.1) werden geanalyseerd en met behulp van een eindlid model ontmengd in drie eindleden. Deze drie eindleden werden geïnterpreteerd als grof-siltig eolisch stof, fijn-siltig eolisch stof en fijn-siltig tot kleiige hemipelagische modder. Door ervan uit te gaan dat de hemipelagische component oorspronkelijk fluviatiel is getransporteerd, kunnen de relatieve proporties van de eindleden worden geïnterpreteerd in termen van klimaatveranderingen. De mengverhouding van de twee eolische eindleden is een maat voor de gemiddelde korrelgrootte van het eolische stof en wordt geïnterpreteerd als maat voor de sterkte van de zuidoost passaat. De mengverhouding van de twee eolische en de hemipelagische eindleden wordt geïnterpreteerd als maat voor de ariditeit op land. De zo verkregen windsterkte-tijdserie wordt vergeleken met een uit literatuur bekende opwellings-tijdserie. De twee tijdseries

Uit de combinatie van chemische- en korrelgrootte data, gemeten aan kern MD962094, blijkt dat deze nauw samenhangen met het klimaat. Echter, de afzonderlijke data mogen niet direct worden geïnterpreteerd in termen van klimaatschommelingen. Zo lijken de variaties in de calcium- en ijzertijdseries van Walvis Rug direct te zijn gerelateerd aan de aanvoer van ijzerrijk stof door de passaatwind. Echter, het indirecte verband tussen de passaatwind en de oplossing van calcium carbonaat heeft een veel groter effect op deze variaties. De oplossing van calcium carbonaat wordt veroorzaakt door opwelling, die op haar beurt weer wordt aangedreven door de passaatwind. Daardoor is het logisch dat de ijzer-tijdserie

Samenvatting

correleert met de passaatwind-tijdserie maar is het verband indirect. Dat wil zeggen, de twee verschillende processen hebben een gemeenschappelijke oorzaak. Door de complexe combinatie van aanvoer van ijzerrijk stof en verhoging van het ijzersignaal door oplossing van calcium carbonaat is het onmogelijk om alleen aan hand van de bulk chemie uitspraken te doen over klimaatvariaties op land. De combinatie van korrelgrootte analyses van zowel bulk sediment als van de terrigene fractie van het sediment, ontmengd in eindleden, levert de benodigde informatie over de variaties in windsterkte en ariditeit in zuidwestelijk Afrika gedurende de afgelopen 300.000 jaar. Vergelijking met tijdseries van de ariditeit in Zuid Amerika en de temperatuur op Antarctica laat zien dat de ariditeit in dit gedeelte van de wereld gestuurd wordt door schommelingen in het ijsvolume op de Zuidpool. Door aangroei van de ijskap op Antarctica worden kenmerkende fronten in de oceaan en atmosfeer in de richting van de evenaar geduwd waardoor delen van Zuid Amerika en Afrika ten noorden van de 35° breedtegraad onder invloed komen van de zone van vochtige westenwinden. De ogenschijnlijke tegenstelling tussen de ariditeit-tijdseries van Zuid Amerika en Zuidwestelijk Afrika en die van het noordelijk halfrond blijken dus een lokale gevoeligheid voor veranderingen in het ijsvolume op Antarctica in plaats van een mondiale tegenstelling in het klimaat.

Appendix A

Gebruikte analysemethoden

De toegepaste methoden worden beschreven in appendix A.

Acknowledgements

This Ph.D. study started with a phone call by Fred Jansen, who asked me if I would like to join an international expedition with the *N.O. Marion Dufresne* from La Reunion to offshore Namibia and back in the fall of 1996. The sediment cores taken from Walvis Ridge could then be studied during a Ph.D. project. I am still very grateful for this particular phone call and for the support that Fred gave me throughout the years whenever I needed it. I also want to thank in particular George Postma, my supervisor in Utrecht, for introducing me into marine geology and sedimentology and helping me putting all the ideas on paper. During the project Poppe de Boer became my promotor and he is acknowledged for his support. Two more key-players I want to thank; Ralph Schneider, for guiding me into the world of sea-going research, and Maarten Prins, of course, for all the support in the world of grain sizes, analyses, texts, and general problems that accompany any Ph.D. project. Both Ralph and Maarten were always available to put things into perspective over a nice glass of beer, thanks!

I highly appreciated working with Rik Tjallingii, who collected a lot of data during his M.Sc. work. His contribution resulted in chapter 6 of this thesis.

I am much indebted to all the people I met at the expeditions IMAGES II (1996) onboard *N.O. Marion Dufresne*, M41/1 (1998) with *F.S. Meteor*, Mare II (2000) with *S.A. Agulhas*, Mare III (2001) onboard *R.V. Pelagia*, and SUPO (2001) also onboard *R.V. Pelagia*. During these trips I had great fun and learned lots of things from many inspiring people. A few I want to mention in particular: Jacques Giraudeau, John Rogers, Gaute Lavik, Ralph Schneider, Thom Wagner, Mattias Zabel, Sabine Kasten, Anne Meier, Gerald Ganssen, Frank Peeters, Marcel Bakker, Lorendz Boom, Rikus Kloosterhuis, Leon Wuis, Astrid van Veldhoven, Laura de Steur, Elise Willemse, Karel Bakker, Evelien van Weerlee, Geert-Jan Brummer, Jan van Ooijen, Peter deMenocal, Sanne Lassen and Enno Schefuß.

I wish to thank my roommates Maarten Prins, Sjoukje de Vries, Rik Tjallingii, and Aart-Peter van den Berg van Saparoea (Utrecht) and Bas West, Neven Loncaric, and Sanne Lassen (Texel), for their pleasant company during parts of the last four years. Next to that I enjoyed lunchtime and numerous coffees and beers with the Ph.D. students at both Texel and Utrecht, in particular with the rest of the 'sedi-clan'; Jelmer Cleveringa, Max van Heijst, Bastian van Dijk, Wessel van Kesteren, Xander Meijer, and Quintijn Clevis, and the rest of the 'MCG-clan'; Marc Grutters, Frank Peeters, and Jerome Bonin, thanks!

The advantage of working at different institutes is the fact that you get to know a lot of interesting people. Always when I returned to my 'home base' Utrecht, I felt very stimulated by the interest many colleagues had shown in my work. I owe a lot to the people from the Marine Chemistry and Geology (MCG) department at NIOZ. I felt that I could always "knock on someone's door" for a specific question about my research or a general question about things at NIOZ. In particular the guys from the 'Dienst Zeetechniek' and 'Electro' always knew to help me out with another last-minute-problem.

Aad Vaars, Bob Koster and Sjerry van der Gaast are acknowledged for introducing me into the world of X-rays and for stimulating discussions on how to cope with the wiggles. Wim Boer is acknowledged for many fruitful discussions about grains and how to measure them and of course for allowing me in his volleyball team!

From the many great people I got to know in Bremen I want to thank in particular Frank Lamy for stimulating discussions about the Southern Hemisphere, and Gaute Lavik, of course, for many good talks and parties!

Another institute I frequently visited is the Vrije Universiteit in Amsterdam. I want to thank the people there for their hospitality, co-operation and interest in what I was doing (there). Especially Kay Beets, Ron Kaandorp, Saskia Kars (nice pictures!), Rink Kruk (now in Utrecht), Simon Troelstra, Hubert Vonhof, and again Maarten Prins, are thanked!

I had a great time at the Faculty of Earth Sciences in Utrecht, where I spent most of my Ph.D. time. Next to the people from the Sedimentology department, I enjoyed working with (and joining lunch/coffee breaks with) people from Stratigraphy/Paleontology and Paleobiology/Palynology and Geochemistry. I thank all you people and mention in particular: Albert Oost, Gert Jan Weltje, Johan ten Veen, Julia Becker, Erwin van der Laan, Frank Huiskamp, Sandra Langezaal, Ivo Duijnste, Cindy Looy, Sander Ernst, Natasja Jannink, Tanja van Kouwenhoven, Luc Lourens, Frits Hilgen, Joris Steenbrink, Hayfaa Abdul Aziz, Michiel van der Meulen, Tom van Hinte, Wil den Hartog, Jan van Dam, Johan Meulenkamp, Albert van der Meulen, Jan-Willem Zachariasse, Bert van der Zwaan, Christian Mulder, Henk Brinkhuis, Karin Boessenkool, Erica Crouch, Gert-Jan Reichart, Helen de Waard and Gijs Nobbe.

I thank Marnella van der Tol, Pien van Minnen, Marjolein van Wijk, and Boudewijn 't Hart for solving many logistical problems.

Paul van Oudenallen and Fred Trappenburg from the audiovisual facilities are thanked for their time and patience in correcting and printing my posters.

My colleagues from the 'promovendi-platform' are also acknowledged for the encouraging meetings we had. I want to mention in particular Jeroen van Hunen, Froukje Brouwer, Bart Bos, Edith Hafkenscheid (keep going, it's only a thesis!) and Menno van de Zedde for their interest in my whereabouts.

My colleagues from NITG/TNO are also thanked for discussions and help. I want to mention in particular Nikolaj Walraven, Bertil van Os, Gerard Klaver, Kenneth Rijdsdijk and Kathrin Reimer, thanks!

The members of the dissertation committee Gert de Lange, Jef Vandenberghe, Ralph Schneider, Jan de Leeuw, and Dick Kroon are thanked for evaluating this thesis and for their helpful comments.

Beside all my colleagues I want to acknowledge my family and friends. They have always shown a lot of interest in my work (“when are you going to find a **real** job?”, “so you’re going to lie on your back on one of those ships again!?”) and they always had the patience to listen to me telling what I really was doing (“dust!?, I have some dust for you too, come and clean my house!”). Besides, they always took great care of Meta whenever I had to go abroad for a while again. In this respect I particularly want to mention Hilbrand & Tjitske, Marc & Hester, Nico & Agnes and my family, thanks!

I’m afraid that –owing to my work– my social life has known some ups and downs during the last few years. I am grateful for having many friends around with whom I could have fun. I want to thank in particular my friends (or rather ‘vague acquaintances’) Peter Paul, Jan, Esther, Fred, Remco and Leon. Also the guys from Kampong 4 have to be mentioned in this respect, the ball may be round but the bottle remains angular! In quite a different way I have been stimulated and inspired by the people from ‘Silo’, thanks!

I am very grateful to my parents, who are always there to care for me. Next to supporting me, they spent a good deal worrying about me whenever I had to go and travel again, and doing so, they took great care of Meta and Mathilde too. Thanks!

Finally, I want to thank Meta and Mathilde for being my first and last.

Curriculum Vitae

Jan-Berend Willem Stuut was born on 26 August 1971 in Weener, Germany. He attended primary schools in Heerenveen, Rotterdam and Harderwijk and secondary schools in Harderwijk and Assen. In 1990 he started to study geology at the Utrecht University. His main subjects were marine geology and sedimentology. He developed a strong affection for sea-going research during a half-year internship at the Laboratory of Marine Geology and Physical Oceanography, University of Patras (Greece). His graduation research 'grain-size analysis of siliciclastics in the Arabian Sea' was followed by another study after the application of the 'grain-size method' in the Southeastern Atlantic Ocean at the Netherlands Institute for Sea Research (NIOZ). These studies resulted in a Ph.D. project at the Institute for Paleoenvironments and Paleoclimate Utrecht (IPPU), Sedimentology Division, Faculty of Earth Sciences, University Utrecht and at NIOZ, from May 1997 until November 2001. During these four years he further developed his fondness of sea-going research during five expeditions with various research vessels. He married his girlfriend Meta in 1996 and they got a beautiful daughter named Mathilde in October 2000. From November 2001 on he is working as a temporary lab assistant at the Vrije Universiteit in Amsterdam, awaiting an application for a post-doc position.



The author was already fascinated by aeolian sediments
when he was very young...
Ameland, May 1973

Stellingen behorende bij het proefschrift:

**Late Quaternary SW African terrestrial-climate signals
in the marine record of Walvis Ridge, SE Atlantic Ocean**

Jan-Berend Stuut

- 1) Size matters!
- 2) As long as detailed information about the transporting agents of sediments are lacking, the ratios of chemical elements cannot be used as proxies for continental aridity or wind strength.
- 3) If a machine yields precise and reproducible measurements, it does not matter if they are not very accurate, as long as the absolute deviation is known.
- 4) Fragmentation of foraminifers can be adequately determined by measuring the size distribution of the carbonate fraction of the sediments
- 5) Late Quaternary rainfall in Southwestern Africa was determined by the latitudinal position of the Southern Westerlies, related to the changes in the Antarctic ice volume.
- 6) Omdat de promovendus gedurende zijn/haar onderzoek vrijwel volledig op zichzelf is aangewezen is het niet vreemd dat het dankwoord het meest gelezen deel van het proefschrift is.
- 7) Als het werkelijk geen zin heeft om over smaak en kleur te twisten kan men geen bekeuring meer krijgen voor het rijden door rood licht.
- 8) Als het GAK het ziek gemelde NS personeel net zo streng zou controleren als de WW dat doet met nog niet gepromoveerde AiO's wiens contract is afgelopen, zouden de meeste treinen wél op tijd rijden.
- 9) Wie niet hoeft te rennen om de trein te halen, gaat niet efficiënt met zijn tijd om.
- 10) Globalisering is uitgevonden door eenlingen die zich realiseren dat ze in een steeds individualistischer samenleving toch ergens bij willen horen.
- 11) Waarheid en werkelijkheid zijn niets anders dan constructies, opgebouwd uit zelf gekozen axioma's. Hetzelfde geldt voor onwaarheid en onwerkelijkheid. Conclusie is: de wereld om u heen is een constructie, opgebouwd uit uw eigen keuzen (net als elk proefschrift...) (J. Bouman)
- 12) Omdat iedereen wil rijden, moeten we allemaal staan (Y van 't Hek)